



The additional value of a sonic drill in a new compaction method

J.D. Keuzenkamp



*Cover image made during the field test in Amsterdam, The Netherlands*

# The additional value of a sonic drill in a new compaction method

an experimental approach

by

**J.D. Keuzenkamp**

in partial fulfilment of the requirements for the degree of

**Master of Science**

in

Civil Engineering

at the Delft University of Technology,

to be defended publicly on Monday December 11, 2017 at 15:00 PM

Thesis committee

Dr. Ir. W. Broere	Delft University of Technology
Prof. dr. K.G. Gavin	Delft University of Technology
Ir. J.S. Hoving	Delft University of Technology
Dr. Ir. Ing A.E.C. v.d. Stoel	Crux Engineering b.v.
Ir J. W. Vink	Cofra b.v.

*This thesis is confidential and cannot be made public until December 11, 2022.*

An electronic version of this thesis is available at <http://repository.tudelft.nl/>.



# Abstract

Cities are growing and more land is reclaimed. Reclamation is the process of creating new land from ocean, riverbeds or lake beds. New land is created by hydraulic placement of sand. The hydraulically placed fills are characterized by low densities and show a high variety in packing throughout the field. The relative density of the fills depend on placement method and whether the placement takes place aqueous or subaqueous. After the placement Vibro-densification techniques are used to densify the soil. Conventional vibro-densification techniques have difficulties penetrating hard soil layers to reach the loosely packed layers. This makes that land reclamation is not always financially feasible. The Sonic drilling technique might be used to improve the penetration in hard layers. Reducing the process time make the use of land reclamation more accessible. However, the sonic drill technology is not well understood at the moment. There are no reliable guidelines that make it able to estimate the driveability of a certain profile in to the ground with the help of sonic vibrations. This research focusses on better understanding of the sonic drill technology and the contribution of a sonic drill to a new compaction technique.

On a reclaimed land site in Amsterdam an innovative method for installing elements in dense and hard sand layers was tested. The method focuses on sonic drilling/installation with vibrations up to 180Hz to reduce soil resistance whilst pushing the elements into the ground. This method has shown to generate less disturbances to the surroundings whilst achieving a higher penetration rate in comparison to conventional installation methods. The sonic vibrator generates pressure waves at the top of the element. The elasticity together with the inertial properties of the element allow the waves to propagate through the element. The pressure waves travel through the element and become partially transmitted to the surrounding soil. At the sides the mainly shear waves occur while at the tip both pressure and shear waves are present. During the wave propagation energy is lost due to scattering, radial damping and proper damping.

The sonic drill technology uses high frequency vibrations to strongly reduce soil resistance. The resistance of the element against penetration is reduced by liquefaction, inertia effects and a temporary reduction of porosity of the soil.

The observations from the tests form the basis for the establishment of model which simulates vibratory pile driving. The model is able to describe the installation process for different type of elements. The model might be used in the future to predict the penetration time using only the CPT data.

It can be concluded from the tests that the sonic vibration method is an effective solution for installing elements in a short amount of time in challenging ground conditions and with minimal vibration and settlement disturbance.

Finally, in terms of further study, it must be noted that several major simplifications and assumptions underlie the model, which may be improved upon with more rigorous constitutive modelling and numerical analysis.

# Acknowledgements

This thesis is the final product of my graduation research, performed in order to complete the master degree in Civil Engineering with a specialization in Geo-Engineering at Delft University of Technology.

I would like to use this opportunity to thank some people for their contribution.

First of all, I would like to express my gratitude to my graduation committee. During meetings they were always willing to share their knowledge and experience with me.

Further I would like to thank Almer van der Stoel for introducing me to the research topic and providing guidance and support.

I want to thank Crux Engineering bv, Cofra bv and H5s to give me the opportunity to be part of the field test. Being part of the test gave knowledge and insight in pile driving and greatly contributed to understanding the data.

I would like to thank my supervisor Jan-Willem Vink for always providing detailed feedback during the different stages of the research.

Last but not least I would like to thank my family for their support and confidence in me during my entire studies and for providing me with the opportunities to achieve my goals.

*J.D. Keuzenkamp  
Delft November 2017*

# Nomenclature

## Abbreviations

NAP	Normal Amsterdams Peil
CPT	cone penetration test
EPP	excess pore water pressure
CSR	cyclic stress ratio
CSL	Critical state line
WC	Weight compensation
MC	Mohr Coulomb

## Subscripts

<i>1D</i>	one – dimensional
<i>ampl</i>	dynamic component
<i>crit</i>	critical
<i>deg</i>	degradation
<i>e</i>	elastic
<i>ecc</i>	eccentric
<i>f</i>	(at) failure
<i>gen</i>	generated
<i>grav</i>	gravity
<i>i, 0</i>	initial
<i>liq</i>	liquefaction
<i>min, max</i>	minimum, maximum
<i>n</i>	normal
<i>nc</i>	normal consolidated
<i>p, s</i>	P – wave, S – wave
<i>pd</i>	pull down
<i>ref</i>	reference
<i>res</i>	resonance
<i>s, w</i>	soil, water
<i>sh</i>	shaft
<i>stat, cyc, kin</i>	static, cyclic, kinematic
<i>t</i>	tip
<i>v</i>	wave velocity
<i>x, y, z</i>	Cartesian components
$\sigma$	Stress
10,20,50	percentage at which particle diameter is smaller
1, 2, 3	principal components

## Superscripts

<i>fric</i>	friction
-------------	----------

## Symbols

Symbol	Unit	Description
$D_r$	[%]	relative density
$I_{SBT}, I_c$	[-]	Robertson soil behaviour type
$R_f$	[%]	friction ratio ( $f_s/q_c$ ) * 100 %
$f_s$	[MPa]	sleeve friction
$p_a$	[kN/m <sup>2</sup> ]	atmospheric pressure, 0.1 MPa
$q_c$	[MPa]	cone resistance
$r_u$	[-]	excess pore water pressure ratio
$u_{1,2}$	[m]	displacement model components
$\alpha_E$	[-]	Robertson factor
$\alpha_d$	[-]	material damping coefficient
$\alpha_s$	[-]	pore pressure development coefficient by Seed
$\alpha_s$	[-]	pore pressure coefficient
$\beta_B$	[-]	suitability number vibroflotation method
$\sigma, \sigma'$	[kN/m <sup>2</sup> ]	total, effective stress
$\varphi'$	[°]	effective internal friction angle
$\nu$	[-]	poisson ratio
$A, B$	[-]	Skempton parameter
$E$	[kN/m <sup>2</sup> ]	Youngs modulus
$F$	[kN]	force
$G$	[kN/m <sup>2</sup> ]	shear modulus
$H$	[m]	thickness soil layer
$K$	[m/s]	permeability
$L$	[m]	length
$N$	[-]	number of cycles
$R$	[-]	reflection coefficient
$S$	[%]	degree of saturation
$T$	[-]	transmission coefficient
$c$	[kNm/s]	damper
$d$	[mm]	particle diameter
$f$	[Hz]	Ffrequency
$g$	m/s <sup>2</sup>	gravity 9.81
$k$	[kN/m]	spring stiffness
$m$	[kg]	mass
$q$	[kN/m <sup>2</sup> ]	deviatoric stress
$r$	[m]	radial distances
$s, v, a$	[m], [ m/s], [ m/s <sup>2</sup> ]	Displament, velocity, accelaration
$t$	[sec]	time
$u$	[kN/m <sup>2</sup> ]	pore water pressur
$v$	[m/s]	wave velocity
$w$	[m/s]	wave amplitude
$\alpha$	[-]	cone resistance reduction factor
$\beta$	[-]	damping amplification factor
$\gamma$	[-]	shear strain
$\zeta$	[-]	damping ratio
$\nu$	[-]	Poisson ratio
$\rho$	[kg/m <sup>3</sup> ]	density
$\tau$	[kN/m <sup>2</sup> ]	Shear stress
$\omega, \omega_0$	[rad/sec]	radial velocity $2\pi f$ , natural radial velocity

# List of figures

Figure 1.1 Hydraulic placement rainbow method .....	1
Figure 2.1 Santa Marina, Panama city, Panama .....	5
Figure 2.2 CPT data Santa Marina .....	6
Figure 2.3 Vibro installation record(left), vibrating probe Bauer (right) .....	7
Figure 3.1 Vibroflot tool.....	9
Figure 3.2 Rearrangement of the grains contractive soil.....	10
Figure 3.3 Grain size distribution for effective densification (Mitchell, et al., 1981) .....	12
Figure 3.4 Schematic overview vibroflot .....	16
Figure 3.5 Vibrodisplacement top feed (Bauer, 2014) .....	17
Figure 3.6 Vibrodisplacement bottom feed (Bauer, 2014) .....	17
Figure 3.7 Examples of compaction probes fltr: terra probe, vibro-rod and Y-probe (Massarsch, et al., 2015) and vibro-wing .....	19
Figure 3.8 a) MRC compaction equipment b) MRC compaction probe .....	20
Figure 4.1 Test location .....	21
Figure 4.2 Soil layers Centrumeiland, Amsterdam.....	22
Figure 4.3 Local soil condition .....	22
Figure 4.4 Open-ended element vibroflot shape 300mm .....	23
Figure 6.1 Cross section vibrator head (Lucon, 2013).....	31
Figure 6.2 Resistance element.....	32
Figure 6.3 Sonic drill in resonance condition (Lucon, 2013).....	33
Figure 6.4 Influence confining pressure on development pore pressure ratio (DU & Chian, 2015) .....	36
Figure 6.5 Undrained shear response (Yang, et al., 2015).....	36
Figure 6.6 Schematic view soil behavior.....	37
Figure 6.7 Undrained response of loose sand under non-symmetrical cyclic loading ( $D_r=10\%$ , $\sigma'_{nc}=300\text{kPa}$ , $q_{stat}=60$ , $q_{cyc}=95\text{kPa}$ .....	37
Figure 6.8 Degradation shear modulus after N load cycles (Abel, 2014) .....	40
Figure 6.9 Illustration soil fatigue.....	41
Figure 6.10 Hysteresis loop (Abel, 2014).....	46
Figure 6.11 P-wave .....	48
Figure 6.12 S-wave .....	48
Figure 6.13 Wave propagation radiation damping (P-waves & S-waves) .....	49
Figure 6.14 Wave reflection and transmission .....	49
Figure 6.15 Attenuation vibration velocity test4 location5 .....	52
Figure 7.1 Simple mathematical model.....	54
Figure 7.2 Applied force 180 Hz.....	55
Figure 7.3 Upward slippage enabled.....	58
Figure 7.4 Upward slippage disabled .....	58
Figure 7.5 Soil interaction.....	60
Figure 7.6 SBT chart based on CPT cone resistance.....	61
Figure 7.7 SBT chart showing $I_{SBT}$ contours.....	62

Figure 7.8 Soil Unit Weight SBT chart .....	63
Figure 7.9 Identification soil type .....	63
Figure 7.10 Results for different number of steps per wavelength.....	64
Figure 7.11 Time step, 10 per wave length.....	65
Figure 8.1 Field test results open- and closed-ended elements.....	71
Figure 8.2 CPT data test location 1 .....	71
Figure 8.3 Model vs field test data test location 1 .....	72
Figure 8.4 Model vs field test data test location 2.....	73
Figure 8.5 CPT data test location 2.....	73
Figure 8.6 Model vs field test data test location 2.....	74
Figure 8.7 CPT data test location 5.....	75
Figure 8.8 Model vs field test data test location 5.....	75
Figure 8.9 Model vs field test data test location 5.....	76
Figure 8.10 CPT data test location 3.....	77
Figure 8.11 Model vs field test data test location 3.....	77
Figure 8.12 Installation curve open- vs closed-ended elements.....	79
Figure 9.1 Sensitivity analysis reduction factor $\alpha$ .....	82
Figure 9.2 Sensitivity analysis amplification factor $\beta$ .....	83
Figure 9.3 Sensitivity analysis Poisson ratio.....	84
Figure 9.4 Shear modulus reduction curve .....	85
Figure 9.5 Sensitivity analysis shear modulus.....	86
Figure 9.6 Sensitivity analysis dynamic frequency .....	86
Figure 9.7 Sensitivity analysis pull down load .....	87
Figure 10.1 Resonance frequency at different damping ratio's .....	89
Figure 10.2 Simplification soil strata test location 5.....	90
Figure 10.3 cone resistance with depth test location 5 .....	90
Figure 10.4 Resonance frequency undamped system test location 5.....	91
Figure 10.5 F.l.t.r penetration, resonance frequency test location 5.....	91

# List of tables

Table 3.1 Suitability vibroflotation method by Brown .....	13
Table 4.1 Overview performed tests.....	24
Table 6.1 Fatigue factors according to Verbeek et al. ....	41
Table 6.2 Degree of influence on penetration rate .....	47
Table 7.1 Forces acting in the system.....	55
Table 7.2 Soil type classification .....	63
Table 7.3 Computing time for different number of time steps.....	64
Table 8.1 Field tests for validation .....	70
Table 8.2 test description location 1 .....	72
Table 8.3 Test description location 2.....	74
Table 8.4 Test description location 5.....	75
Table 8.5 Test description location 5 (adapted).....	76
Table 8.6 Test description location 3.....	77
Table 8.7 Factors $\alpha$ and $\beta$ for the different tests.....	79
Table 9.1 Shear modulus reduction curve characteristics .....	85
Table 10.1 Soil characteristics test location 5 .....	90

# Table of Contents

Abstract.....	i
Acknowledgements.....	ii
Nomenclature.....	iii
List of figures.....	v
List of tables.....	vii
1 Introduction.....	1
1.1 Motivation.....	1
1.2 Structure of the thesis.....	3
2 Problem description.....	5
2.1 Introduction.....	5
2.2 Example projects.....	5
2.3 Objective and scope.....	8
3 Vibro-densification.....	9
3.1 Introduction to vibro-densification.....	9
3.1.1 Applications of vibratory densification methods.....	10
3.2 Principles behind deep vibratory densification methods.....	10
3.2.1 Soil type.....	11
3.2.2 Soil gradation/grain size distribution.....	12
3.2.3 Degree of saturation & location of the water table.....	13
3.2.4 Pretreatment density.....	13
3.2.5 Initial in-situ stresses.....	13
3.2.6 Time effect on strength and stiffness.....	14
3.2.7 Project related requirements & machine characteristics.....	14
3.3 Deep densification techniques.....	15
3.3.1 Vibroflotation method.....	16
3.4 Vibro-compaction methods.....	18
3.4.1 Vibro-rod.....	18
3.4.2 Vibro-wing.....	18
3.4.3 Foster Terra probe.....	18
3.4.4 Y-Probe.....	18
3.4.5 Müller Resonance Compaction (MRC) probe.....	19

4	Field-test.....	21
4.1	Test location .....	21
4.2	Elements .....	23
4.3	Tests .....	23
4.4	Conclusions .....	24
4.5	Recommendations.....	25
5	Research questions.....	27
5.1	Objective & scope.....	27
5.2	Limitations.....	28
6	Sonic drilling .....	29
6.1	Introduction to sonic drilling.....	29
6.1.1	History.....	29
6.2	Sonic drilling process .....	31
6.2.1	Resonance.....	32
6.2.2	Energy transfer.....	33
6.3	Parameters of influence.....	42
6.3.1	Crane base unit.....	43
6.3.2	Crane Leader.....	43
6.3.3	Sonic vibrator.....	43
6.3.4	Element .....	44
6.3.5	Soil .....	45
6.3.6	Degree of influence .....	47
6.4	Wave propagation.....	47
6.4.1	Type of wave .....	47
6.4.2	Interfaces .....	49
6.4.3	Scenario's .....	50
6.4.4	Attenuation of wave amplitude.....	51
6.5	Recommendations.....	52
7	Modelling Sonic drilling .....	54
7.1	Spring Mass model.....	54
7.2	Model components .....	55
7.3	Model conditions .....	56
7.4	Equations of motion.....	57
7.5	ODE-Solver Matlab.....	57

7.6	Initial conditions .....	58
7.7	Sonic drill parameters .....	59
7.8	CPT correlations.....	61
7.8.1	Soil type .....	61
7.8.2	E-modulus .....	61
7.8.3	Soil Unit Weight .....	62
7.8.4	Poisson ratio .....	63
7.9	Limitations of the model .....	63
7.9.1	Spring Mass Model .....	63
7.9.2	Element.....	66
7.9.3	Crane.....	66
7.9.4	Soil properties .....	67
7.10	Recommendations .....	68
8	Model results & validation .....	70
8.1	Introduction.....	70
8.2	Results .....	70
8.2.1	Test 1 .....	71
8.2.2	Test 3 .....	73
8.2.3	Test 4 .....	75
8.2.4	Test 5 .....	77
8.3	Conclusions model.....	78
9	Sensitivity analysis .....	82
9.1	Parameters.....	82
9.1.1	Factor alpha .....	82
9.1.2	Factor beta .....	83
9.1.3	Poisson ratio .....	84
9.1.4	G-modulus .....	84
9.1.5	Dynamic frequency .....	86
9.1.6	Pull down load.....	87
9.1.7	Conclusion.....	87
10	Optimization .....	88
10.1	Introduction.....	88
10.2	Test location 5.....	90
10.3	Conclusion.....	92

11	Discussion.....	93
11.1	Field test.....	93
11.2	Model.....	94
11.3	Soil.....	96
12	Conclusion.....	97
13	Recommendations.....	99
14	References.....	100
	Appendices.....	106
A	Test results.....	106
A.1	Test results.....	106
A.2	Location.....	106
A.3	SonicSampDril.....	107
A.4	Elements.....	107
A.5	CPT.....	108
A.6	Time-Depth Registration.....	109
A.7	Execution tests.....	109
A.8	Results.....	109
A.9	Conclusions.....	115
A.10	Appendices.....	116
B	Modelling.....	129
B.1	Introduction.....	129
B.2	Pseudo code.....	129
B.3	Governing equation.....	130
B.4	Model processes.....	132
C	Zone of influence.....	133
D	Test field conditions.....	134
E	Influence factor Beta.....	135
F	Damping.....	136
G	Parameter values damping and spring stiffness.....	137
H	Pore pressure ratio.....	139
I	Cyclic mobility.....	141
J	Densification based on accelerations.....	143
K	Conference paper.....	145



# 1

## Introduction

### 1.1 Motivation

Over the years more and more people are moving towards large cities. The space available for housing and industrial activities is often scarce. One is eagerly looking for opportunities to expand the living/working domain of these cities. This generally results in taller buildings and underground constructions. These solutions are very costly and not always feasible. For cities adjacent to water, reclamation of land is another possibility to expand the city area. New land is reclaimed from ocean, lake, or riverbeds and offers great potential to the demand for extra space. At land reclamation the ground surface is lifted above the water table by the addition of a land fill, mostly sand. The sand is added by dredging vessels, Figure 1.1. High costs are involved by such an operation and time is therefore an important factor. This makes that land reclamation is not always financially feasible. Hydraulic placement does not always lead to the desired results. Especially the variety of relative density throughout the fill is a great concern when observing reclaimed land originated by hydraulic filling. Hydraulic sand fills are characterized by relative low density, low strength and high liquefaction potential. The insitu density of soil is highly dependent on the type of soil, grains size distribution and if segregation occurs during placement.



**Figure 1.1 Hydraulic placement rainbow method**

There are several types of hydraulic placement techniques like rainbow placement and pipe placement. The possible range of achievable density per technique varies largely (Lee, 2001). Subaqueous placement methods result in low density placements while above the water table, higher densities can be obtained. The maximum mean relative density that can be obtained by hydraulically placed sand fills is around 60%. Some cases even show relative densities of only 20%. Furthermore, the range of the relative densities around the mean can be very large. This large spread involves high risk potential. Failures can easily be triggered by weak spots and causes failure in stronger layers. The low and variable strength of the soil makes the area less suitable for further

construction works. It is important to compact the loose layers, to secure the stability of structures and other constructions at ground surface.

Vibratory soil improvement techniques are used to increase the density and to create a more homogenous soil conditions. Unfortunately, conventional methods face often difficulties compacting deeper loosely packed soil layers underneath hard sand layers.

Nowadays there are several methods to densify granular soil. The soil needs to be densified to avoid liquefaction, limit settlements and to increase the bearing capacity. Most of these methods are straight forward and simply consist of using an overburden to compact the soil. These static techniques require a relatively long timeframe and are not able to compact deeper layers. It is of high interest to compact the soil in a short amount of time, because extra costs are involved for a longer compaction time. Shortening the time by starting construction work before the soil is adequately compacted results in extra settlement in the future leading to higher unexpected costs/maintenance and is therefore not recommended.

More sophisticated vibro-densification techniques can decrease the time needed to compact large quantities of soil and are able to reach great depths. However, these cyclic loading techniques are not always capable in penetrating dense sand layers ( $q_c > 20$  MPa). The dense sand layers make the penetration of the probe difficult and the densification of deeper layers troublesome. To be able to adequately compact the loosely packed soil underneath stronger layers, the method should be able to penetrate the overlying layers. A vibro-densification method that is capable of penetrating stronger layers is the vibroflotation method. However, the downside of this method is that it requires large quantities of water (Broms, 1991). Water is not always available, or the usage is not allowed due to environmental regulations. An alternative drilling technique that is able to penetrate stronger layers without the use of additional water is the sonic drill. The sonic drill method is a vibration drilling method that uses high frequency vibrations ( $f > 60$  Hz) to lower the soil resistance.

Vibratory densification methods have become more and more attractive due to several important developments such as the availability of powerful construction equipment and more reliable electronic equipment. Several companies invest in these new technologies to stay ahead of their competitors. A collaboration between CRUX Engineering, Cofra and H5s is established to find an innovative deep compaction technique which makes use of high frequency vibrations to insert different types of elements. A unique crane is designed to investigate the possibilities to rapidly insert elements and compact the surrounding soil. The crane is provided with a sonic drill motor from the company Eijkelkamp SSD and is installed on the leader of the crane. The amount of vibrations per second is variable and can be found in order of 0-180 oscillations per second. The element is vibrated into the ground whilst pushing it with a maximum load of 10 ton. The newly designed crane performed several tests at IJburg in Amsterdam. The installation effects were monitored using CPT's and Geophones. Several types of elements were vibrated into the ground in different patterns at various ground conditions.

The compaction and insertion of elements are considered to be two different components in finding a new compaction technique that can compete with the existing techniques. Each of them will be treated individually to better understand their fundamental workings.

## **1.2 Structure of the thesis**

In the following chapter of this thesis the problem is presented and explained with the help of a reference project. In chapter 3 a literature study on vibro-compaction is performed and different techniques are briefly explained. In the next chapter the field test is described and main conclusions of this test are presented. The results obtained from the field test determine the research direction of this thesis. In chapter 5 the research questions of the thesis are presented. The test results show that more effort needs to be spend in understanding the sonic drilling process. Next, a literature study on sonic drilling is presented in Chapter 6. The findings of the field test together with the literature study are used to come up with a mathematical model to simulate the sonic drilling process. The next chapter extensively explains how the model is constructed. In chapter 8 the model is validated with the field test results. This chapter is followed by a sensitivity analysis. The knowledge obtained in chapter 9 is then used to optimize the model to enhance the penetration rate of an element. In the discussion more attention is paid to the reliability of the result. At last a conclusion will be given on the applicability of the crane setup and recommendations will be given.



# 2

## Problem description

### 2.1 Introduction

Time is a very important factor at the construction of new projects. At every aspect of the project one tries to save as much time as possible to reduce the costs. One of the processes that has great potential in decreasing the time needed is the preparation of the project area. The basis for every project is the foundation of the construction. A proper foundation meets limited settlements and high calculability. By having a dense and homogenous subsoil one is able to fairly well describe the behaviour of the soil in the future as result of the load of the construction. To meet these requirements the soil has to be densified over the entire area in an equal way. A method that is able to densify the soil in a relatively short amount of time is a vibro-densification method. With the help of vibrations, the soil is densified. Although this method has proven itself there are still some limits to this method. To be able to densify deeper soil layers a probe needs to be vibrated into the soil to that specific layer prior the densification process. Sometimes it has to penetrate stronger layers to reach the loosely packed layers. The penetration of hard layers can form problems and takes more time. By improving the penetration rate in these hard layers, it is possible to save time and reduce the costs. The problem of having hard soil overlaying loosely packed soil is further elaborated with the help of an example project.

### 2.2 Example projects

#### Punta Pacifica

In 2011 Boskalis started with the construction of an artificial island called Santa Marina, off the coast of Panama city (Boskalis, 2013). Before the construction works could start, Boskalis started with dredging to remove soft soil sediments overlaying the weathered rock. After the disposal of the soft soil material a rock dike was created to form the perimeter of the island. The enclosed circuit was then hydraulically filled with sand, Figure 2.1.



Figure 2.1 Santa Marina, Panama city, Panama

Boskalis performed several cone penetration tests (CPT's) to check the relative density before they started to compact the soil using vibro-densification. The result of one of the CPT's is presented in Figure 2.2. The local reference height is indicated with respect to CID. The CPT data shows various values of cone resistance over the depth. This indicates the high variety in soil density throughout the fill. The rock base can be found at -7 m CID.

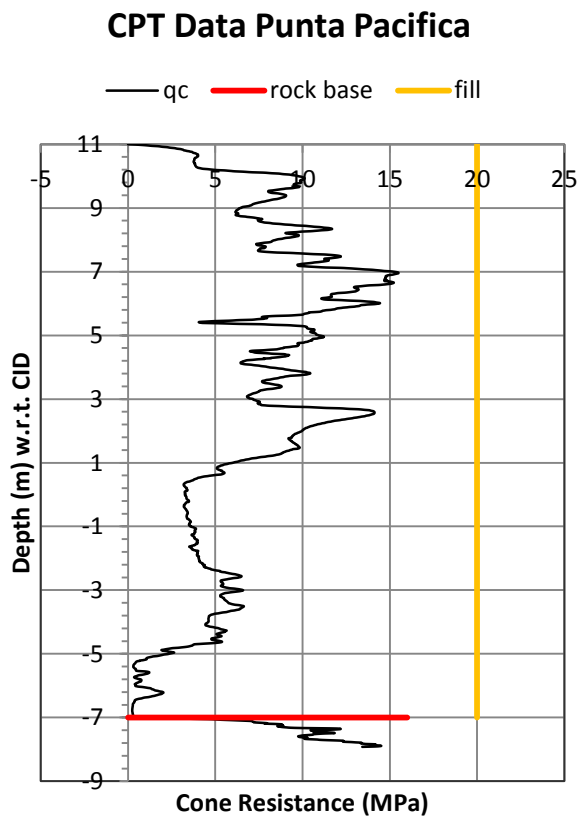


Figure 2.2 CPT data Santa Marina

The fill has to be compacted before further construction works could start. The ground surface before compaction can be found at 11 m CID.

The first 10 meters of the fill is dominated by soil with an average cone resistance of 10 MPa. The lower 8 meters mainly consist out of loosely packed soil with an average cone resistance of about 3 MPa. Underneath this soft soil layer, the weathered bed rock is found. The difference in cone resistance is the result of the placement of the sand. The phreatic surface can be found at 2.5 m CID. There is a clear difference between the cone resistance of the fill above the phreatic surface and underneath it. The layers of sand beneath 2.5 m CID were subaqueous placed and due to a reduced settling velocity by the water result in a loose packing. The soil above the water table was sprayed and spread out by dozers. This results in more densely packed soil.

To compact the underlying soft soil layers a vibro-densification technique by Bauer was used, see Figure 2.3. This vibro-densification method uses a vibrating probe that is lowered into the ground under its own weight. At the tips of the probe a vibrator generates horizontal vibrations. These vibrations cause the surrounding soil particles to rearrange themselves in a denser configuration. During vibration of the probe, water is jetted to enlarge the densification zone and increase the penetration rate. As the probe reaches its final depth it is gradually retracted in steps while extra sand is added to

compensate for the volume loss as result of the densification (Bauer, 2014). During the densification process the time needed to penetrate the soil was recorded. The recorded data of the rig shows that the penetration of the first 9 meters of soil cost most of the time, Figure 2.3. The first 9 meters correspond to the strong layers above the water table. The total penetration time takes around 4.5 minutes of which 3.5 minutes were needed to penetrate the first 9 meters and only one minute was needed to penetrate the following 8 meters.

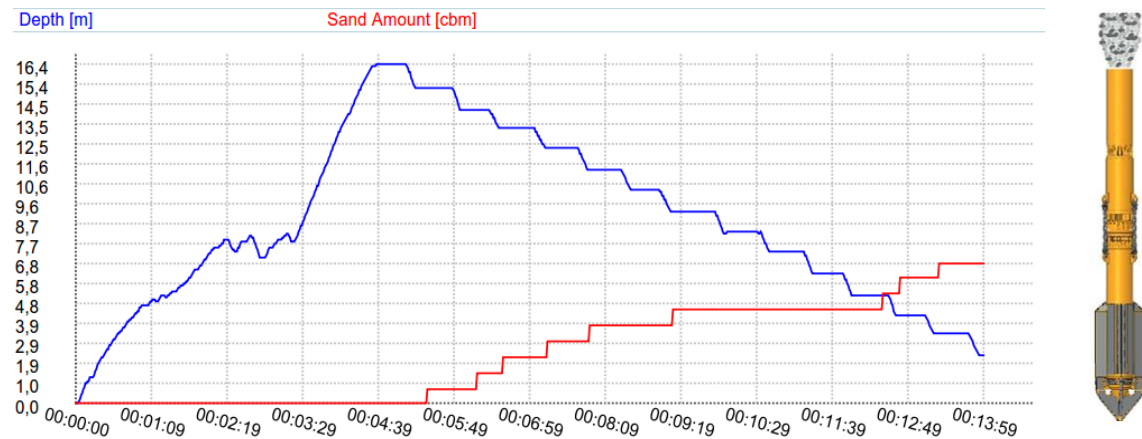


**Figure 2.3 Vibro installation record(left), vibrating probe Bauer (right)**

A project usually does not consist out of one drill hole. Big projects can have hundreds of vibro-densification locations or even more. The large penetration time in the hard layers have significant influence on the total time needed to adequately densify the project area.

### Embankments

The same variety in densities can be found at a newly placed embankments. Sand is deposited in different manners leading to a large spread of possible densities. The top layer of the newly placed sand can be densified due to construction works. Heavy machinery cause densification of the soil at the top due to static and dynamic loads. The deeper layers are not adequately densified and settlements in the future are not prevented. The densified top layer can cause problems when deeper soil layers need to be densified.

Contemporary vibro-densification methods are not able to adequate densify the deep loosely packed layers as they have difficulties penetrating the stronger layers. By reducing the penetration time in the stronger layers, it is possible to save time and eventually significantly reduce the cost of the compaction process. This research focusses on finding a method to increase the penetration through the hard layers.

### **2.3 Objective and scope**

To scope of the thesis is to find a new compaction method that is able to rapidly insert elements and densify the surrounding soil with the help of vibrations. The method should be able to reach great depths and is able to penetrate strong layers ( $q_c > 20\text{MPa}$ ) without having difficulties. The compaction and the installation process are considered to be two individual components. During this research they will be investigated separately.

The research is divided in different sections:

- Compaction of contractive soils (loose) via vibrations
- Field test and results
- Vibrational drilling
- Mathematical Modelling to simulate vibrational drilling
- Comparison model and field test results

The knowledge obtained in this research can be used to improve the crane setup to make it compete with existing vibro-densification techniques.

# 3

## Vibro-densification

In this chapter a literature study is performed on the available vibro-densification techniques. This chapter gives more insight in how the soil can be densified with the help of vibrations and which techniques are available at moment.

### 3.1 Introduction to vibro-densification

Vibro-densification methods are invented to compact the soil with the help of vibrations. Densification is achieved by vibrating the soil particles into a denser state. The air and or the water is expelled from the voids during the compaction process resulting in a volume decrease of the bulk. The vibrations in cohesionless soils have to be sufficient to overcome the frictional resistance between the grains and make densification of the soil possible. By increasing the density, one is able to improve soil properties as shear strength, stiffness and bearing capacity. Compaction is a standard process for the construction of embankments, earth structures, fills, subgrades for roads and airfields. The compaction of soil with the help of vibration methods is not something new. The first insitu deep densifications method for granular soil deposits was patented in the 1930's by Germans (Griffith, 1991). The method consisted out of a vibrating probe provided with two wings at the sides to enhance the densification. The method was first used without the use of a backfill material to compensate for volume loss.

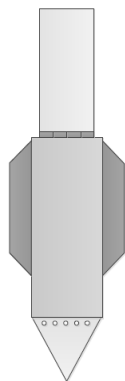


**Figure 3.1 Vibroflot tool**

Until 1970's the vibroflot tool was the only tool available for the densification of soil. During the years several variations have been developed to make it suitable for both cohesionless soils as cohesive soils. Several improvements enhanced compaction rates and made it possible to use backfill to compensate for volume loss. After the 1970's the terra probe was introduced. The terra probe process consists of driving an open-ended steel pipe into the ground while it is vertically vibrated. With this new method densification rates almost four times as high as the vibroflot tool were achieved without the use of water (Nicholson, 2015). From then several new methods were introduced with different characteristics to achieve better compaction rates.

Lately the vibratory compaction methods have become more and more attractive due several important developments such as the availability of powerful construction equipment and more reliable electronic equipment. Next to the improvement of equipment the monitoring of the compaction process becomes more and more important in assessing the quality of the vibro-densification technique.

The vibro-densification methods might be an effective and relatively inexpensive method. However, the method does not have unlimited capacities. By describing the fundamentals, a better understanding of the effectiveness and the applicability of the technique can be obtained.

### 3.1.1 Applications of vibratory densification methods

Densification methods are used to:

- Mitigation liquefaction
- Reduce settlements
- Increase engineering properties of the soil such as bearing capacity, shear strength, stiffness, dynamic shear modulus, reduced compressibility, etc.
- Decrease permeability
- Increase uniformity of the soil

### 3.2 Principles behind deep vibratory densification methods

All of the vibratory methods densify the soil with the help of a vibratory probe. The probe comes in different shapes and sizes depending on several factors such as: the required depth, degree of compaction, gradation of the soil, content of fines, degree of saturation, location of groundwater table, risks involved, available equipment and time, experience of the contractor and costs (Broms, 1991).

The vibratory methods are most effective in granular soils with low contents of fines. To increase the relative density the volume taken by the voids should be minimized. To decrease the volume of the voids the grains have to rearrange themselves in a denser configuration. This new configuration leads to settlements at ground surface. The total settlement is the result of the drained volume of water and the displacement of the grains in a closer configuration.

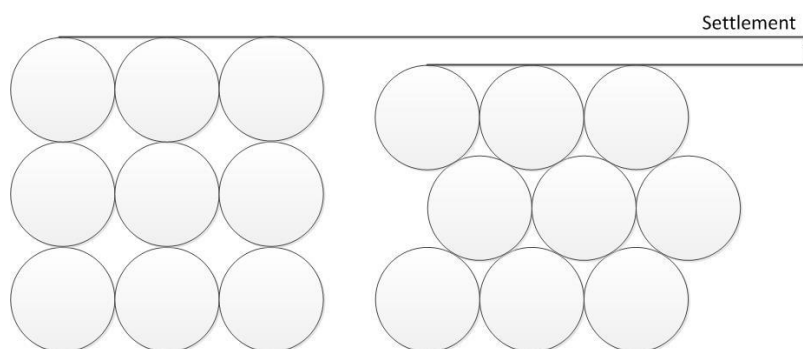


Figure 3.2 Rearrangement of the grains contractive soil

The vibrations on the probe are generated with the help of an external or internal vibrator. The vibrations are transferred from the probe to the surrounding soil and causes rearrangement of the soil particles. The rearrangement of particles results in contraction of the soil leading to a volume loss. The volume reduction of reclamation projects is

usual between the 5 and 15% depending on the initial relative density (Broms, 1991). To rearrange the particles the grains, have to slide on top of each other. Before there is any interference in the condition of the deposit the excess pore pressure is assumed to be equal to zero. In this situation the deposit is considered to be drained; the water is “free” to flow out. At this moment the sliding of the grains is prevented by the shear resistance between the grains. The drained shear resistance between the grains is a function of the external confinement, inter-particle friction and the degree of interlocking (Course Risk and Variability, M. Hicks 2016). The external confinement causes shear stresses between the individual grains. The total stress is the sum of the effective stress and the pore pressure (Terzaghi).

$$\sigma = \sigma' + u \quad (1)$$

The shear stress is dependent on the effective stress and the internal friction angle of the soil for non-cohesive type of soils.

$$\tau = \sigma' \tan \varphi' \quad (2)$$

The vibrations caused by the vibrator result in a sudden increase of water pressure adjacent to the probe. Even though the deposit was considered to be drained such rapid pressure increase cannot fully dissipate through the grains. The result is that the soil starts to behave partly undrained. The additional pressure is fully taken by the water. As the pore water pressure increases the effective pressure drops and the soil starts to liquefy. This process is known as liquefaction. The definition of liquefaction is stated as ‘the phenomenon wherein a saturated sand loses a large percentage of its shear resistance (due to monotonic or to cyclic loading) and flows in a manner resembling a liquid until the shear stresses acting on the mass are as low as its reduced shear resistance’ (Castro & Poulos, 1977)

The reduction in shear resistance enables the rearrangement of the loose, cohesionless grains as the soil re-consolidates.

The sliding resistance is determinative for the type of compaction method that can be used. The following factors influence the densification effect (Nicholson, 2015) & (Broms, 1991):

- Soil type (1)
- Soil gradation (2)
- Degree of saturation & location of the water table (3)
- Pretreatment density (4)
- Initial in-situ stresses (5)
- Time effect (6)

Next to the soil conditions other factors related to the project have influence on the type of method that can be used:

- Project related requirements & machine characteristics (7)

### 3.2.1 Soil type

The area of influence and the amount of compaction is highly dependent on the type of soil. As the grain size starts to increase the permeability increases and the soil becomes less prone to liquefaction. Furthermore, larger grains have to undergo more displacement to rearrange themselves and are therefore more difficult to compact.

In case of compaction of layers with a low permeability such as silts and clays the potential for liquefaction is high. However practically none of the water volume flows away when the probe is pulled out from the ground. The vibrations only result in some plastic deformation around the probe and no actual densification (Griffith, 1991). Furthermore, the cohesive forces of cohesive material increase the intergranular forces and make vibratory densification less successful.

### 3.2.2 Soil gradation/grain size distribution

A well graded sand is more difficult to compact than a sand with an uniform distribution. The fines fill up the voids and damp out the vibrations imparted by the vibrator. The amount of fines are also influencing the water flow through the soil. Clean sand has relatively large voids and thus a higher permeability. Increasing the percentage of fines decreases the permeability of the soil. The fines fill up the voids and reduce the water flow through the soil and make vibratory methods less effective (Griffith, 1991)

Fines are considered to be grains smaller than the minimal size of sand of 0.063 mm. The type of soil is known as silt (0.002-0.063 mm) and clay (<0.002 mm) (Verruijt, 2001). Several studies describe the limits of the amount of fines that can be present in soil to make compaction via vibrations effective. Percentages of fines below 10% can be easily compacted by vibratory methods. The methods become ineffective if the percentage of fines becomes greater than 25% (Mitchell, 1981).

A certain permeability is required to make re-consolidation of the soil possible. The time needed for the soil to consolidate is highly dependent on the permeability and the relatively density of the soil (Broms, et al., 1984). For soils with an intermediate permeability ( $k < 10^{-3}$  m/s) the water pressure first highly increases and the soil in the close vicinity of the probe liquefies. The excess pore pressure (EPP) decreases further away from the point of application until zero again. The pressure gradient in granular soils allows the soil to drain of the EPP and cause the particles to settle in a denser configuration resulting in a decrease of void volume. The lower the permeability of the soil the smaller the area of influence.

A fast and effective way to check whether or not a soil can be effectively densified by the vibro-densification method is to check its grain size distribution of the local soil.

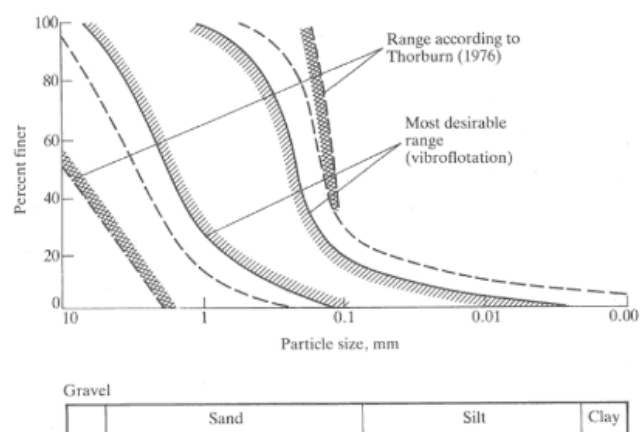


Figure 3.3 Grain size distribution for effective densification (Mitchell, et al., 1981)

Brown (1997) comes up with suitability number to express the effectiveness of the vibroflotation method.

$$\beta_B = 1.7 \sqrt{\frac{3}{d_{50}^2} + \frac{1}{d_{20}^2} + \frac{1}{d_{10}^2}} \quad (3)$$

Values for  $\beta_B$  less than 10 indicates that the soil is excellent for vibroflotation. When the value of beta exceeds the 30 the vibroflotation is ineffective for the compaction of the soil.

**Table 3.1 Suitability vibroflotation method by Brown**

(1)	(2)	(3)	(4)	(5)	(6)
<b>Suitability number</b>	0-10	10-20	20-30	30-50	>50
<b>Rating</b>	Excellent	Good	Fair	Poor	Unsuitable

### 3.2.3 Degree of saturation & location of the water table

Water is needed to take over the stress when the effective stress is decreased. The degree of saturation determines to which extend the stress is transferred to the water. If the soil is not fully saturated some of the energy generated by the vibrator gets lost in plastic deformation of the soil. As result the method becomes less effective.

For saturated soils it is important that the soil starts to behave undrained when it is vibrated to develop liquefaction. Whether or not the soil behaves drained or undrained depends on: (Brinkgreve, 2015)

- Degree of saturation S
- Permeability  $K_x, K_y$
- Loading rate  $dq/dt$
- Material stiffness E
- External conditions drainage length

The effectiveness of a vibro-densification technique depends on the availability of water and is therefore less effective in partially saturated and dry soils. In the region above the water table false cohesion occurs. The cohesion comes from suction as result of capillary forces between the grains. The forces increase the effective stress and therefore more energy is required to compact the soil. Vibrations in dry soil are more damped by plastic deformation in the near surroundings of the element and are therefore less effective in compacting large areas. There are techniques that can add water during the vibrations to enhance to compaction rate and zone. These methods will be explained later in this study.

### 3.2.4 Pretreatment density

Vibro-densification increases the relative density of the soil. Soils with low relative densities are easier to densify than soils that already have a very dense matrix. This is mainly due to an increase in shear resistance. As the void ratio decreases more grain interfaces are in contact with each other resulting in a higher intergranular friction. More energy, in the form of vibrations, is needed to overcome this friction.

### 3.2.5 Initial in-situ stresses

The initial effective stress has to be reduced to zero to make densification possible. Stronger vibrators are needed to obtain compaction in deeper layers were the in-situ stress is greater. However, a certain stress is needed to compact the soil during re-consolidation. Soil near the surface is less compacted as result of the limited load. The bigger the stress as result of the overburden the better the compaction effect.

### **3.2.6 Time effect on strength and stiffness**

Even after the EPP is dissipated an increase in strength and stiffness can be found with time. An explanation of this increase in time can be that due to heterogeneous stress conditions a rearrangement of the soil particles is taken place to find a new equilibrium (Massarsch & Fellenius, 2015). The penetration resistance after a month can increase up to 50 to 100% compared to the resistance directly after the densification process (Broms, 1991).

### **3.2.7 Project related requirements & machine characteristics**

The type of project influences the amount of compaction that is needed prior the construction works. The degree of compaction determines the durability and stability of the structure in the future. Also, the time available for compaction is an important factor in finding the best compaction method. Projects are restricted to a tight time schedule. The compaction time can reach from some weeks up to several months depending on the type of method and the area/volume that needs to be densified. The location of the project determines in a large extent which method will be used. Next to the allowable disturbance the space available for the crane to maneuver is also an important factor.

The maximum relative density than can be obtained for all vibro-densification methods is around 80%. However, the different techniques do not have the same time efficiency. Some methods can obtain the maximum relative density in a shorter time span and with less compaction locations.

The energy that can be generated and transmitted to the element determines the degree of densification. The efficiency of a particular method can be increased by:

#### **1. Pattern**

The probe pattern influences the densification effect. Most of the time squared of triangular patterns are used to densify the soil. The densification obtained with a squared pattern is often less than with a triangular pattern. According to (Brown, et al., 1977) 5-8% more probe insertions are needed with a squared pattern to get the same densification rate as with a triangular pattern in case of vibro flotation.

#### **2. Vibration frequency**

The probe can be vibrated with a high frequency to bring the probe as fast, as possible, at depth. A high frequency reduces the soil resistance between the probe and the surrounding soil. Once the probe reaches depth a lower frequency can be used to densify the soil. A frequency between 15-20 Hz results in the best densification. At this frequency the probe vibrates in resonance with the soil. The relative displacement between the soil and the probe becomes minimal. During the resonance the energy generated by the vibrator is transferred to the soil in an efficient way. At the resonance frequency the dynamic shaft friction increases to a maximum value and approaches the static state shaft resistance (Massarsch & Westerberg, 1995). At this point more dynamic energy can be transferred to the soil.

### **3. Efficiency in probe operation**

- **insertion, suspension, withdrawal**

To be able to increase the density of deeper soil layers the soil needs to be penetrated first. At penetration it is not the intention to densify soil beneath the probe, as this only counteracts the penetration of the probe. As the probe is withdrawn, the soil is densified with the help of vibrations. If the probe is withdrawn too fast the compaction becomes inadequate. When the withdrawal is too slow the probe/flot can become stuck.

### **4. Duration of vibration**

Nowadays the probe is vibrated until the moment that the machines operator notices that the machine requires more energy to vibrate at the same velocity. This is done by listening to the sound of the rig or by reading off the hydraulic pressure. It is important to find the exact time needed to densify the soil. A longer vibration time will not result in extra densification and is therefore useless.

## **3.3 Deep densification techniques**

The vibro-densification can be divided into three different densification methods (Broms, 1991):

- Vibroflotation
- Vibro-compaction
- Blasting

Blasting will not be further elaborated as a result of the purpose of this study. The vibroflotation method is considered to be one particular method while the vibrocompaction method consist out of several different methods which are based on the same technique. Vibroflotation and vibrocompaction differently transfer vibrations to the surrounding soil. The vibroflotation vibrator generates lateral vibrations while in the vibrocompaction methods vertical vibrations are created. During the vibrations the probe is either pushed, vibrated and/or jetted into the ground.

There are two different techniques that are commonly used to compensate for the volume loss: vibrodisplacement and vibroreplacement.

### Vibrodisplacement

During this process all the existing soil remains in the ground. This technique is used in loose sand and gravels that are relatively easy to densify by vibrations. As result of the compaction of the soil the volume reduces. The reduction of the volume is typically backfilled with clean sand. In some cases, a lowering of the site elevation is preferred in those cases the amount of backfill is reduced.

### Vibroreplacement

This technique is used in soils which are difficult to compact. The soil consists out of a high percentage of fines or is not suitable for compaction, e.g. clay. Water is injected during penetration to flush out of the fines and keep the borehole stable while the hole is backfilled with granular soil. At the process existing soil material is replaced by a coarse aggregate which is then densified, resulting in a stone column. These stone columns can act as a drain which can decrease the consolidation time. However, a high hydraulic

gradient in these drains can promote internal erosion and/or clogging of the drain. These columns can also be used for reinforcement in slope stabilization.

### 3.3.1 Vibroflotation method

Most of the vibro-densification methods use a probe which is vibrated in to the ground. The probe for the vibroflotation method is also known as the vibroflot and comes in a variety of sizes and configurations. The vibroflotation method, in contrast to other vibro-densification methods, can be used in cohesive, mixed and layered soils. The vibroflotation method increases its effectiveness in these soils with the help of air- and waterjets at the tip and sides of the probe.

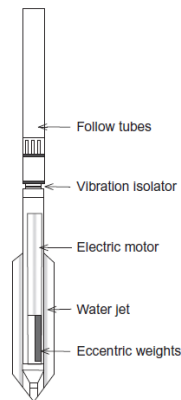


**Figure 3.4 Schematic overview vibroflot**

Normally the diameter of a vibroflot can be found in the range of 300-450 mm (Nicholson, 2015). On the sides of the vibroflot steel plates are welded to prevent rotation of the vibroflot and to increase the range. Inside the vibroflot eccentric weights rotate on an internal vertical shaft inside the motor. This causes lateral vibrations of the probe. By changing the amount of revolutions per second the frequency of the vibration changes. The lateral vibrations propagate radially away from the probe making densification possible. During the penetration of the probe water or air can be added via jets to enhance the penetration rate and densification of the soil.

There are two types of vibrator systems on the market at the moment. Both the vibrators can vibrate at variable frequencies. The length at which the vibrations are transmitted is different. The Keller systems transmits the vibrations of the entire length of the vibroflot while a Bauer system only vibrates at the tip (Broms, 1991).

The effective range of the vibrating probe is around 1.5 to 3 meters (Welsh, 1991)& (Griffith, 1991). The relative density that can be obtained with vibroflotation method is 70 to 85 % (Baker, 2010). The maximum relative density that is achieved during the compaction process is highly dependent on the spacing and power of the vibrator.

#### *Process*

The vibroflot is attached to the crawler crane leader and is positioned to a selected point. The vibroflot is lowered into the ground by its own weight and vibratory action. The vibroflot can be installed with water- and airjets. Most of the time waterjets are used. Airjets are used in specific circumstances when no water can be used. During the penetration of the ground the water jets at the tip of the flot are flushing water to enhance the penetration. When the vibroflot reaches depth the jets at the tip are turned off and the jets at the side are activated. The purpose of the side jets is to loosen the soil above the vibrator. From this point on the densification process starts. The flow rates have to be monitored at all the time to control the densification of the in-situ particles. The water stabilizes the borehole and creates an open channel along the sides of the vibroflot to prevent stick and make the addition of backfill possible (Brown & ASCE, 1977). The

flowrate should be sufficient enough compensate for seepage losses and keep the channel open. The water stabilizes the borehole. From this point the vibroflot is slowly raised to the surface in intervals of 0.5m to compact the soil around the probe. At each interval the probe compacts the soil for at least half a minute up to one minute. As the vibroflot retreats from the soil layer the EPP dissipates and the grains settle in a new and denser configuration.

Backfill of coarse grained sand is often used to fill up the volume loss as result of the densification of the soil. The amount of backfill needed is dependent on the degree of compaction but can be up to 1.5 m<sup>3</sup> per meter length (Griffith, 1991).

There are two ways to add the backfill material to the end of the probe.

### Wet top feed method

- **Replacement and displacement methods**

In this technique the water jets first remove the soft material and stabilizes the probe hole. The tip is now free and surrounded by water. From the top backfill material is added to the probe hole by using an excavator.

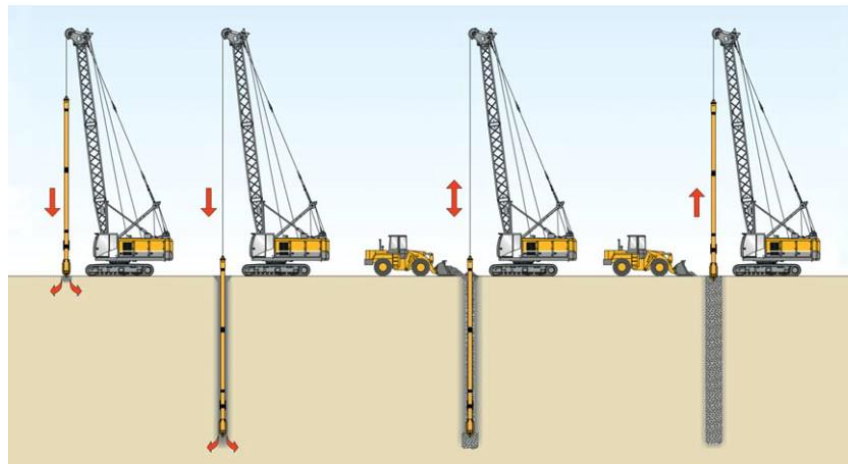


Figure 3.5 Vibrodisplacement top feed (Bauer, 2014)

### Dry bottom-feed method

- **Displacement method**

The granular back fill material is added with a hopper to the supply tube. The supply tube feeds the granular backfill to the tip of vibrator. This operation is completely dry.

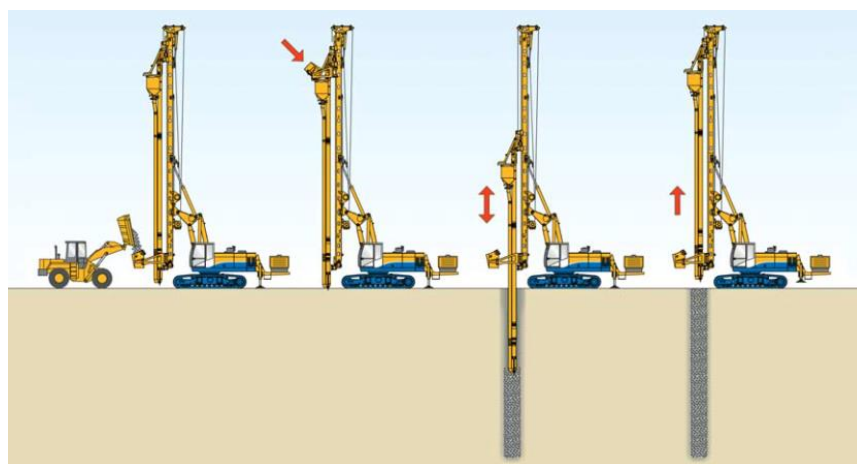


Figure 3.6 Vibrodisplacement bottom feed (Bauer, 2014)

### **3.4 Vibro-compaction methods**

The different techniques make use of a probe which is vibrated by an external vibrator on top of the probe. The vibrator creates vertical vibrations which are transferred into horizontal vibrations, in the surrounding soil, via the shear resistance between the probe and the soil. The probe is vibrated into the ground and then pulled out again while the probe keeps on vibrating. Backfill can be added from the top of the probe hole to counteract for the volume loss. The rate at which the probe is pulled out depends on the time needed to get the required relative density. The vibration frequency used for most of the vibro-compaction methods can be found in the order of 15-60 Hz (Broms, 1991).

The differences between the techniques can be found in the shape and size of the vibratory probe resulting in different compaction rates. In this study the most popular methods are presented.

#### **3.4.1 Vibro-rod**

The vibro-rod was developed in Japan and consists out of closed pipe together with a number of protrusions on the sides of the rod, Figure 3.7. The probe is driven by a vibratory pile driver (Saito, 1977).

#### **3.4.2 Vibro-wing**

The vibro-wing method is an evolution of the vibro-rod method. The vibro-wing systems were developed in Sweden and utilize a steel rod with 0.8 meter long wings welded to the rod (Massarch, 1990), Figure 3.7. The probe is inserted by a piling rig. The piling rig offers better control of the penetration of the probe than a pile driver.

The efficiency of the vibro-wing method is dependent on the length of the wings and the distances between them. Relatively short wings are used in coarse grained sand. Long wings in coarse grained soil can cause problems during the pull-out operation of the rod. The excess pore water pressure in coarse grained soil rapidly decreases leading to a vacuum of water pressure when the probe is retrieved out of ground. To prevent this, wings are placed relative far apart from each other and the size is decreased. Because of the smaller wings more intensive vibrations are needed to liquefy the soil. In fine sand longer wings can be used which are placed closer to each other.

#### **3.4.3 Foster Terra probe**

The terra probe was invented in the United States by Foster Engineering (Massarch, 1990). The open ended has a diameter of 0.76 m (Figure 3.7). The probe is vibrated by a vibratory hammer. The frequency that is used to drive the probe is around 15 Hz (Broms, 1991). The probe itself is around 3 to 5 meters longer than the required depth of compaction. The probe is driven into the ground and pulled out again after compaction of the soil

#### **3.4.4 Y-Probe**

The probe consist out of three 0.5 meter wide steel blades welded to a steel probe at an angle of 120 degrees to each other, Figure 3.7 (Massarch, 1990). Small ribs are attached to the wings in order to increase the friction between the blades and the soil. The probe is inserted with the help of a crane.

Field tests have shown that the vibrations from the probe to the ground are transferred the best with a Y-shape arrangement. Between each of the wings there is an angle of 120. The frequency that is used varies between the 15 and 20 Hz.

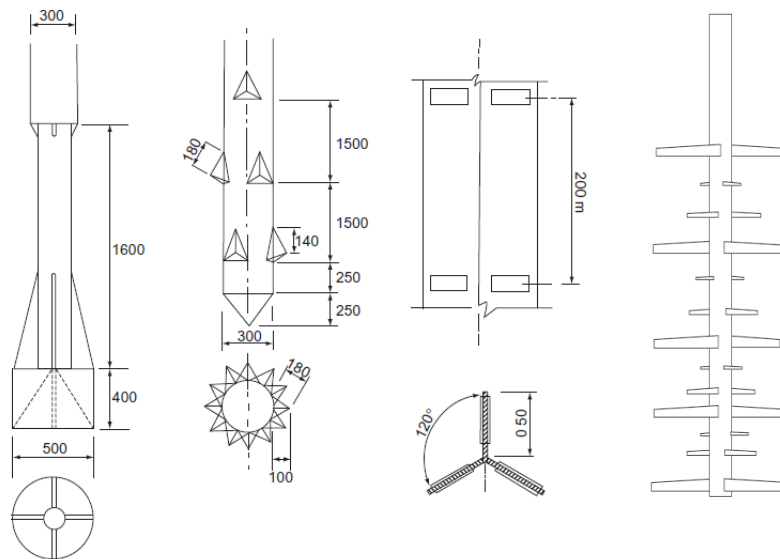


Figure 3.7 Examples of compaction probes fltr: terra probe, vibro-rod and Y-probe (Massarsch, et al., 2015) and vibro-wing

### 3.4.5 Müller Resonance Compaction (MRC) probe

The probe of a resonance compaction system is provided with openings to decrease the weight and increase the contact area. As results of the opening the probe behaves less stiff. This results in more energy transfer to the soil, resulting in better compaction rates than a massive probe.

The probe is vibrated into the ground with high frequency vibrations ( $f=50$  Hz). As the probe reaches depth the frequency is lowered to the resonance frequency. The resonance frequency is the frequency at which the vibrator and the soil mass vibrate at the same frequency. This frequency is also known as the natural frequency of the soil mass.

The resonance frequency of a soil layer can be determined. By knowing the resonance frequency better compaction rates can be obtained. The frequency is dependent on the wave velocity and the thickness of the soil layer (Massarch, 1990).

$$f_{res} = \frac{v_{soil}}{4H} \quad (4)$$

The wave velocity in soil can range from 100 m/s for soft soils to 700 m/s for gravelly soils. The exact velocity depends on the porosity, water content, stress state and mineralogy. To obtain resonance over a soil column with a length of 8 meters and a wave velocity of the soil of 500 m/s the resonance frequency is 16 Hz. This frequency corresponds to the frequencies used at other compaction methods.

One should be aware that the formula assumes that the wave velocity is constant over the entire layer. In practice the resonance frequency is obtained at site during execution of the compaction. The frequency is increased or decreased until resonance of the soil is

visible. This value is more reliable because of the fact that the soil is not homogeneous. The optimal frequency for compaction of the soil changes during compaction process. As the soil becomes denser the wave velocity of the layer changes and therefore also the resonance frequency (Massarch, 1990).

Settlement at ground surface can be expected within a zone of 2 times the radius of the probe.

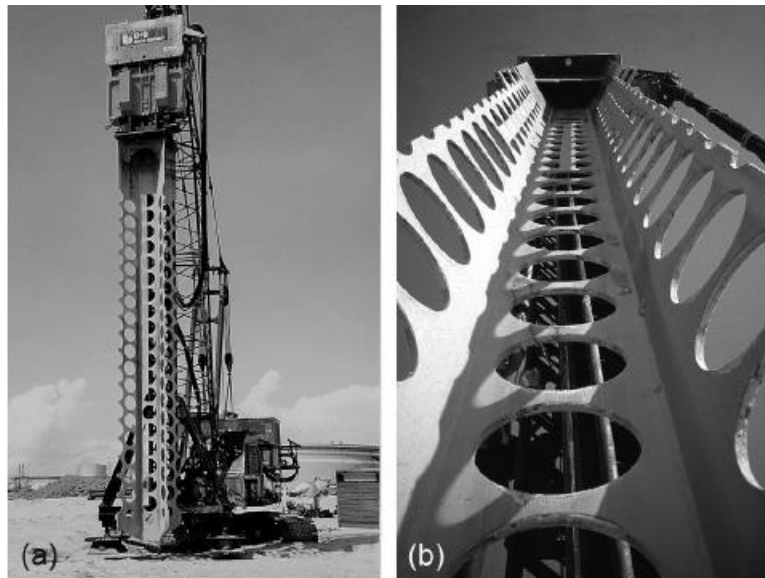


Figure 3.8 a) MRC compaction equipment b) MRC compaction probe

# 4

## Field-test

Together with the knowledge obtained from the literature study on vibro-densification techniques it is possible to review the densification and penetration results obtained by the field test.

From the 27<sup>th</sup> of February up to the 8<sup>th</sup> of March a full scale test, in which an innovative method for installing foundation elements in dense and hard sand layers, has been performed. The test was executed on a piece of reclaimed land in Amsterdam, The Netherlands. In this period several types of elements were vibrated, whilst pushing it, into the ground with an entirely new crane setup. The vibrations were generated by a sonic vibrator from the company SonicSampDrill. The vibrator can reach frequencies up to 180 Hz and is installed on the leader of the crane (see front page). The leader is placed on a wooden board to ensure that the element stays straight during insertion. The applied load on the elements is varied between 4 and 10 ton. The purpose of the test is to investigate the possibilities of the crane to rapid insert elements and to compact the surrounding soil.

During insertion of the elements the particle acceleration, velocity and frequency were measured by different geophones. The geophones were installed at respectively 2 m, 5 m and 10 m radial distance from the point of insertion. At the same time the element is vibrated into the ground the time needed for 1 meter of penetration was manually recorded. Together with the CPT-data a relation between the  $q_c$ -value and the penetration time can be obtained. More specific information about the test can be found in appendix A.

### 4.1 Test location

The tests were performed on a piece of reclaimed land in Amsterdam named IJburg. In the years 2014 until 2015 IJburg was further extended by the company named Boskalis. The extension was made to make further development of the IJburg possible. The land was lifted 2 meters above the water surface using hydraulic- and dry placement of sand. Underneath the water table layers of 0.5 m were deposited. Between each layer a period of rest of 4 weeks was taken to let the soil consolidate. Above the water table layers of 1.0 meter thick were used for the elevation of the island.



Figure 4.1 Test location

The soil underneath the fill consist out of fine grained sediments deposited by the IJsselmeer. The alluvial deposition took place over hundreds of years and mainly consist out of weak clayey silt and is considered to be very organic (Zaalberg, 1985). The soil layering at the location of Centrumeiland look as illustrated in Figure 4.2.

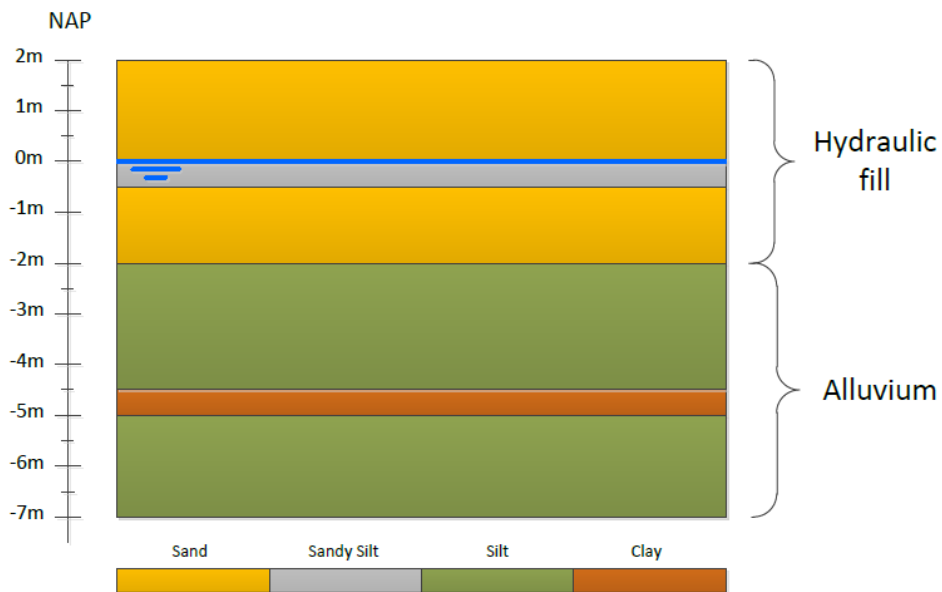


Figure 4.2 Soil layers Centrumeiland, Amsterdam

The total test area was split up into 15 different compartments e.g. test locations in which different tests were executed. At each test location the same type of elements were installed under different conditions to measure its influence on the penetration rate.



Figure 4.3 Local soil condition

## 4.2 Elements

During the field test different type of elements were tested:

- Closed tube vibroflot shape with a diameter of 300 mm
- Open tube vibroflot shape with a diameter of 300 mm
- Closed tube vibroflot shape with a diameter of 400 mm
- Open tube with a diameter of 800 mm
- Closed tube with a diameter of 800 mm

The 300mm and 400mm are 8 meters in length, the 800mm is 4 meters long. The vibroflot shape is characterized by two wings at the sides of the element. These wings prevent the element from rotating when it is drilled into the ground.



Figure 4.4 Open-ended element vibroflot shape 300mm

## 4.3 Tests

The field test was performed to test the capabilities of the crane setup to install elements in different soil conditions and the possibility to densify the surrounding soil. The method used for the installation of the elements was entirely new but based on the fundamentals of vibro-densification techniques, Chapter 3.

The different elements were installed with the help of high frequency vibrations (150-180 Hz). The closed 300 mm and 400 mm and the open 800 mm were also used to test to ability to densify the soil with the help of low frequency vibrations. When the elements reached depth a lower frequency vibration (+/- 40 Hz) was used to densify the surrounding soil. The frequency was kept constant for around 40 seconds.

In table Table 4.1 the different tests are shown. Each test was performed at a different test location. Some of the elements were also used to test the densification effect, these are indicated with a X.

**Table 4.1 Overview performed tests**

<b>Test nr.</b>	<b>Description</b>	<b>Densification</b>	<b>Test location</b>
<b>Test 1</b>	Closed 300 mm		1
<b>Test 2</b>	Closed 300 mm	X	8
<b>Test 3</b>	Open 300 mm		2
<b>Test 4</b>	Open 300 mm	X	5
<b>Test 5</b>	Closed 400 mm		3
<b>Test 6</b>	Closed 400 mm		10
<b>Test 9</b>	Open 800 mm		11
<b>Test 10</b>	Open 800 mm	X	13
<b>Test 11</b>	Open 800 mm	X	14
<b>Test 12</b>	Open 800 mm	X	4
<b>Test 13</b>	Open 800 mm	X	15
<b>Test 18</b>	Open 300 mm		6

#### **4.4 Conclusions**

The main conclusion from the field test is that the crane setup was not able to compact the soil. On the other hand, it shows great results in penetrating strong soil layers with cone resistances up to 40 MPa.

The SonicSampDrill vibrator generates vertical vibrations onto the element. The geophones show that the influence zone around the element is very small when vibrating both at high (>150 Hz) and low (+/- 40 Hz) frequency vibrations. The transformation of vertical to horizontal vibrations via shear forces at the sides was limited and made densification impossible. The limited transfer of vibrations can be appointed to the smooth surface of the elements and not using the optimal frequency for densification. A frequency of 15-20 Hz is more convenient for soil densification, see Chapter 3. Unfortunately, the sonic drill was not able to drill at these frequencies due to resonance of the vibrator.

When vibrating at high frequencies (>150 Hz) the friction between the element and the surrounding soil decreases resulting in a reduction in resistance at the tip and sides of the element. Together with a large static load, applied by the crane, it was possible to rapidly insert several types of elements through hard soil.

Other important conclusions are:

At further distances from the vibrator both the acceleration as the velocity of the particles decreases. The geophone data shows minimal particle velocity in the surroundings. Low particle velocity is equivalent to less disturbance to the surroundings. The wave velocity at 5 meters distance from the vibrator during the installation of an element did not exceeded 2 mm/s in any of the tests.

The geophones measured higher frequency vibrations than what the SonicSampDrill vibrator is capable of according to the specifications. The highest frequency recorded was 180Hz.

The installation time of the elements reduces when more load is applied on to the elements. However the additional load on the elements caused instability of the crane leader. At some points the installation of the element had to be stopped to re-align the leader to secure straight insertion.

At some tests water was added to measure its influence. The addition of water at the tip of the element reduces the penetration time. However, the water flushes out the fines in the soil. The wash out of fines affects the soil characteristics locally and changes the soil characteristics. This can have negatively impact the future use of the area.

The time needed to vibrate an element of 8 meters length into the ground was relatively short in comparison to conventional drilling techniques, see reference project. Certainly, given that the first four meters of soil consist out of very hard soil layers. The open 300 mm elements reached depth in about 2 to 3 minutes and easily penetrate strong layers with a cone resistance up to 33 MPa. The insertion time for the closed version of the 300 mm tube is around 2-4 minutes. The element was able to penetrate a hard sandy soil layer with a peak value of 29 MPa without having problems.

The 300 mm closed-ended and open-ended have more or less the same penetration time. It is supposed that the equal penetration time is due closure of the tip by a soil plug. This results in an equal behaviour of an open and closed-ended element.

The closed 400 mm tube was vibrated into the ground within 5 to 7 minutes and penetrated soil layers with a cone resistance of 32 MPa. The 800 mm open-ended element was able to penetrate through a soil layer with a cone resistance of 30 MPa in 1-2 minutes. The crane was not able to drive the closed-ended 800 mm version into the soil. The large surface caused too much resistance against penetration.

More conclusions and detailed information about the field test can be found in Appendix A

#### 4.5 Recommendations

For a future testing program, I would recommend to apply the following proposals:

- Perform additional tests with different types of element. The influence of the end appearance on the installation time could not be clearly distinguished due to plug formation. Using larger diameter element will reduce the risk of plug formation. It is recommended to perform the additional tests on a more homogenous soil profile. This reduces the influence of side effects makes it easier to compare the different type of elements.
- Monitor more and more accurately the installation characteristics of the tests. The results show that the pull down load greatly affects the penetration time. It is of high interest to have a continues data log of the pull down load over time. In addition more information about the used vibration frequency will help to better understand the influence of the frequency on the drilling process. Additional monitoring such as pore pressure development will improve the knowledge about the soil response. The pore pressure development is highly dependent on the displacement amplitude. The displacement amplitude gives more insight in the stiffness of the soil. Together with the pore pressure development this enables better understanding of the degradation of shear resistance with increasing amount of loading cycles.
- To increase the penetration rate even further rotary action of the element might be used. The provided sonic vibrator can rotate with a torque of 10.000 Nm. The influence is not tested during the field test but might influence the penetration rate significantly. The rotary action can also reduce the risk of plug formation.

- The inertia effects play an important role in finding the most efficient type of element. The optimum mass/vibratory displacement ratio have to be found for this specific crane setup. Using the optimum mass results in larger displacement amplitude at equal energy consumption.
- More effort needs to be spend on the quantification of resistance at both the tip and shaft of the element. Measuring the degradation of penetration resistance, with increasing number of loading cycles, provides a better understanding of how phenomena as liquefaction and friction fatigue develop.
- Perform an extensive site investigation to obtain more detailed information about the soil characteristics. Identify the distribution of loose and dense sand and the permeability of the deposits. This will give more insight in the type of failure that is expected. Furthermore, the influence of fines on the potential of liquefaction needs further investigation. A grain size contribution of the local soil will contribute to this.
- The data from the geophone contains a lot of noise. Better installation of the apparatus will improve the measure data. The installation of geophones at different depth makes is possible to better distinguish pressure waves generated by the tip and the shaft of the element.
- Adapt the crane setup in order to make it able to compact the soil. There are two possibilities according to the literature study on vibro-densification methods. First, enable the vibrator to vibrate at frequencies of 15-20 Hz. Secondly equip the elements with an additional vibrator at the tip of the element. This vibrator should be able to transfer horizontal vibrations to the surrounding soil.
- The test results show minimal disturbance to the surroundings. When considering the installation of foundation elements close to existing structures this technique might be a better solution than existing installation techniques. Additional research has to be performed on the influence of the vibrations on neighbouring structures.

# 5

## Research questions

From the conclusions obtained by the field test more specified research questions are formulated. The field test results show that the crane setup was not able to densify the surrounding soil. Nevertheless, it achieved great success in penetrating strong layers of densely packed sand. Soil layers of almost 40 MPa were penetrated in a relatively short amount of time, especially when the installation time is compared to Punta Pacifica project illustrated in chapter 2.2. A high penetration rate is an important factor in finding a new method that is competitive with other deep compaction techniques.

At this moment there are only a limited number of tools available to help to estimate the pile and soil behaviour during vibratory driving at high frequencies. This thesis will investigate the process of pile driving intensively to gain more knowledge about the fundamentals of the vibratory driving and the environmental impact.

### 5.1 Objective & scope

The main goal of this research is to find a new deep compaction technique that is able to rapidly penetrate strong layers in order to reach the loosely packed soil. The field test results show that the newly designed crane setup was not able to densify the surrounding soil and therefore the densification process is omitted.

From this point on the research is more focussed on understanding the installation process rather than the densification process. The literature study on the vibro-densification together with the knowledge obtained in following chapters can be used to find a new compaction technique.

The following research question can be formulated:

***“What is the science behind the sonic drill technology and how does it improve the installation of elements?”***

In this research a mathematical model will be developed to be able to better understand the drilling process and to give answer to the formulated research question. The main research question is split up into sub-questions.

#### Theoretical concepts sonic of drilling

- what is the loading mechanism during sonic drilling?
- what is the soil response on dynamic loading?
- how does liquefaction influence the soil characteristics?
- how do the waves propagate in soil and element?
- what is the zone of influence for the vibrations?
- in what way is sonic drilling different than conventional drilling techniques?
- how do the initial stress conditions influence the pile driving?

- What are the main components that cause resistance against penetration?

### **Modelling pile installation**

- which parameters play a role in modelling the pile behaviour?
- what causes damping of the vibration?
- how do the results from the developed model differ from the field test data
- what is the maximum depth that can be reached using vibratory drilling?

### **Practical approach**

- in what way can the process be optimized?

## **5.2 Limitations**

Some of the approaches are simplified to be able to better deal with the problems.

The following aspects are not taken into account in this research:

- expansion of the drill pipe
- vibration drilling in rock
- group effects
- negative skin friction
- time effects

# 6

## Sonic drilling

To better understand the great success of the sonic drill technology in penetrating hard soil layers a literature study is performed. The entire system is split up in different components to better understand their individual influence on the drilling process. The process is approached by using the crane setup, used during the field test, as reference.

### 6.1 Introduction to sonic drilling

Sonic drilling is a vibration drilling technique that makes use of high frequency vibrations to penetrate soil and/or rock. Sonic drilling includes all drilling methods that use frequencies above 60 Hz. Frequencies between the 30 and 60 Hz are considered to be high frequencies and frequencies lower than 30 Hz fall within the low frequency range. Sonic drilling is very energy efficient and can be used in both dry and wet conditions. In wet conditions the technique takes advantage of the degradation of shear strength as result of cyclic loading. In dry conditions it uses its destructive power to make its way through soil or rock. The sonic drill is able to drill through boulders, consolidated materials and bedrock formations. Sonic drilling might be the solution to drill through hard soil layers to make the densification of deeper soil layers, with the help of another soil improvement technique, possible.

The sonic vibrator is used for various purposes. It is used to drill holes to create monitoring wells and pump installations. Beside that is also used for the installation of elements for foundations and retaining structures. The sonic drill technology can also be used for core recovery. It is capable in obtaining undisturbed soil samples from great depths.

This research focusses on the drilling performance in cohesionless granular soils. Especially cases where a strong soil layer overlays a loosely packed layer. To be able to compact the loose layer, with the help of a vibro-densification method, the stronger layer need to be penetrated first. The test results already showed that the sonic drill method is able to penetrate soil layers with a cone resistance of almost 40 MPa. The drilling process is considered to be very complex and is dependent on the loading/deformation rate of the drill, the density of the soil, the presence of water and soil characteristics such as mineralogy and grain size distribution.

The sonic drilling system consists out of three components; the vibrator, the resonator and the surrounding soil. The resonator in this case is a steel element which is vibrated during drilling. Each of the three components are influencing each other during the drilling process. Together with base unit this total system enables rapid penetration of various types of element through strong soil layers. To make the drilling as efficient as possible minimal energy should dissipate during the process.

#### 6.1.1 History

The first time vibrations were used for drilling was during the Roman empire. By using vibrations the Romans were able to overcome the earth's elastic resistance and

penetrate the soil (Lucon, 2013). It became clear that by increasing the amount of vibrations per time interval the penetration rate was increased. However, it was not possible to generate high frequency vibrations for many years. After the industrial revolution more machines were invented that were able to reach higher frequency vibrations. However, the fundamentals of drilling with 'high' frequency vibrations were not understood. In 1913 more research on sonic technology was performed by George Constantinesco from Romania (Janes, 2009). In the 1930's this research was used by Dr. Ion Basgan to apply sonic vibrations onto a drill pipe string. The result was a greater drilling depth and a higher penetration rate of the drill rig. At that moment this was a great leap forward in the drill rig industry. More companies saw the potential of drilling with high frequency vibrations and started doing their own research. In the 1940's the government of the USA became interested and started to develop their own sonic drilling technique. Initially the sonic drilling technique was mainly focused on speeding up the oil well drilling operations but was later used for other purposes. In the period of 1948 to 1959 Dr Albert G. Bodine worked together with Borg Warner on a new down hole vibrator. They named this new vibrator 'the sonic drill'. The vibrator uses rotating eccentric masses to generate vertical oscillating vibrations. This sonic drill vibrator was capable of reaching higher frequencies with an increase in peak force accelerations in comparison to existing methods. However, this extra energy caused some mechanical failures of the drilling components and was therefore not rated to be a success. In the 1960's Albert G. Bodine increased the performance and reliability of the equipment. Albert G. Bodine was the first to discover a method that is able to generate high frequency vibrations with a very high force output without destructing the machine. Several companies tried to refine the technology but the fundamental methodology is still kept secret by Albert G. Bodine. Together with more than 300 U.S. patents Albert G. Bodine is world leader on the topic of orboresonance (Lucon, 2013). All the rights of Bodine's inventions belong to the Resodyn Corporation. In the 1980's Hawker Siddely and Ray Roussy worked on the development of the sonic drill technology. However due to several setbacks Hawker Siddely decided to stop with working in the development of the technology. Ray Roussy continued to develop the technology for small diameter drilling with success. Nowadays there are 3 major sonic drill companies worldwide that deliver sonic drilling techniques: Sonic Drill group, Boart Longyear and Eijkelkamp SonicSampDrill.

### **Sonic Drill group**

The Sonic Drill Group consist out of the Sonic Drill Corp. and Sonic Drilling Ltd. At the moment Ray Roussy is president of the group. Sonic Drilling Ltd is based in British Columbia. Sonic Drilling Corp is based in Bellingham, Washington, US. The Sonic Drill Cooperation manufactures and supplies sonic drill heads, rigs and tooling.

### **Boart longyear**

Since the 1990's Boart Longyear became interested in the potential of sonic drilling technology. Boart longyear is based in Salt lake City, Utah, US and is one of the world's largest drilling contractors. Boart Longyear mainly focusses on the exploration of minerals around the world.

### **Eijkelkamp SonicSampDrill**

Royal Eijkelkamp SSD is a Dutch company established in 1911 and is based in Giesbeek, The Netherlands. Eijkelkamp started in 1996 with the research for an

innovative drilling technique. In 2006 Fons Eijkelkamp started with the manufacturing of sonic drilling equipment. The equipment is sold under the name SonicSampDrill.

Even though there has been great progress in the development of drilling technology the understanding of the principles behind the operation of sonic drilling is still not totally clear. There are no reliable guidelines available that makes it possible to estimate the driveability of a certain profile in to the ground with the help of sonic vibrations.

## 6.2 Sonic drilling process

The vibrations are mechanically generated by an oscillation of at least 2 rollers inside the vibrator. By combining the two rollers it is possible to create a centrifugal force. The rollers have to be exactly synchronized and counter rotating to ensure there will only be a movement in the vertical direction. The number of rotations per second determine the frequency of the vibration. The amount of repetitions per second can be found in the order of 0-180 oscillations per second for a sonic vibrator. The centrifugal force is dependent on the eccentric rotation ( $r$ ), the mass of the rollers ( $m$ ) and the rotation speed ( $\omega$ ) (Borrow, 1994).

$$F_{ecc} = m\omega^2r \quad (5)$$

In Figure 6.1 a cross section of a vibrator head is shown.

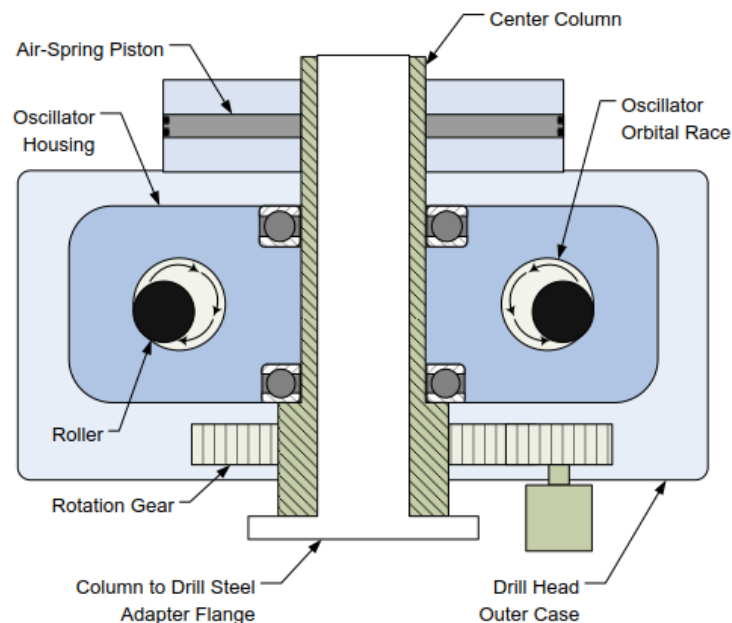
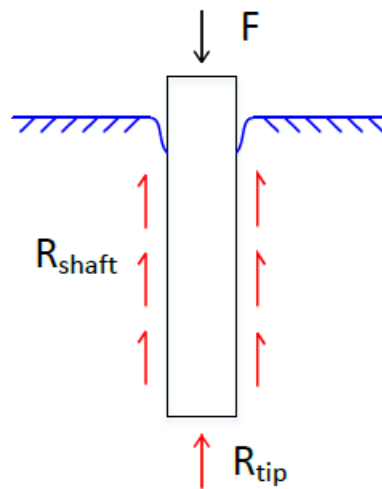


Figure 6.1 Cross section vibrator head (Lucon, 2013)

The back and forth movement of the vibrator is repeated periodically creating a sinusoidal compressive and expansive pressure wave on top of the element. The elasticity together with the inertial properties of the element allow pressure waves to propagate through the element. The waves cause the element to contract and expand over its length leading to a fast up and down movement of the element. The fast movement decreases the soil resistance at both the tip and sides of the element during penetration. The air spring piston on top of the vibrator makes sure there is limited transfer of vibrations to the crane. Some vibrators are provided with a rotation gear. This rotation gear enables the vibrator to rotate the element on its central axis.

The total resistance is the sum of the shaft and tip resistance. The decrease of soil resistance makes it possible for the element to easily penetrate through hard types of soil which would not be possible with monotonic loading.



**Figure 6.2 Resistance element**

The penetration of the element in the soil is the result of a net force pointing in downward direction,  $F > R_{\text{shaft}} + R_{\text{tip}}$ . The total force consists out of the dynamic force, the gravitational force and in some cases a static force applied by the crane. The sum of all these forces must be positive in downwards direction to enable penetration.

The frequency at which the energy transfer through the resonator is at its best can be found at the natural frequency of the steel element. At this particular frequency the steel element starts to resonate. At the natural frequency the element contracts and expands just like a spring and allows energy to be stored in the element resulting in a limited energy dissipation.

### 6.2.1 Resonance

The resonance frequency at which one wave travels through a steel element back and forth can be determined with the following formula (Borrow, 1994):

$$f_{res} = n \frac{v_{steel}}{2L} \quad (6)$$

The  $n$  indicates the number of vibrating nodes. For  $n$  is equal to 1 the system vibrates in a half wave mode. The maximum wave velocity in a steel element ( $v_{\text{steel}}$ ) can be found in the order of 5800 m/s.

During resonance the pressure wave inside the resonator appears to stand still. Each induced energy pulse wave is exactly superimposed on each reflected energy pulse wave. In this situation the direction and magnitude of movement of each individual steel molecule, with respect to other molecules, stay the same, Figure 6.1 (Borrow, 1994). By repeatedly pulling and pushing at the top of the element more energy is built up resulting in an increase of the wave amplitude. The build-up of extra energy enhances the penetrate rate of the system as there will be more energy available to penetrate the soil. The moment the element penetrates the soil the available energy reduces and the

natural frequency changes. To keep the acceleration of the element the same the frequency needs to be adjusted to maintain resonance.

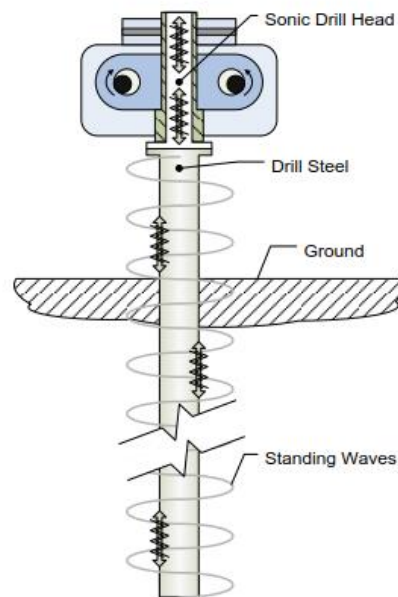


Figure 6.3 Sonic drill in resonance condition (Lucon, 2013)

One should be careful with the build-up of energy. If there is no release of energy the amount of energy becomes so high that the vibration starts to get out of control. This can lead to failure of the element and other parts of the system.

### 6.2.2 Energy transfer

The penetration rate is highly dependent on the amount of vibratory energy, produced by the vibrator, that reaches the tip of the drill string. The amount of energy that is transported by the wave is proportional to the square of the amplitude of the wave. A decrease of the amplitude by a factor two causes the energy to decrease by a factor four. As the pressure waves travel away from the source (vibrator) some of the energy starts to dissipate resulting in a decrease of force amplitude. The decrease in amplitude is also known as the decay. In literature three different types of decay are classified (Voznesensky, et al., 2011)

#### 1. Scattering on obstacles

The pressure waves are scattered on obstacles with different compressibility and density.

Occurs during the transmission of energy from the element to the surrounding soil and between different soil types.

#### 2. Radiation

The energy is spread over an increasing area. Resulting in a decrease of specific energy per unit area.

#### 3. Proper damping

The dissipation of energy due to plastic and nonlinear elastic deformations and in creating heat.

Most of the generated energy by the vibrator is lost due friction and internal mechanisms in the soil. The residual energy that reaches the tip of the element is used by the system to enable displacement. The contribution of the vibration frequency on the soil damping is not well understood but seems to increase the damping as the frequency increases. Voznesensky et al. performed tests at low frequencies and found that the amount of damping grows linearly with the frequency (Voznesensky, et al., 2011).

### **6.2.2.1 Cyclic loading**

Cyclic loading enables the element to penetrate hard types of soil. The driving force behind vibratory drilling in saturated soils is an applied force greater than the resisting force and the reduction of the soil resistance. The resistance is reduced by various processes. As the element vibrates at high frequencies the high acceleration impedes the soil particles to stick onto the element resulting to a reduction in shaft resistance. This inertial effect reaches its maximum at around 1.5g. During cyclic loading excess pore water pressure develops and causes a degradation of the shear resistance of the soil close to the element. This phenomenon is later explained as liquefaction and mainly occurs around the tip of the element. Other mechanisms, both temporary and long term, such as grain crushing and the decrease of horizontal stress (friction fatigue) do also contribute to the reduction of soil resistance. These mechanisms can be found at respectively the tip and along the shaft of the element.

### **6.2.2.2 Liquefaction**

Liquefaction is the loss of strength in cohesionless soils due to a decrease in effective stress as result of an increase in pore water pressure. The soil, surrounding the tip, becomes cyclically loaded when the resonator vibrates. The vibrations cause cyclic shear stresses to develop in the vicinity of the element. The applied stress makes the soil skeleton want to change in a denser configuration. The volume reduction can be triggered by rearrangement of the grains or by grain crushing. The volume reduction is prevented by the water in the pores. The rapid loading does not give the water enough time to fully dissipate, resulting in a gradually increase of the pore water pressure. The soil starts to behave partially undrained resulting in a temporary development of local excess water pressure in the pores. As the EPP increases the effective stress decreases and the soil resistance reduces, equation 1. The development of EPP increases with every loading cycle resulting in further decrease of soil resistance over time. The decrease in resistance after cyclically loading of the soil is known as the degradation.

The buildup of pore water pressure is often described by Skempton:

$$\Delta u = B[\Delta\sigma_3 + A(\Delta\sigma_1 - \Delta\sigma_3)] \quad (7)$$

The parameters A and B are known as pore pressure coefficients and describe to amount of pore pressure that is developed when deviatoric stress is applied. The values can be determined by undrained Triaxial tests (Skempton, 1948). The relation does not take the influence of rapid cyclic loading into account.

In the last decades more and more research has been conducted on the cyclic loading behavior of soil during earthquakes. This loading behavior is similar as what can be seen at vibratory drilling, despite the fact that at earthquakes the loading mechanism occurs at much lower frequencies. In the past multiple cyclic tests were performed to obtain more

knowledge about the soil response at low frequency loading. Low frequencies are considered within the earthquake range 0.1-2.0 Hz.

The different tests show that the soil response is considered to be very complex and dependent on several factors. The main factors are explained here.

#### 1. Strain/stress amplitude

The strain amplitude is the greatest influencer of the development of EPP. Several studies have been performed on the influence of strain amplitude on the development of EPP. In general, the larger the shear strain/stress amplitude the faster the development of EPP (DU & Chian, 2015) & (Rodger & Littlejohn, 1980). On the other hand, there is an optimal shear displacement amplitude at which the energy to develop liquefaction is at its minimum. Larger strain amplitudes may even counteract to the development of excess pore water pressure. At larger strains certain types of soil can undergo a phase transformation. The pore pressure starts to decrease due to dilatancy effects of the soil. This phenomenon especially plays a role when medium to dense sands are cyclically loaded.

In 1968 Thiers and Seed performed several cyclic direct simple shear tests under strain-controlled conditions to measure the degradation of the shear modulus at undrained conditions. The results show that the shear modulus was reduced by 50% to 80% when the strain amplitude of the cyclic loading was increased from 0,5% to 2%. The results do also show that increasing the strain amplitude above 2% does not result in a further reduction of the shear modulus. The largest reduction of the shear modulus can be found within the first 50 load cycles (Thiers & Seed, 1968)

#### 2. Cyclic frequency

The knowledge about the influence of the cyclic loading frequency on the development of EPP is still limited. Sassa et al. performed different ring shear tests on a very loose soil to investigate the influence of the loading frequency on the development of excess pore water pressure on sands (Sassa, et al., 2005). Frequencies of shear loading were varied between the 0.01 and 2.00 Hz. As the loading frequency increases the number of cycles needed to develop liquefaction increases and the total shear displacement reduces with increasing frequency. Nevertheless, the time needed to obtain full liquefaction reduces at higher frequencies.

Dash et. al investigated the influence of the frequency on liquefaction and dynamic properties of the saturated sand on a denser type of soil. He observed that the rate of generation of pore water pressure increases with frequency (Dash & Sitharam, 2016). At higher frequencies less cycles are needed to develop liquefaction.

The relative density seems to be an important factor in how the excess pore water pressure develops at increasing loading frequency. In both cases the increase of frequency seems to have a positive effect on the development of liquefaction per unit of time.

All of these tests were conducted at very low frequency vibrations,  $f < 2\text{Hz}$ . Most advantage of the higher cyclic load frequency is probably obtained in the frequency range  $0 \rightarrow 50\text{Hz}$ . The additional benefit in generating EPP at very high frequencies is limited. The added value of high frequency vibrations is found in other processes than the development of EPP, especially when considering low depth applications.

### 3. Initial effective stress

Full liquefaction occurs when the EPP becomes equal to the current effective stress. The larger the depth the higher the effective stress that needs to be taken over by the water. S. Du and S.C. Chian performed several cyclic triaxial tests at different confining pressures. The results show that as the applied confining pressure increases the number of cycles to obtain full liquefaction increases (DU & Chian, 2015).

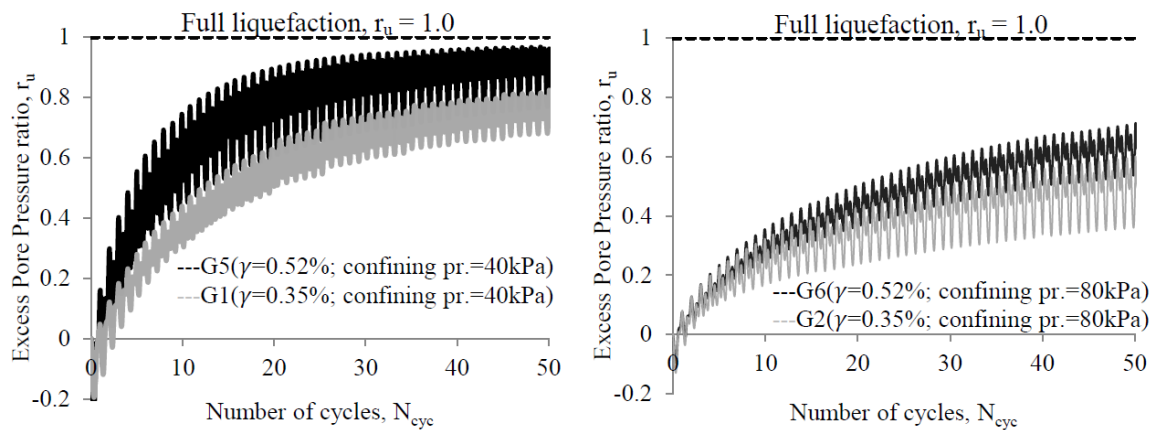


Figure 6.4 Influence confining pressure on development pore pressure ratio (DU & Chian, 2015)

- Number of cycles

Cyclic loading of the element results in the development of cyclic shear stresses in the soil. These cyclic shear stresses cause a generation of EPP. The larger the number of cycles the larger the generation of excess pore water pressure. As the loading frequency increases the number of loading cycles per unit of time increases.

#### 6.2.2.2.1 Types of liquefaction

The response of the soil on cyclic loading is dependent on the different soil characteristics and the confining stress. As the soil is extensively loaded it tends to contract (red) or dilate (green), Figure 6.5.

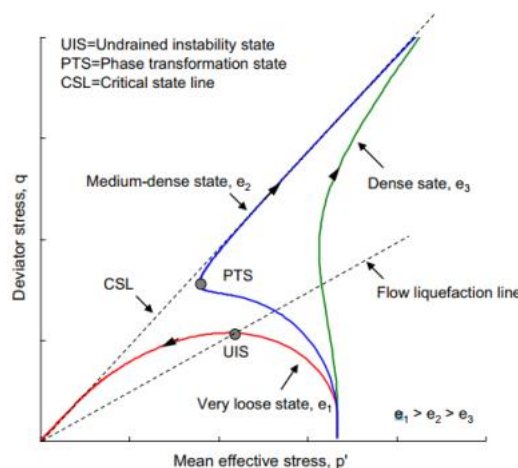
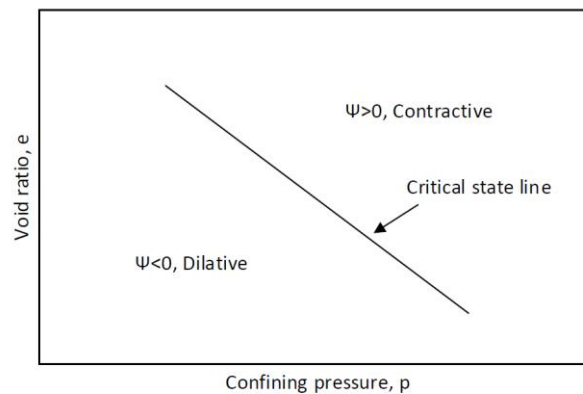


Figure 6.5 Undrained shear response (Yang, et al., 2015)

The blue line shows the intermediate response where both contraction and dilatation of the soil occurs at different stages on the stress path.

If the soil contracts or dilates during loading depends on both the void ratio and the initial effective stress. The critical state line (CSL) depicts the conditions when there is no volume change during shearing. Below the CSL the soil shows dilatant behavior and

above the CSL the soil contracts. The type of behavior is often indicated with the state parameter  $\psi$ . The state parameter is equal to the current void ratio minus the critical state void ratio.



**Figure 6.6 Schematic view soil behavior**

Considering undrained conditions, a contraction of the soil directly results in an increase of EPP. As the pore water pressure increases the strain amplitude increases and the rate of the pore water pressure development increases progressively.

In literature two main types of phenomena that can induce liquefaction can be recognized:

- Flow liquefaction
- Cyclic mobility

The different phenomena are explained with the help of illustration obtained by cyclic Triaxial tests.

**Flow liquefaction** is the consequence of dynamic loading of loose and sensitive types of soil. As soon as the soil is subjected to additional loads it wants to change its structure in a denser configuration. The volume change is prevented by the water in the pore resulting in an increase of pore water pressure (Berghe, 2001). At every load cycle the pore water pressure increases and the stiffness/strength of the soil decreases. This process is known as shear degradation.

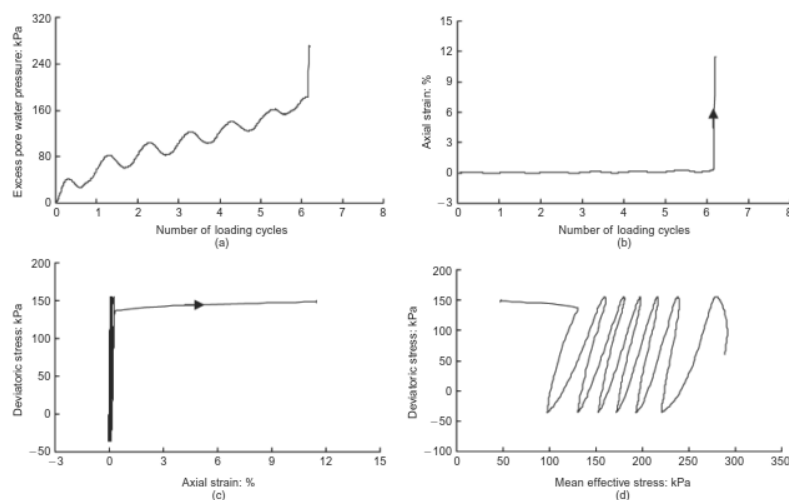


**Figure 6.7 Undrained response of loose sand under non-symmetrical cyclic loading ( $D_r=10\%$ ,  $\sigma'_{nc}=300\text{kPa}$ ,  $q_{stat}=60$ ,  $q_{cyc}=95\text{kPa}$ )**

The moment the stress condition reaches the flow liquefaction line it loses a significant part of its effective stress, see Figure 6.6. The applied load does not influence the stress condition anymore. This point is characterized by a sudden loss of strength. Figure 6.7 illustrates the complete loss of strength after 7 load cycles. Large deformations may arise as the applied shear stress exceeds the residual strength of the soil. The residual strength is the resistance against sliding when the soil reaches its minimum effective stress. The residual resistance can be assigned to the intergranular friction between the grains. When flow liquefaction is engaged it cannot immediately be stopped. Only time allows the EPP to dissipate. Flow liquefaction leads to progressive failure of the soil and is not affected by stress reversal (Yang & Sze, 2011).

**Cyclic mobility** occurs when medium dense to dense sand is subjected to shear stresses. The soil does not fail as a result of flow liquefaction but due to a gradual accumulation of strains. As the soil is cyclically loaded the pore water pressure increases progressively resulting in net softening of the soil. The deformations stop as the cyclic loading ceases because of dilation effects of the soil. Due to the dilatancy the soil recovers a substantial part of its effective stress and stiffness (Yang & Sze, 2011). This is not the case for flow liquefaction.

The behavior of the soil is highly dependent on the loading condition. If the soil is symmetrically loaded or not and if stress reversal occurs. Three types can be described:

1. Isotropically consolidated samples with stress reversal
2. Anisotropically consolidated samples with stress reversal
3. Anisotropically consolidated samples without stress reversal

The different types of response are further described in Appendix I.

Seed performed several tests on the cyclic behavior of cohesionless soils with different relative densities and suggested that for values of  $D_r$  larger than 0.45 the soil response is as described for cyclic mobility (Seed & Idriss, 1971). For lower values of the relative density it is more likely that the soil suffers from flow liquefaction.

#### 6.2.2.2.2 Threshold value

At very low values of strain the potential increase in pore water pressure is limited. Only as the strain exceeds a particular threshold value permanent volume changes and the development of EPP become of significant value. At strains below this value the soil behavior is considered to be linearly elastic and no hysteresis occurs. Hysteresis is known as the loss of energy due to non-elastic behavior. The threshold value is dependent on the over consolidation Ratio (OCR), initial stress state, plasticity index and the degree of saturation. The threshold value for strain can be found in the order of  $10^{-4}$  for most types of sand (Rascol, 2009). For clays the threshold value can be as low as  $10^{-5}$  (Diaz-Rodriguez & López-Molina, 2008). If this threshold value is exceeded a progressive decrease in shear modulus is produced.

#### 6.2.2.2.3 Excess pore pressure generation

The generation of excess pore water pressure is often expressed as the ratio between the developed excess pore water pressure and the initial effective stress. The development of excess pore water pressure by cyclic loading is predominately described

by empirical formulations. There are often large uncertainties in these empirical approaches but an analytical approach is still missing.

In the literature there are several methods to determine the pore pressure ratio as result of cyclic loading. Total liquefaction occurs when the pore pressure ratio becomes equal to 1. In the 1970's Seed B.H. et al. proposed an empirical formula to calculate the increase in excess pore water by the application of cyclic loading (Seed & Idriss, 1971):

$$r_u = \frac{u_{gen}}{\sigma'_{v0}} = \frac{1}{2} + \frac{1}{\pi} \sin^{-1} \left( 2 \left( \frac{N}{N_{liq}} \right)^{\frac{1}{\alpha_s}} - 1 \right) \quad (8)$$

Where N is the number of applied load cycles with equal strain amplitude and  $N_i$  is the required number of load cycles to obtain liquefaction at an equal stress amplitude. The value  $\alpha_s$  is an empirical value and is soil related. The value for  $\alpha_s$  is dependent on the soil properties and stress condition. Seed chose an average value for  $\alpha_s$  of 0.7 as an average curve for the behaviour for different soil properties and test conditions (Seed, et al., 1976).

The relation proposed by Seed assumes that the soil is initially subjected to hydrostatic and isotropic stress conditions.

The number of cycles to liquefaction can be determined with undrained cyclic Triaxial tests. A cyclic Triaxial test shows many similarities with the stress conditions during vibratory pile driving. Rahman et al. came up with an empirical relationship to obtain the cycles to liquefaction (Rahman & Jaber, 1986) & (Faccioli, 1972).

$$N_{liq} = \left( \frac{\tau}{\frac{\sigma'_{v0}}{aD_r}} \right)^{-\frac{1}{b}} \quad (9)$$

The ratio  $\tau/\sigma'_{v0}$  is also known as the cyclic stress ratio (CSR),  $D_r$  the relative density and a and b are empirical parameters that soil dependent. Typical values of the parameters are  $a=0.48$  and  $b=0.2$  for sands.

For triaxial conditions the CSR can be determined by using the deviatoric stress and the effective normal stress on the 45° plane.

$$CSR = \frac{q_{cyc}}{2\sigma'_n} \quad (10)$$

The effective normal stress on the 45° plane at Triaxial test conditions is equal to  $p' + q_{st}/6$  (Yang & Sze, 2011).

Several researches tried to make the empirical relation proposed by Seed more dependent on the different soil characteristics (Tokimatsu & Yoshimi, 1983), (Chern & Chang, 1995) (Chang, et al., 1983) and (Booker, et al., 1976). Chang et al tried to improve the relation to make is applicable for anisotropic stress situations. Other researches tried to take the residual strength of the soil into account and to estimate the development of pore water pressure in cohesive types of soil (Berghe, 2001) Appendix H. These correlations might have better results at specific soil conditions.

#### 6.2.2.2.4 Shear Modulus degradation

The increase of the pore water pressure decreases the shear modulus of the soil. F Arduino et al. proposed a relation between the pore pressure ratio and the shear modulus for contractive types of soils as sand (Arduino, et al., 2014).

$$G_{deg} = G_0 \sqrt{1 - r_u} \quad (11)$$

$G_{m0}$  is the initial stiffness

This relatively simple relation can be used to quickly estimate the stiffness reduction caused by an increase in pore water pressure. In Figure 6.8 the degradation of the shear modulus is illustrated. Increasing numbers of load cycles cause the hysteresis loop to rotate clockwise. The gradient of the backbone curve is approached by the square root in formula 11.

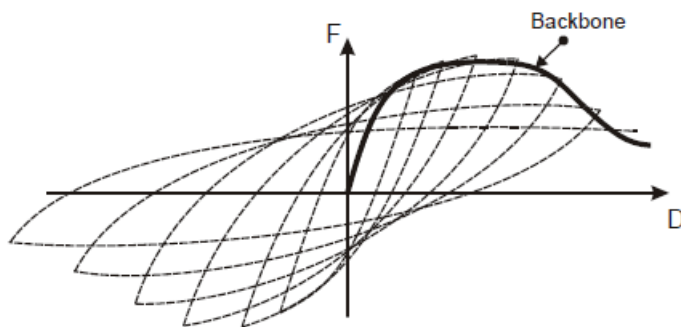


Figure 6.8 Degradation shear modulus after N load cycles (Abel, 2014)

#### 6.2.2.3 Other factors influencing the shear strength reduction

At the sides of the element other mechanisms play a role in the degradation of the shear resistance. Several laboratory tests show a reduction of shear stress when shearing air dried granular soils, Barkan (1962), Bernhard (1967), O'Neill and Vipulanandan(1989), and Viking (1998). This indicates that the increase in pore water pressure is not the primary factor for shear stress degradation.

Especially at the sides of the element this shear degradation mechanism is from significant contribution to the reduction in shear resistance. The maximum shear stress at which granular soil fails can be determined using Mohr Coulomb.

$$\tau_f = \sigma'_n \tan \delta \quad (12)$$

Where  $\tau_{sf}$  is the resistance at failure  $\sigma'_{rf}$  the normal effective stress acting on the shaft and  $\delta$  mobilized friction angle between the shaft and the surrounding soil. The friction angle is dependent on the pile shaft roughness and on the grain size. The normal stress acting on the shaft is a certain percentage of the effective vertical stress. For sandy soils the horizontal effective stress is around 30% of the vertical effective stress. The effect of the vertical effective stress on the shear resistance is limited up to a certain value (White, 2009). The normal effective stress acting on the shaft determines the shear resistance between the element and soil. During rapid cyclic loading the resistance decreases due to a phenomenon known as friction fatigue. The reduction of resistance due friction

fatigue can be up to 90% for soil displacement piles with respect to the initial resistance at full insertion (Verbeek, et al., 2005).

### 6.2.2.3.1 Friction fatigue

When vibrating the element in the soil Inertial forces are developed. As the vibration acceleration exceeds 1-1.5g, the soil particles at the sides of the element start to experience a free fall (Viking, 2002). The reduction of vertical confining stress allows the soil, close the element, to densify gradually with every loading cycle. The local densification results in a decrease of horizontal stress acting on the pile shaft. The net reduction of volume is observed at both loose and dense sands. The amount of compressibility in the shear zone is dependent on the packing of the soil, stress state and the mobilized friction angle. The shear resistance between the element and soil decreases gradually with increasing number of displacement cycles. The maximum degradation is limited to a certain value and is highly dependent on the mobilized friction angle.

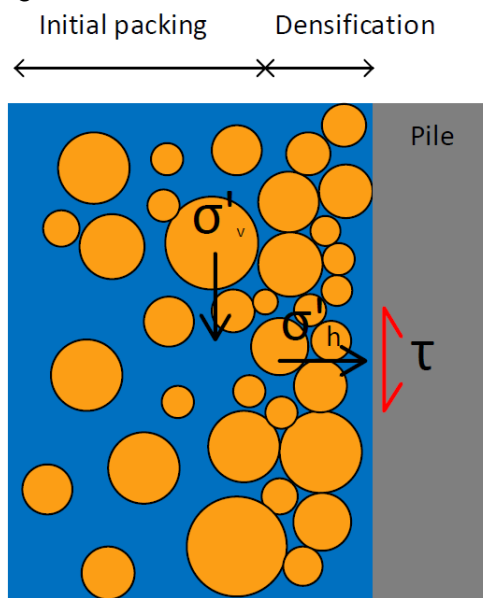


Figure 6.9 Illustration soil fatigue

D.J. White investigated several laboratory tests and concluded that the shaft resistance in carbonate sands can drop by around 75 percent of its peak value after 10000 cycles (White, 2009). Verbeek et al. came up with a fatigue factor to determine the soil resistance reduction along a pile shaft at failure. By multiplying the fatigue factor with the maximum shear resistance at the start one is able to determine the resistance after an infinite number of load cycles.

$$\tau_{max} = \tau_{f,0} \cdot r_f \quad (13)$$

Table 6.1 Fatigue factors according to Verbeek et al.

Type of soil	Fatigue factor, $r_f$
Round Coarse Sand	0.10
Soft Loam/Marl, Soft Loess, Stiff Silt	0.12
Round Medium Sand, Round Gravel	0.15
Fine Angular Gravel, Angular Loam, Angular Loess	0.18
Round Fine Sand	0.20

<b>Angular Sand, Coarse Gravel</b>	0.25
<b>Angular/Dry Fine Sand</b>	0.35
<b>Marl, Stiff/Very Stiff Clay</b>	0.40

One should be aware of the fact that these numbers are obtained using vibratory drivers at a frequency of 20-40Hz and are only applicable for closed-ended type of elements. For open-ended elements the reduction is less due to lower radial displacement of the soil (White, 2009). At the moment there are no results available from tests performed at higher frequencies. At higher frequency vibrations it is expected that the mobilized friction angle drops even further resulting in an even smaller shear resistance between the element and the soil. The reduction in horizontal stress would probably less at higher frequency as the transfer of shear waves through the soil skeleton becomes limited and therefore the densification in the vicinity of the elements becomes less.

The reduction becomes more pronounced at large sliding displacements (Evgin & Fakharian, 2001). The reduction in maximum shear stress degrades faster when failure occurs than when no failure of the soil mass occurs. Large displacements enable crushing of the grains closely to the shaft. The pulverization of the soil particles decreases the friction angle between the soil and element and enhances the degradation of the shear resistance along the shaft even further.

The densification of the soil occurs only in close vicinity of the element. The densification of the soil requires a change in the configuration of the soil skeleton. The water present in the pores should be able to dissipate, this is only possible close to the element. Close to the element the water can be dissipated via the shaft. Behind the densification zone there might be a zone which experiences an increase in pore pressure. The water is not able to easily flow away when the soil is subjected to shear waves. The densified zone prevents any dissipation of EPP in the direction to the element. The zone where EPP can be found is considered to be limited. In 1994 Wang conducted pore-pressure measurements in combination with finite element analysis of vibratory-driven model piles (Wang, 1994). He found out that the increase of excess pore water pressure was far more significant close to the pile shaft than further away from the pile. There was a rapid decay of pore water pressure with increase radial distance from the vibrating shaft.

The reduced shear resistance between the element and the soil eventually reduces the transfer of shear waves to the surroundings. A large part of the transferred shear waves are damped by the local development of EPP. The minimal disturbance of sonic drilling to the surrounding also became clear from the field test results. The results show low particle velocities and accelerations at two and five meters radial distance, see Chapter 4 and Appendix J.

### **6.3 Parameters of influence**

The total system is broken down into different components to better understand the entire drill process. Each of the components influences the penetration rate to a different degree. The penetration rate is defined as the distance that the element travels into the ground per unit of time. A high penetration rate is preferred. Most of the time extra costs are involved when the drilling operation takes more time. The total system can be divided into 5 major components: The crane base unit, the crane leader, the Sonic vibrator, the element and the surrounding soil. Each of the components is further elaborated and its influence on the drilling process is explained. By optimizing each of the components the

total operation time can be further improved. Decreasing the drilling time is from high interest to be competitive with existing drilling techniques. The crane setup from the field test is used as a reference.

### **6.3.1 Crane base unit**

During the field tests a Caterpillar 336F L was used for the installation of different elements.

#### *Pull down force*

The static load created by the crane is essential for penetration. The crane is able to put a static load on the element of 9 á 10 tons. The larger the static load the higher the penetration rate, see test results Chapter 4. However larger loads increase the risk of instability during the drilling process.

#### *Maneuverability*

A project usually does not consist out of one drill hole. Big projects can have hundreds of drill locations or even more. These locations are spread over a large area. To save time and thus money it is of interest to reach each of the locations within a short amount of time. The type of crane determines the time needed to get from one location up to another. The time needed depends on the speed of the crane and the maneuverability. The maximum speed of the caterpillar 336F L is around 5 km/h which is equal to 1.3 m/s (Caterpillar, 2017). The crane is equipped with Caterpillar tracks which allows the vehicle to rotate around its central axis. Furthermore, with the Caterpillar tracks the crane is able to drive at difficult ground conditions.

### **6.3.2 Crane Leader**

Instead of using a normal crane leader a different type of leader was installed onto the crane. The sonic drill is mounted on the leader and can move up and downwards along the leader with the help of a hydraulic motor. The leader guides the element as it is pushed into the ground. The stability obtained by the leader significantly improves the penetration process.

#### *Pedestal of the leader*

The type of pedestal influences the stability of the leader and therefore the penetration rate of the installation of the elements. When the pedestal is directly placed onto ground surface there is a possibility that the pedestal of the leader sinks into the ground at soft soil conditions. A pedestal with a larger surface area can be used to spread to load over a larger area. During the test the pedestal was placed on a wooden board with an area of 2X4 m to reduce the load per unit area.

### **6.3.3 Sonic vibrator**

The LargeRotoSonic drill from the company Eijkelkamp SSD was used to generate a dynamic force onto the elements.

#### *Dynamic Force frequency*

The key element of the vibrator is to transfer as much as possible energy to the tip of the element and have a minimal amount of energy loss. At resonance no energy gets lost in re-mobilization of the pile resulting in less energy loss (Janes, 2009). Additionally, it is possible to store extra energy in the elastic properties of the pile.

The frequency is also of importance on the degradation of shear resistance of the soil. At higher frequencies the excess pore water pressure has less time to dissipate in between the impact forces resulting in a higher and faster increase in built up excess pore water pressure. Eventually leading to a larger degradation of shear resistance.

#### *Force amplitude*

The dynamic force of the sonic vibrator that was used during the field test was 227 kN. It generally applies that the greater the force the larger the strain amplitude for a constant stiffness. The amount of degradation of soil resistance is dependent on shear strain amplitude, relative density and the initial stress state (Berghe, 2001). The larger the strain amplitude the larger the built up of pore water pressure the larger the potential for liquefaction. For very large strain amplitudes (>3%) the pore water pressure built up becomes independent of the strain amplitude in loosely packed soil. In medium dense to dense soil large strain amplitudes might cause the soil to dilate and negatively influence the build-up of EPP, see cyclic mobility chapter 6.2.

#### *Inertial effects*

D.D. Barkan researched the influence of the vibratory acceleration on the frictional forces from the sandy soil (Barkan, 1963). Barkan discovered that the influence of the acceleration amplitude on the soil resistance measured on the lateral surface during extraction is bounded. At an acceleration of around 1-2 g the maximum reduction in friction resistance occurred for web sheet piles and U-shaped sheet piles. Higher values for the acceleration do not result in any further reduction of friction forces along the shaft. Therefore, the shaft friction seems to be independent of the frequency but very dependent on the acceleration of the vibrations. This is in agreement with the findings of K. Viking (Viking, 2002).

#### *Mass of sonic vibrator head*

The amount of energy that is transferred to the element by the sonic vibrator is highly dependent on the mass of the vibrator. As the mass increases the relative movement of the sonic vibrator compared to the element decreases. For an infinite heavy head, no energy is transferred to the drill system (Lucon, 2013). However, as the mass of the sonic drill head is reduced the driver oscillates with a higher amplitude resulting in more energy transmission at the same amount of input force. A certain mass of the head together with a certain frequency lead to the best energy transfer for a particular type of element at a certain depth.

### **6.3.4 Element**

The function of the element is to transfer vibrations from the vibrator to the tip of the element to enable penetration.

#### *Geometry*

Increasing the diameter of the element increases the interaction between the soil and the element resulting more resistance against penetration. The same is true for the roughness of the element. A rough interface between the soil and element enlarges the mobilized friction angle and eventually increases the friction between the soil and the element.

As the penetration of the element increases the resistance increases. More soil comes in contact with the shaft of the element. For closed-ended type of elements larger volumes have to be displaced resulting in greater resistance.

#### *Material*

Most of the time steel is used as drill string material. Steel has a high strength and can easily be manufactured in different shapes and sizes. During the vibration of the element energy is lost due to the development of heat. The dissipation of energy is accompanied by a decrease in amplitude of the pressure wave (Kramer, 1996).

#### *Mass of the element*

The same applies for the mass of the element as for the mass of the hydraulic head. Heavy elements reduce the transfer of energy and decrease the vibration amplitude. Nevertheless, the weight of the element does contribute to the static load that is needed to penetrate the soil, only in a lesser extent than the dynamic force. There is an optimum between the weight of the element and the displacement amplitude. The optimum is dependent on the element as on the power of the vibrator.

### **6.3.5 Soil**

The soil gives direct response to the applied vibrations. The soil properties at the location determine the possibility in inserting a certain type of element.

#### *Friction*

The type of soil significantly determines the penetration rate that can be obtained during insertion. High penetration rates can be achieved in soils with low strength such as clay and silt. These soil types offer little resistance against penetration. A dense sand gives more resistance at the pile tip and lowers the penetration rate significantly. The contribution of the shaft resistance is relatively small compared to the tip resistance when considering the penetration through hard soil. The role of the shaft resistance becomes more significant in soft soils than it is in strong types of soils. The shaft resistance accumulates during the drilling process while the tip resistance is only dependent on the soil resistance at the tip. The degree of shaft is dependent on the vertical effective stress and friction angle between the soil and element. The total resistance increases with depth due to an increase in effective stress.

In practice most of the time the friction angle between soil and steel is taken in the order of 2/3 of the internal friction angle of the soil. Laboratory tests show however that it can be as low as 50% and as high as 90% of the internal friction angle (Rinne, 1985) depending on the surface roughness of the element, density of the sand, rate of deformation, grain size and angularity and mineralogy. Using 2/3 times the internal friction angle is considered to be very conservative.

#### *Damping*

The soil damps the incoming cyclic load by means of hysteresis. Hysteresis is known as the loss of energy due to non-elastic behavior. Hysteresis is the phenomena that different stress-strain loops are formed during loading, unloading and reloading of the soil. Hysteresis is mainly the result of friction between the grains. The area within such a loop represents the dissipated of energy, Figure 6.10.

The moment the soil fails there is continuous plastic deformation without a significant increase/decrease in force. Plastic strain results in a direct loss of energy.

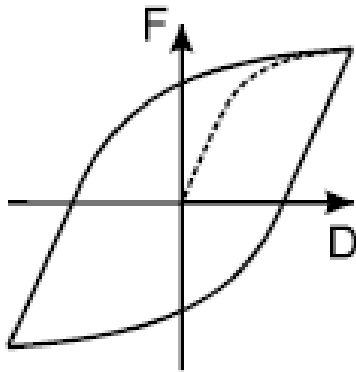


**Figure 6.10 Hysteresis loop (Abel, 2014)**

Hysteresis damping only occurs at above the linear cyclic threshold value, Chapter 6.2.2.2.2 . At very low strains the energy loss due hysteresis is minimal (Kramer, 1996). Above the threshold value the contribution of hysteresis to the energy loss becomes substantial. The threshold value is the strain that occurs at 70% percent of the small shear strain. Hysteresis is not frequency dependent and is proportional to the amount of strain. The larger the strain the larger the area within the hysteresis loops.

In saturated soils damping also occurs as result of viscous drag. Viscous drag is the flow of pore fluid relative to the soil skeleton. The viscous drag slows down the displacement. The amount of viscous damping is dependent on the velocity of the element. Another type of damping is breakage of soil particles. This type of damping is minimal with respect to the other two mechanisms.

The total amount of damping depends on the strain amplitude, void ratio, mean stress, plasticity index, overconsolidation ratio, moisture ratio, dispersity of the soil and the number of cycles applied (Berghe, 2001), (Brinkgreve, 2016) & (Voznesensky, et al., 2011).

#### *Soil conditions*

The degradation of soil resistance by means of creating EPP is highly dependent on the initial stress state. At a higher stress level more cycles are needed to degrade the soil resistance as there is more effective stress to overcome. The more cycles needed the more energy and time it cost. Large values for the void ratio influences the soil degradation positively. The higher the initial void ratio the larger the soil degradation (Berghe, 2001).

### 6.3.6 Degree of influence

Each of the components influence the penetration rate to a different the degree. Table 6.2 displays their relative influence.

Table 6.2 Degree of influence on penetration rate

Component	Type	Degree of influence
Crane	Pull down force	+++
	Manoeuvrability	+
Crane leader	Leader	++
	Pedestal	+
Sonic vibrator	Dynamic force frequency	++
	Force amplitude	+++
	Mass vibrator	+
Element	Material	+++
	Mass element	+
Soil	Friction	++
	Damping	++
	Soil conditions	+++

## 6.4 Wave propagation

To have more insight in the drilling process is it important to know how waves travel through the system. As the pressure waves travel through the element part of it is reflected, within the element, and part of it is transferred to the soil. The wave propagation in wet and dry soil is different (Hölscher, 1992). Especially the radial velocity of pressure waves in saturated soil is significantly less than it is in dry soil. Due to the water there is less friction between the grains and the element which reduces the amount of shear forces that can be transmitted.

To enable penetration of the element there should be plastic deformation of the soil underneath the pile tip. The zone of plastic deformation is in the same order as the zone of the increase pore water pressure (Hölscher, 1992). The influence zone is dependent on the void ratio, grains size and amplitude of the pressure wave.

### 6.4.1 Type of wave

When considering pressure waves in soil, two types of waves can be described: body waves (P-wave & S-wave) and Rayleigh waves. The particle motion of a Rayleigh wave is a combination of the particle movement of P and S-waves and does only affect the soil near the surface. Rayleigh waves are not further elaborated for the sake of the research.

#### *P-wave*

The P-wave is known as primary wave and produces areas of compression and extension in the soil when it propagates through the soil. P-waves have the highest propagation rate of all the different type of waves. The direction of the particle movement is parallel to the wave direction in which the wave is travelling (Kramer, 1996). Pressure waves are transferred by the element via compressional and extensional vibrating forces of the element.

The P-wave velocity in a certain medium is given by:

$$v_p = \sqrt{\frac{2G(1-\nu)}{\rho(1-2\nu)}} = \sqrt{\frac{E(1-\nu)}{\rho(1-2\nu)(1+\nu)}} \quad (14)$$

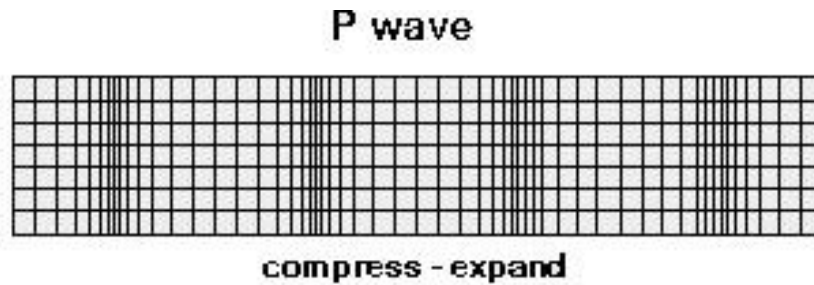


**Figure 6.11 P-wave**

*S-wave*

S-waves are known as secondary or transverse waves and produce shear stresses in the soil as they propagate. S-waves do not travel through liquids as liquids cannot sustain shear. The wave is transferred by the intergranular friction between the grains. The particle movement is perpendicular to the direction of the wave, resulting in shear stresses. Shear waves can only propagate through solids as liquids cannot sustain shear. The shear waves are transferred by the element via shear forces between the steel and the surrounding soil.

The S-wave velocity can be calculated with the following formula.

$$v_s = \sqrt{\frac{G}{\rho}} = \sqrt{\frac{E}{2\rho(1+\nu)}} \quad (15)$$

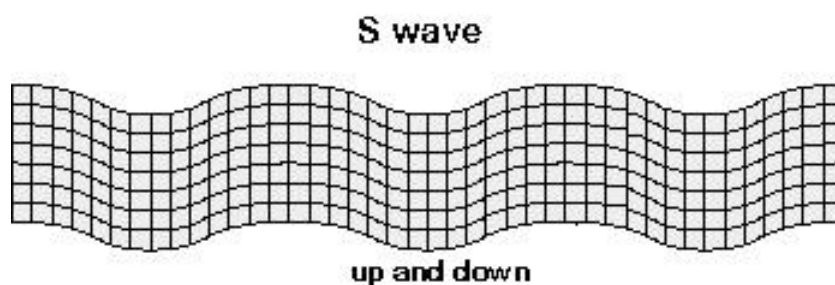


**Figure 6.12 S-wave**

In general the P-waves propagate faster than the S-waves. The P-waves cause volume changes in the soil whilst S-waves cause shear deformation of the soil. In case of vibrating the element in vertical direction, shear waves and compression waves propagate in a spherical wave front from the pile toe. At the sides of the pile mainly vertical shear waves are transmitted. The shear waves travel outwards over a conical wave front. The wave amplitude decreases with distance from the element due to mechanisms discussed in chapter 6.2.2.

The wave propagation of the body waves is illustrated in Figure 6.13.

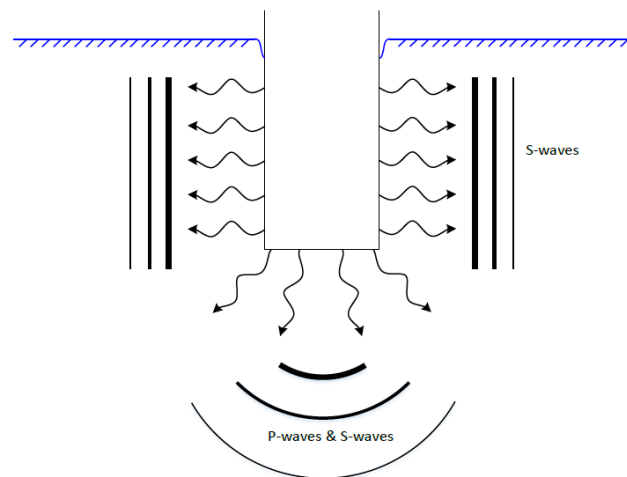


Figure 6.13 Wave propagation radiation damping (P-waves & S-waves)

### 6.4.2 Interfaces

As been explained energy is lost due to scattering of waves onto obstacles with different density and compressibility. This is especially the case during the transmission of energy from the element to the surrounding soil and between different soil types, e.g. clay and sand.

Let's consider for the sake of simplicity an element which is inserted into the ground and has only interaction with the soil at the tip of the element. A dynamic load is applied at the head of the element creating a compression-extension waves with a wave velocity  $v_p$ . The waves travel straight in a downward direction to the interface without transmission or reflection of the wave, assuming that there is no loss of energy. As soon as the waves reach the tip-soil interface part the wave is transmitted and part of it becomes reflected. The amount transmission and reflection is dependent on the interaction of the pile with the soil particles and the characteristics of the soil and element.

The values of R and T indicate the degree of reflection and transmission of the pressure wave.

$$F_{reflected} = R \cdot F_{incoming} \quad (16)$$

$$G_{transmitted} = T \cdot F_{incoming} \quad (17)$$

The reflection and transmission of pressure waves is illustrated in Figure 6.14.

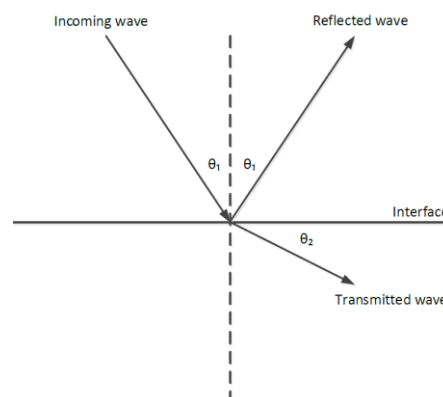


Figure 6.14 Wave reflection and transmission

### *Reflected wave*

When the wave strikes the boundary between the end of the steel element and the soil, part of the wave is reflected in opposite direction. In case that the wave strikes the boundary perpendicularly it becomes perfectly reflected in opposite direction (Kramer, 1996). The reflection coefficient of the magnitude of the wave velocity can be calculated with the following formula according to (Verruijt, 2008):

$$R_v = \frac{\rho_1 c_1 - \rho_2 c_2}{\rho_1 c_1 + \rho_2 c_2} \quad (18)$$

Where  $\rho_1$  is the density of the element,  $\rho_2$  the density of the soil. The values for  $c_1$  &  $c_2$  are the wave velocities for the respectively the element and the soil. Depending on requested results one could either calculate the reflected/transmitted p-wave ( $c=v_p$ ) or s-wave ( $c=v_s$ ).

The stress of the reflected wave changes sign, the incoming stress waves is reflected into tension waves. The reflection coefficient for the reflected stresses is given by equation 18.

$$R_\sigma = -\frac{\rho_1 c_1 - \rho_2 c_2}{\rho_1 c_1 + \rho_2 c_2} \quad (19)$$

### *Transmitted wave*

Part of the incoming wave is dispersed into the soil. The number of incoming waves that are transmitted is represent by the transmission coefficient T.

The transmission coefficient for the wave velocity is given by:

$$T_v = \frac{2\rho_1 c_1}{\rho_1 c_1 + \rho_2 c_2} \quad (20)$$

Magnitude of the wave stress is given by:

$$T_\sigma = \frac{2\rho_2 c_2}{\rho_1 c_1 + \rho_2 c_2} \quad (21)$$

In the perfect world there would not be any loss of energy due to reflected and transmission of the waves. However, this is not the case in reality. The wave amplitude decreases and becomes refracted. As results of inhomogeneity's and skewed interfaces part of the wave gets refracted. Refraction of the wave includes the change of direction when a wave hits an interface.

### **6.4.3 Scenario's**

In case of infinitely soft soil underneath the pile. The pile is able to move freely, resulting in  $R_v = 1$  and  $R_\sigma = -1$ . All of the incoming compression waves are reflected and turned into tension waves. The magnitude of the reflected wave is the same as for the incoming wave. No energy is lost.

When the soil becomes infinitely stiff then  $R_v = -1$  and  $R_\sigma = 1$ . The compression wave is entirely reflected as compressive wave. In between those extreme scenario's energy is lost.

### *Practice*

In practice energy is always lost. There is no such a thing as a perfectly reflected wave or a perfectly transmitted wave between the different media. In some cases, the reflected wave can even cause problems. When the soil underneath a pile is very soft than the situation occurs that tension waves are reflected onto the element. This does not form a problem for steel elements but could give some issues at installing concrete elements in soft layers. The concrete element might not able to withstand the tensile stress.

#### **6.4.4 Attenuation of wave amplitude**

As the pressure wave propagates through the soil the wave amplitude decreases due to damping mechanisms as radiation damping and proper damping as explained in Chapter 6.2.2. The pressure wave causes the soil particles to undergo a displacement. The further away from the source the smaller the acceleration/velocity/displacement amplitude of the particles. The amplitude largely determines the influence zone of the vibration. When the value for the amplitude becomes lower than a certain limit value the particle motion will not affect the surroundings. The SBR norm describes limits for different categories related to different type of constructions. The SBR norm is used in the Netherlands to describe the environmental impact of vibrations.

The attenuation for an arbitrary wave amplitude in soil is often described with formula 21 proposed by G. Bornitz (Bornitz, 1931).

$$w_2 = w_1 \left( \frac{r_1}{r_2} \right)^n e^{-\alpha_d(r_2-r_1)} \quad (22)$$

Values  $w_1$  and  $w_2$  are the vibration amplitudes at  $r_1$  and  $r_2$ ,  $n$  is the geometric damping coefficient and  $\alpha_d$  is a material damping coefficient. The value of  $\alpha_d$  depends on the loss factor  $\eta$ , the frequency of the wave and  $c$  the propagation velocity of the wave (Kim & Lee, 1999)

$$\alpha_d = \frac{\pi\eta f}{c} \quad (23)$$

The value of  $\eta$  is equal to zero for waves that propagates at the surface(surface waves) and 0.5 when considering waves in the subsurface (body waves). During the full scale tests, the geophone were installed at approximately 0.5m below ground surface. The relatively small depth made that the geophones only registered surface waves. Therefore, a value of  $\eta$  equal to zero is taken to describe the attenuation of the surface waves during the field test.

$$w = w_{\text{ref}} \left( \frac{r_{\text{ref}}}{r} \right)^n \quad (24)$$

The value for the exponent  $n$  is equal to 0.5 for surface waves according to Kim et al. (Kim & Lee, 1999).

The attenuation for the wave velocities in x,y and z direction for the field test at test location 5 are further elaborated. During pile driving the velocities in the different directions varied. Therefore, average values of the wave velocity at different radial distances are taken to illustrate the attenuation of the amplitude. A large reduction in wave velocity can be recognized in the first few meters of soil next to the vibrating element.

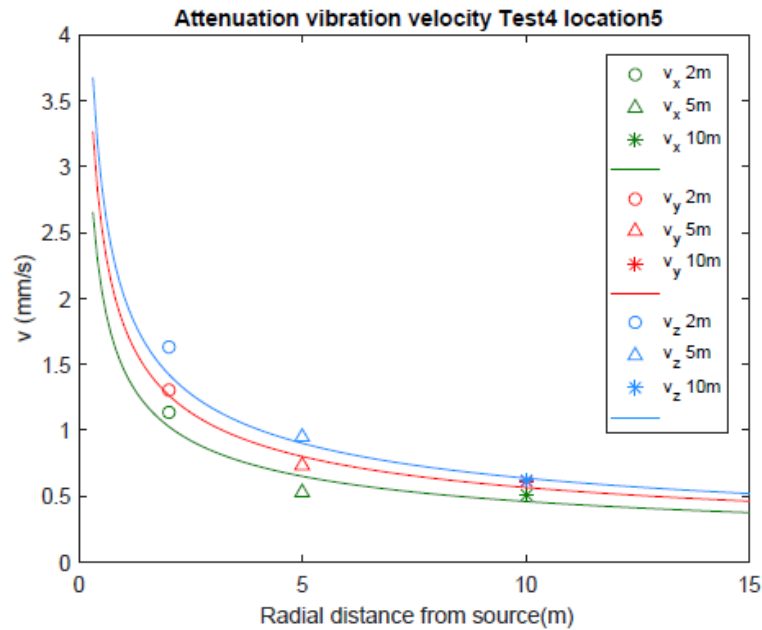


Figure 6.15 Attenuation vibration velocity test4 location5

In Appendix J the environmental impact of pressure waves from the field test are further elaborated using the limit value from the SBR norm and the threshold value proposed by Hergarden.

## 6.5 Recommendations

Considering the literature study on cyclic loading I would recommend additional research to the following topics:

- This research focusses on contractive soil behavior. Loose and dense soil will both suffer from liquefaction when cyclically loaded. Only the phenomena that induce liquefaction is considered to be different. The influence of vibrations on the dilative (very dense) soils needs to be further investigated. Dilatancy of the soil can have significant influence on the strengthening of the soil.
- The development of EPP at high frequency cyclic loading. The development of EPP is crucial for the determination of shear resistance. It seems that the EPP development is very dependent on the cyclic frequency, the initial effective stress, the stress/strain amplitude and the number of loading cycles. The influence of these processes is never been tested at high frequency vibrations. Extending the Triaxial testing program would contribute to a better understanding of the soil behavior under cyclic loading.
- The vibratory movement of the element cause liquefaction of the surrounding soil in the vicinity of the tip of the element. The excess pore water pressure decreases the strength and stiffness of the soil. The residual strength is mostly dependent on the initial effective stress and the amount of fines. Further investigation to the influence of the fine content on the development of EPP is needed.

- Voznesensky et al. found out that the amount of damping is frequency dependent in the low frequency zone (Voznesensky, et al., 2011). Further investigation is needed to validate this statement at higher frequencies.

# 7

## Modelling Sonic drilling

To be able to better understand the sonic drilling technique a mathematical model is developed. The model provides a better understanding of the dynamics of the sonic drill system. By better understanding the drilling process it is possible to further develop this technique and make it more applicable in the future. Furthermore, the model gives insight in the influence of different parameters on the penetration rate of the drill string.

### 7.1 Spring Mass model

A simple model is developed to analyse the influence of the surrounding soil on the penetration rate. The model is a simplification of the reality but gives a first insight in the drilling process. As the element becomes exposed to dynamic forces part of the energy is transferred to the elastic properties of the soil and part of it dissipates. The remainder energy is used to penetrate the soil.

The surrounding soil behaves as a Bingham viscoelastic viscoplastic material. The soil behaves viscoelastic until it reaches a certain yield stress. As the stress becomes greater than the yield stress it starts to have viscoplastic. The model is made out of a combination of a Kelvin-Voight and Maxwell bodies.

The model is presented in Figure 7.1 and has only one degree of freedom. The model consists out of a single mass combined with a spring  $k$  and two (Newtonian) dashpots  $c$  and a friction slider  $F$ . The different parameters describe the behaviour of the soil and do not tell anything about the dynamic response of the element itself. The element is considered to be a rigid body with no length. In Appendix B, a more detailed discretion of the model is given.

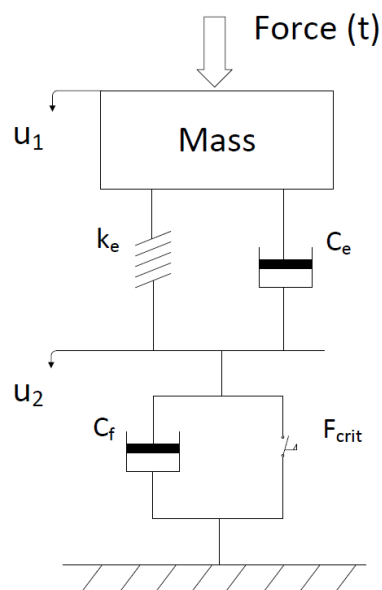


Figure 7.1 Simple mathematical model

## 7.2 Model components

Each of the components of the model features a specific part of the dynamics response of the element. The top half of the model mimics the elastic behaviour of the element in the ground while the bottom half simulates the plastic deformation of the soil and thus the penetration of the element.

### Mass

The mass indicated in the model is the sum of the weight of the element and the mass of the vibrator head.

### Force

The total force applied on the system consist out of a static part and a dynamic part and only acts in vertical direction. The static force is the sum of the pull down force applied by the crane and the gravitational force of the element. The gravitational force is the force acting on the mass and is dependent on the dimensions of element. As the crane places its crane leader onto the wooden footing it pulls down the element into the ground. The maximum pull down force of the crane is 100 kN. The dynamic force is generated by the sonic vibrator. The sonic vibrator transfers a sinusoidal force onto the element with a force amplitude of 227 kN. The dynamic force is time dependent and reaches its peak value 360 times per second when the vibration frequency equalizes 180 Hz.

The total vertical Force applied by the system on the pile is:

$$F(t) = F_{stat} + F_{ampl} \cdot \sin(\omega t) \quad (25)$$

$$F_{stat} = F_{grav} + F_{pd} \quad (26)$$

The sinusoidal Force applied on the element is illustrated in Figure 7.2

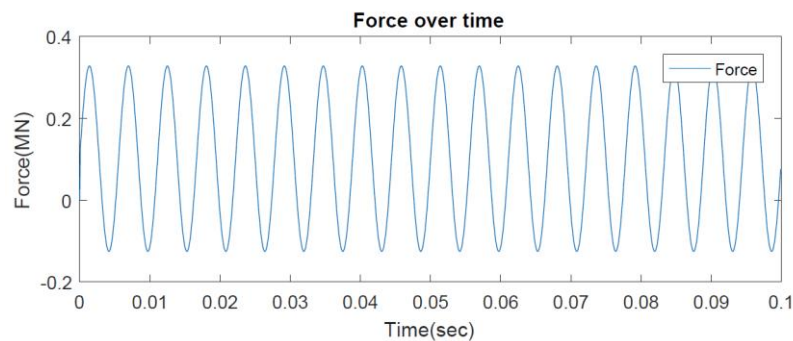


Figure 7.2 Applied force 180 Hz

Table 7.1 Forces acting in the system

$F_{pd}$ [kN]	$F_{stat}$ [kN]	$F_{ampl}$ [kN]	Ratio $F_{stat} / F_{ampl}$ [-]
40	5.23e+01	2.27e+2	0.23
60	7.19e+01	2.27e+2	0.32
80	9.15e+01	2.27e+2	0.40
100	1.11e+02	2.27e+2	0.49

### *Spring*

Part of the generated energy is stored elastically by the soil. The spring constant is denoted by  $k_e$ . The larger  $k_e$  the lower the elastic deformation of the surrounding soil, the stiffer the response.

### *Damper*

The total energy loss during the drilling process is a combination of different mechanisms as explained in chapter 6.2.2. In the model the energy dissipation is represented by viscous damping for mathematical convenience.

The damping in the system is denoted with  $c_e$  &  $c_f$ . The value for  $c_e$  describes the damping as a result of the vibratory movement of the element inside the soil,  $c_f$  describes the damping during the penetration of the soil.

### *Friction slider*

The frictional slider allows the displacement of  $u_2$  only when the applied force exceeds the critical force. From the moment  $u_2$  starts to move, the dashpot  $c_f$  becomes activated. The system is able to slide upwards as downwards, depending on the user's preference. The friction slider simulates the friction of the element with the surrounding soil. There are two types of friction, static friction and kinematic friction. The static friction is the critical resistance against sliding and mimics the resistance of the soil against penetration. As the applied force becomes greater than the static friction force the mass body starts undergo plastic displacement. The displacement of the system causes a decrease of friction force. The friction force during movement of the body is known as the kinematic friction force. The kinematic friction force is 70 % of the static friction.

$$F_{kin}^{fric} = 0,7 \cdot F_{static}^{fric} \quad (27)$$

## **7.3 Model conditions**

The model simulates the penetration of an element into the ground. On top of the mass a dynamic force is applied resulting in a harmonically movement of the mass in vertical direction. Part of the total applied force is directly transferred by the spring  $k_e$  and dashpot  $c_e$  to the second part of the model. As long as the applied force does not exceed the static resistance the model stays in stick condition and does not undergo plastic deformation. From the moment the applied force exceeds the critical force the status of the model changes into slip condition. In this condition the model starts to simulate the penetration of the element in the ground. The displacement of the pile in the ground is indicated by  $u_2$ . During the simulation two transition phases can be described: Stick to slip and slip to stick.

### *Stick to slip*

At  $t=0$  there is no displacement of any of the components of the model. The model is in stick condition. As long as the model is in stick condition the behaviour can be described with a Kelvin-Voigt model. The model stays in this condition until the applied force at the  $u_2$  exceeds the static resistance force. From the moment the applied force exceeds the static resistance the model starts to undergo plastic deformation at a certain velocity. As a consequence, the damper  $c_f$  is activated and the sliding resistance becomes the kinematic resistance. The model is in slip condition

### *Slip to stick*

The model returns from slip condition to stick condition when the velocity of  $u_2$  changes sign. In between that particular moment the velocity passes the zero velocity barrier. Zero velocity means no displacement and therefore the model returns to stick condition until the moment that the applied force exceeds again the static resistance force.

More information about the different model components can be found in appendix B.

## 7.4 Equations of motion

The governing equations can be derived from Newton's second law. Newton's second law states that the force acting on an object is in equilibrium with the product of the mass and its inherent acceleration.

By analysing the model displayed in Figure 7.1 the governing equations of motion can be derived. The over-dot notation indicates a time derivative.

### **Stick condition:**

During stick condition only the top half of the model is activated (Kelvin Voight model).

$$m\ddot{u}_1 + c_e(\dot{u}_1) + k_e(u_1 - u_2) = \text{Force}(t) \quad (28)$$

### **Slip condition:**

During slip condition both the top half as the bottom half of the model are activated (Kelvin Voight + Maxwell model). The following equations of motion can be derived:

Top half model

$$m\ddot{u}_1 + c_e(\dot{u}_1 - \dot{u}_2) + k_e(u_1 - u_2) = \text{Force}(t) \quad (29)$$

Bottom half model

$$c_e(\dot{u}_1 - \dot{u}_2) + k_e(u_1 - u_2) = c_f\dot{u}_2 + \text{sign}(\dot{u}_2) \cdot F_{kin}^{fric} \quad (30)$$

The friction during slip condition is present by the kinematic friction. The direction of the friction force should always be in opposite direction of the movement of  $u_2$ . The value of  $\text{sign}(\dot{u}_2)$  makes sure that this is the case.

## 7.5 ODE-Solver Matlab

Matlab is used to model the penetration of the element in the ground. Matlab is numerical computing program which allows fast and multi-scenario programming. The differential equations obtained in chapter 7.4 are solved by the ode45 solver. The ode (Ordinary Differential Equation) solvers are part of the Matlab software package and iteratively solve differential equations.

The ode45 calculates the values for  $u_1$  and  $u_2$  for each given time step. For this problem two sets of ode solvers need to be implemented. One for the stick condition and one for the slip condition. At every time step the model checks the condition of the model and activates the right ode solver.

## 7.6 Initial conditions

At  $t=0$  there is no displacement and velocity of  $u_1$  and  $u_2$ . This represents the situation of the pile hanging above ground surface. No force is applied to the soil at that particular moment.

As described in the previous chapter the model only allows displacement of  $u_2$  when the applied force exceeds the critical force. Depending on the values for the static and dynamic force it is possible to have both slip in upward and downward direction. For arbitrary values for the dampers and spring the following graph can be obtained when the model is allowed to slip both upwards and downwards.

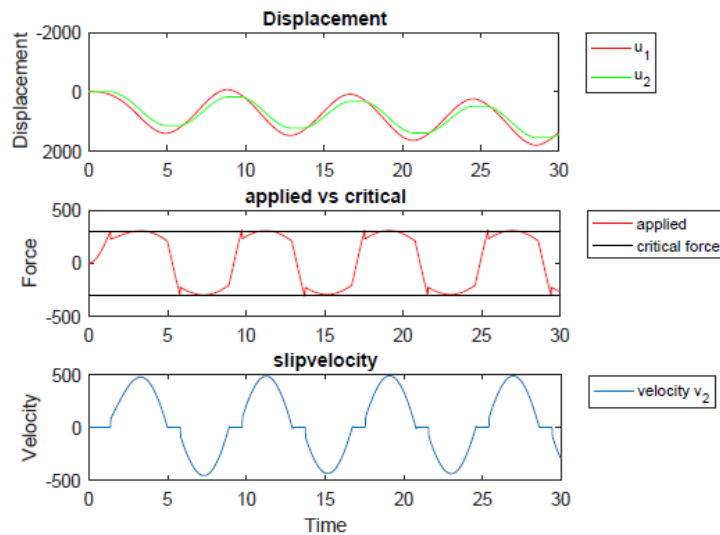


Figure 7.3 Upward slippage enabled

Every time the applied force becomes larger than the critical there is some displacement of  $x_2$ . The force pointing in downward direction is larger than resisting force in opposite direction resulting in a net penetration of the model. For certain circumstances there is only downward slippage possible. This might be the case when there is open connection between the element and the vibrator. An increase in penetration is visible because of the lack of upward slippage.

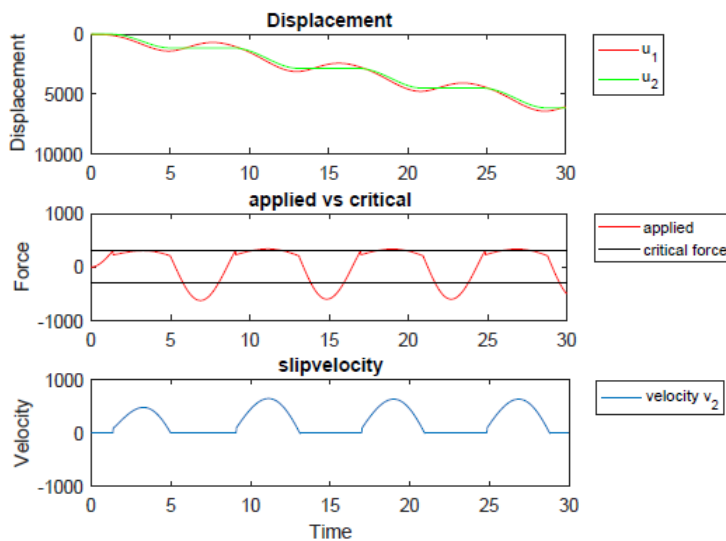


Figure 7.4 Upward slippage disabled

## 7.7 Sonic drill parameters

Parameters related to the soil properties have to be assigned to the different components of the model. As the element penetrates the soil it faces changing soil conditions. The model should be able to take this into account. The relations used to calculate the parameter values in the model are collected from different sources of literature and do not always fulfil the purpose of the model. The different relations are briefly explained in this chapter.

The relation for the spring stiffness and damping at the tip is proposed by Lysmer. Lysmer obtained the equations by simulating the behaviour of a rigid footing resting on a homogenous, isotropic and perfectly elastic half space. The response of the footing was approached for low frequency vibrations. The static spring constant per unit area for a rigid footing is given by (Lysmer, 1965):

$$k_t = \frac{4 \cdot G_s \cdot r_t}{(1 - \nu) \cdot A_t} \quad (31)$$

The damping underneath a rigid footing per unit area can be calculated with the following relation:

$$c_t = \frac{3.4 \cdot r_t^2 \cdot \sqrt{G_s \cdot \rho_s}}{(1 - \nu) \cdot A_t} \quad (32)$$

Warrington research the elastic behaviour and damping of the soil around a circular pile. The spring stiffness per unit area for the shaft is given by (Warrington, 1997):

$$k_s = \pi \cdot G_s \cdot \sqrt{\frac{r_g}{A_{sh}}} \quad (33)$$

The damping per unit area shaft is given by:

$$c_s = \sqrt{G_s \cdot \rho_s} \quad (34)$$

$r_g$  is the geometry ratio of the element. The ratio can be calculated by dividing the area of the pile  $A$  by the square of the pile perimeter  $P$ .

The damping and spring parameters along the shaft are given per unit area. This allows model to increase both these parameters with increasing penetration. As the penetration of the pile increases it faces different types of soil with different engineering properties. The values for the damping and spring stiffness at the tip should constantly be updated to be able to correctly simulate the soil conditions. The resistance at the shaft should accumulate to account for an increase of pile-soil interaction.

The different parameters are combined to fit the model characteristics. The resistance of the soil at the tip of the element greatly influences the penetration rate of the element. The tip resistance is processed in all of the components of the model.

At the start of the installation ( $t=0$ ) only the tip of the element causes resistance against penetration. As the element penetrates the soil the shaft resistance starts to contribute to the total resistance.

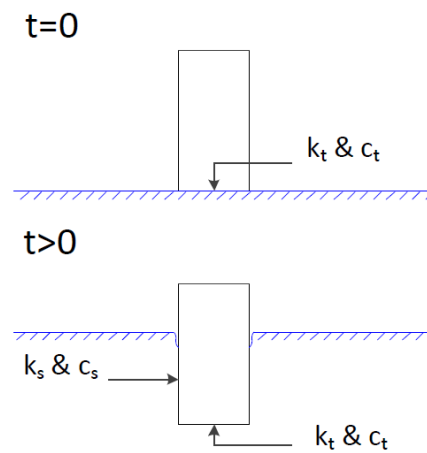


**Figure 7.5 Soil interaction**

At  $t=0$  both the values for  $k_s$  and  $c_s$  are equal to zero. The model uses the following formula's to simulate the element behaviour.

$$k = k_t \quad (35)$$

$$c_e = c_t \quad (36)$$

$$c_f = c_t \quad (37)$$

As the element starts to penetrate to soil for  $t>0$  the shaft resistance starts to contribute to the total resistance. The different component for  $t$  larger than 0 are described as followed.

$$k = \sum (k_s \cdot P \cdot \Delta u_2) + c_t \quad (38)$$

$$c_e = \sum (c_s \cdot P \cdot \Delta u_2) + c_t \quad (39)$$

$$c_f = c_t \quad (40)$$

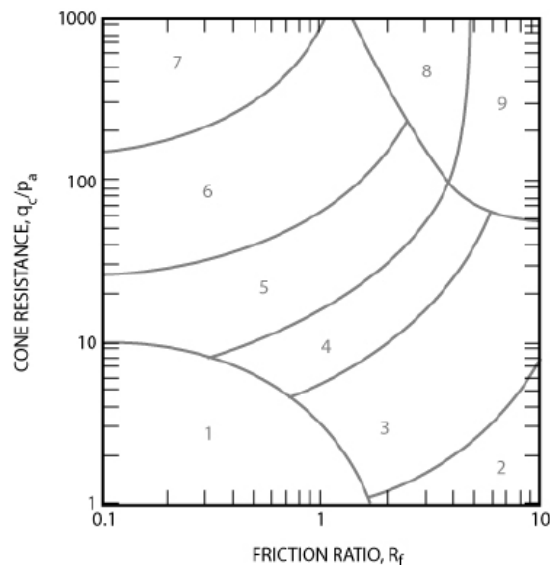
The damping during penetration of the element is solely dependent on the damping created at the tip.

## 7.8 CPT correlations

Correlations between CPT data and soil type/properties are used to define the model components. The model constantly determines the soil characteristics on basis of the cone resistance and friction ratio present belonging to the soil at the tip.

### 7.8.1 Soil type

The type of soil can be identified with the help of a soil index chart proposed by Robertson et al. (Robertson, et al., 1986). The chart uses the friction ratio  $R_f$  and the cone resistance  $q_c$  to identify the type of soil.



Zone	Soil Type
1	Sensitive fine grained
2	Organic soils – clay
3	Clay – silty clay to clay
4	Silt mixtures – clayey silt to silty clay
5	Sand mixtures – silty sand to sandy silt
6	Sands – clean sand to silty sand
7	Gravelly sand to dense sand
8	Very stiff sand to clayey sand*
9	Very stiff fine grained*

\*Heavily overconsolidated or cemented

Figure 7.6 SBT chart based on CPT cone resistance

### 7.8.2 E-modulus

Many researches tried to find a direct correlation between the cone resistance and the Young's Modulus  $E$ . The value for the Young's modulus is very sensitive to stress and strain history, aging and soil mineralogy and therefore difficult to estimate (Robertson, 2015).

A correlation that is used quite often to estimate the stiffness modulus using CPT data is as followed.

$$E = \alpha \cdot q_c \quad (41)$$

The value of  $\alpha$  can be found in the order of 2-5 depending on cone resistance. In general, low values for  $\alpha$  are used for strong types of soil and high values for soft types of soils.

Robertson came up with a more advanced method to determine the Young's modulus. The method is applicable for uncemented predominantly silica sands. The modulus has been defined as the stiffness that is mobilized at 0.1 % strain. The correlation does also take the vertical stress and friction ratio into account.

$$E = \alpha_E (q_c - \sigma_{vo}) \quad (42)$$

$$\alpha_E = 0.015(10^{0.55 \cdot I_c + 1.68}) \quad (43)$$

In case the vertical effective stress is in between 50 and 150 kPa then  $I_c \approx I_{SBT}$  (Robertson, 2010).

$$I_{SBT} = \sqrt{(3.47 - \log \frac{q_c}{p_a})^2 + (1.22 + \log R_f)^2} \quad (44)$$

The soil behaviour type contours are plotted on the SBT chart.

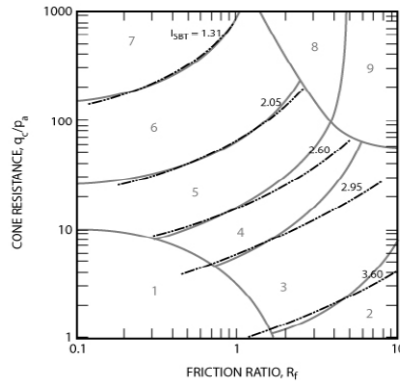


Figure 7.7 SBT chart showing  $I_{SBT}$  contours

The shear modulus can be obtain using the Young Modulus and the Poisson ratio.

$$G = \frac{E}{2(1 + \nu)} \quad (45)$$

### 7.8.3 Soil Unit Weight

An estimation of the unit weight of the soil can be obtained via the following formula (Robertson, 2010). The formula determines the ratio between the soil's unit weight and the unit weight of water. The value  $p_a$  stands for the atmospheric pressure and is equal to 100 kPa.

$$\frac{\gamma_s}{\gamma_w} = 0.27 \cdot \log R_f + 0.36 \cdot \log \frac{q_c}{p_a} + 1.236 \quad (46)$$

The soil unit weight per soil type is illustrated in Figure 7.8

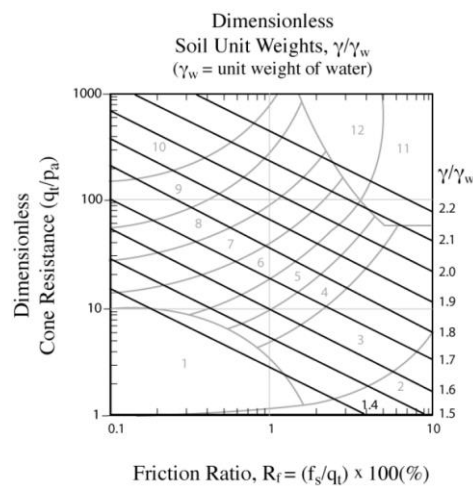


Figure 7.8 Soil Unit Weight SBT chart

### 7.8.4 Poisson ratio

The soil at the test field in Amsterdam is considered to be normally consolidated. Robertson found that most of the  $q_c/R_f$  points for a normally consolidated soil can be found in a certain region in the SBT chart (Robertson, 2010). By assuming that the soil is normally consolidated it is possible to define the soil type by using only the  $q_c$  or  $R_f$  value. The model makes use of this relationship and quantifies the soil type using the  $R_f$  value from the CPT data.

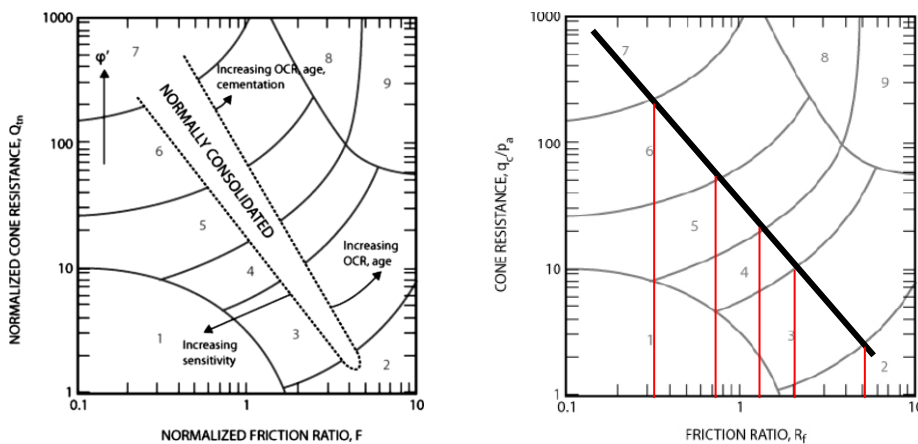


Figure 7.9 Identification soil type

Table 7.2 Soil type classification

SBT zone	Friction ratio $R_f$	Poisson ratio $\nu$	Soil type
7	0.1-0.33	0.3	Gravelly sand to dense sand
6	0.33-0.72	0.3	Sands – clean sand to silty sand
5	0.72-1.33	0.2	Sand mixtures – silty sand to sandy silt
4	1.33-2.00	0.4	Silt mixtures – clayey silt to silty clay
3	2.00-5.00	0.4	Clay – silty clay to clay
2	5.00-10.00	0.4	Organic soils – clay

Each of the SBT zone can be related to a particular type of soil. The Poisson is assumed to be constant at in every SBT zone.

## 7.9 Limitations of the model

The model is considered to be very simple. The dynamic response of the soil is far more complex than the model describes. By the knowing the limitations of the model one is able to develop the model in the future to make it more realistic. The limitations of the model are divided in different categories for clarity.

### 7.9.1 Spring Mass Model

#### *Ode solver*

The total simulation time is divided into small time intervals (time steps). For each time step the differential equations are solved iteratively. Within each time step Matlab creates multiple internal solutions. These internal solutions are not further considered.

The outcome of each time step forms the initial condition for the next time step. If the number of time steps is too low the results become less precise. The ‘incorrect’ solution is then used to calculate the displacement and velocity in the next time step. The error amplifies at every time step resulting in unsatisfying results.

The model simulates the installation of an element while vibrating at 180 Hz. Each second the dynamic load changes 360 times from direction. The times step should be sufficient small in order to follow the change in load. The higher the amount of time steps the more accurate the solution will be. On the other hand, increasing the number of time steps increases the computing time. The computing time is measured for different number of time steps per wavelength. One should be aware that the parallel tool in MATLAB is used to accelerate the calculation process. Without this tool the computing time would be even larger.

**Table 7.3 Computing time for different number of time steps**

No. time steps per wavelength	Calculation time
<3	No reliable results
3	+/- 4 min
5	+/- 10 min
10	+/- 25 min
100	+/- 600 min

The total number of calculations is the number of steps per wavelength times the applied vibration frequency and the total time span. When simulating a penetration time of 200 seconds at a vibration frequency of 180 Hz with 10 time steps per wave length, the total number of calculations is 360.000.

The influence of the number of time steps on the outcome is depicted in Figure 7.10. The lower the amount of time steps per wavelength the larger the penetration time. Results obtained with less than 3 time steps per wavelength are considered to be unreliable. In this case the sinusoidal behaviour of the load cannot be recognized.

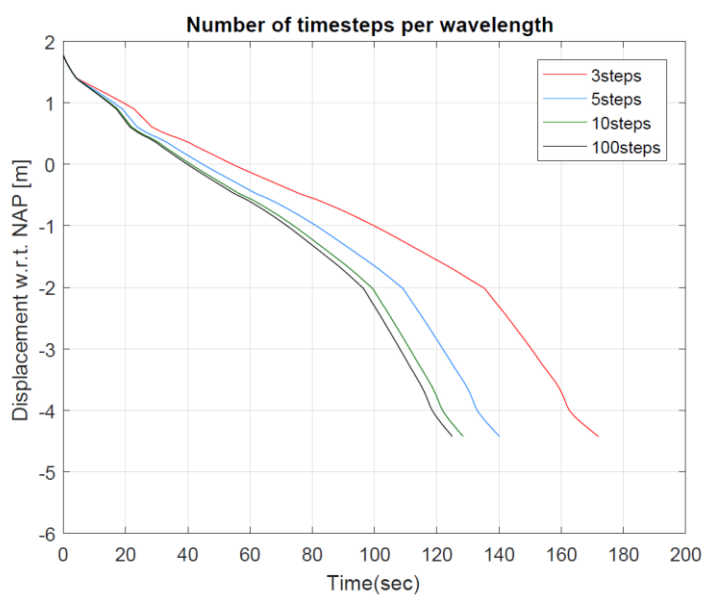


**Figure 7.10 Results for different number of steps per wavelength**

During this research a number of 10 time steps per wavelength is chosen to be accurate enough and within the preferred computing time. At each time step the dynamic load is obtained by the model and used to calculate the displacement and the velocity for the different components.

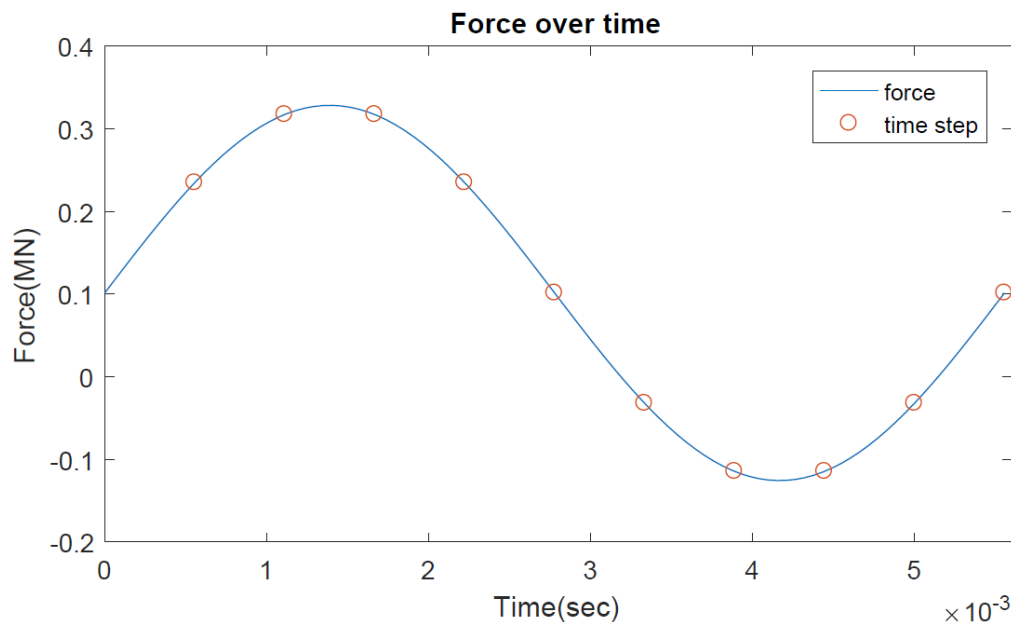


**Figure 7.11 Time step, 10 per wave length**

For each time step the ode solver gives as output the velocity and displacement for the different parts of the model. On basis of these values the applied force is calculated. The applied force together with the velocity  $v_2$  is needed to determine if the model is in slip or in stick condition, see Appendix B. A change in condition can only be implemented in the next time step therefore the model is always one time step too late when it changes from conditions. If the number of time steps is sufficient high the influence is limited

#### *One dimensional*

The model only takes the movement in vertical direction into account. The horizontal stress is not further elaborated but can have significant influence on the penetration process. Especially in overconsolidated clays there are large stresses in the horizontal plane. Large horizontal stresses increase the shaft friction and reduces the penetration rate.

#### *Constant parameters*

The model considers constant values for the vibration frequency and the static load throughout the installation process. However, during the field test these parameters were not kept constant all the time.

#### *Influence zone*

The resistance against penetration is determined by the soil properties directly underneath the pile tip. It is assumed that the resistance against penetration is not influenced by the soil above pile tip level.

In case of static loading the influence zone underneath the pile is considered to be within 4 and 7 times the diameter according the Koppejan method used in the NEN 9997-1.

The rapid changing dynamic load and penetration does not allow the load to be distributed over a large area. A length of two times the diameter is chosen to be more representative. The exact influence zone is not known and might deviate per soil type.

### 7.9.2 Element

#### *Element*

The element is considered to be a rigid body with no length. The loss of energy as result of internal mechanisms is not taken in to account.

#### *Damping*

The damping from internal mechanisms is not taken in to account. The damping in the element is considered to be very small compared to the soil damping and is therefore neglected (Novak, 1974).

#### *Roughness*

The model does not take the roughness of the element in consideration. The roughness of the outer surface influences the resistance against sliding through the soil. The model assumes that the interaction between the element and the soil is the same as the interaction between the soil particles itself. The resistance between the element and the surrounding soil is considered to be less. N.F. Rinne performed research on the mobilized friction angle between sand and steel and came to the conclusion that the mobilized friction angle lies between 50-90% of the internal friction angle (Rinne, 1985).

#### *Pressure waves*

The pressure waves travel with a certain velocity through the element depending on the type of material were its made off. The pressure waves are transmitted and reflected as they travel through the element. This influences the amount of energy that eventually reaches the tip of the element. The model assumes that the vibratory force at the tip is equal to the dynamic force generated by the vibrator. The model is not able to simulate the development of resonance in the element to maximize the energy transfer.

### 7.9.3 Crane

#### *Vibrator*

As the vibrator is activated it passes lower resonance frequency of the soil. The Low frequency vibrations can have influence on the surrounding soil conditions, see vibro-densification chapter 3. The model assumes maximal frequency from  $t=0$  on.

#### *Crane*

The model does not describe the loss of energy due to damping mechanisms of the crane. As the sonic vibrator start to generate some of the vibrations are transferred onto the crane. The model does not take this in to consideration.

#### *Static force*

The elements where pushed in the ground with a dynamic and static force. The static force varied between 40 kN, for the installation with weight compensation, and 100 kN when using no weight compensation. The 10 ton loading caused difficulties during installation. For some cases the installation process had to be stopped and the static

load had to be lowered to sustain stability during the installation process. This influences the total installation time. The model assumes a continuous installation process.

#### 7.9.4 Soil properties

The model uses the CPT data to obtain the soil properties needed for the determination of the parameter values for the different components. The locations of the CPT's does not exactly match the test locations and therefore possibly do not describe the right soil characteristics.

##### *Stiffness*

The correlation proposed by Robertson (Robertson, 2010) over-estimates the stiffness of the soft soil layers at field test location. The deeper soft layers at Centrumeiland, Amsterdam mainly consist out of very fine grained material that has been deposited over the years by the IJsselmeer. These layers are very sensitive to applied load. A reduction for the E-modulus in these layers is applied to better approach the soil properties. The calculated value for the E-modulus by the correlation proposed by Robertson is reduced by dividing it by a factor. The greatness of this value is chosen such that the penetration rate obtained with the model is in comparison with the test results in the weaker soil layers. The stiffness is reduced by a factor 5 at the weak layers. These sensitive layers are more prone to flow liquefaction and therefore a reduction in stiffness is justified. Flow liquefaction is characterized by a sudden loss of strength within a relatively small number of load cycles. A reduction in stiffness by a factor of 5 corresponds to an excess pore water ratio of 96%, see formula 11. This indicates that the soil suffers from liquefaction due to cyclic loading.

##### *Static soil resistance*

The static soil resistance is determined using the cone resistance from the CPT data. The behaviour of a CPT cone pushing in the ground is similar to that of an element penetrating the soil. Multiplying the cone resistance directly with the surface area of the element results in an overestimation of the soil resistance force. To reduce this resistance a factor  $\alpha$  is introduced, later also referred as alpha.

$$F_{stat}^{fric} = (q_c \cdot A_t) / \alpha \quad (47)$$

This method is in agreement with the ICP method developed by Jardine in 2005 (R.J.Jardine, et al., 2005) and the Koppejan method used in the NEN9997-1. These methods use a reduction factor to calculate the pile tip bearing capacity from the measured cone resistance. The reduction factor comprises the influence zone around the pile tip, the type of pile and the shape of it.

The factor alpha is kept constant during the simulation of a test. The static soil resistance is depending on several factors such as vibrating frequency and soil gradation. A constant value for alpha might result in over- underestimation of the resistance in other layers. Further investigation to factor alpha is needed.

##### *Soil damping*

The damping of the soil at the tip of the element is modelled with the parameter  $c_t$ . An amplification factor of  $\beta$  is needed to make to model better fit with the reality.

$$c_f = \beta \cdot c_t \quad (48)$$

The amount of damping at the tip is much more than the value of  $c_t$  proposed by Lysmer (Lysmer, 1965). An amplification factor beta takes this extra damping into account. There are multiple reasons which allow the use of this factor.

The loading frequency used for the determination of  $c_t$  was much lower than the frequencies used in this model. In undrained conditions the soil start to liquefy. High quantities of energy are lost during the development of excess pore water pressure. Besides that, the damping parameter corresponds to damping for homogenous soil conditions. This is not the case in the CPT data that is used by the model. The formulation for damping can only be used when the displacements are small considered to the size of the footing of the element. The displacement calculated by the model are relative high and consist out of displacement in the inelastic range. All these factors prove an increase in damping for the correlation proposed by Lysmer (Lysmer, 1965).

#### *Zone of influence*

The extent of the influence zone around the tip of the element influences the resistance against penetration. The extent is highly dependent on the relative density of a particular type of soil. The applied load is transferred between the grains. In high density types of soil, the grains have more intergranular contact resulting in a better transfer of load. In loosely packed soil the applied load causes the soil to deform. As long as there is no equilibrium between the load and the soil structure there will be limited transfer of load. In the model an influence zone underneath the pile tip of two times the diameter is chosen. The average cone resistance in this zone is used to obtain the soil properties. As result of this thin layers of high and low cone resistances barely influences the penetration of the element.

The different limitations indicate that the process is very complicated. Multiple factors influence the penetration of the element. The installation process is characterized by the shape of the time/depth curve. In chapter 8 the field test data is used to validate the model.

### **7.10 Recommendations**

For future use of the model I would recommend applying the following adjustments

- Subdivide the element into different masses with in between springs and dashpots to take the wave propagation inside the element in to account. It also enables you to locally specify the shaft friction. In this way the degradation of shaft friction with increasing number of load cycles can be taken into account.
- The influence zone around the tip is chosen to be two times the diameter of the element and stays constant for each type of soil. The influence zone might change at different soil types. Stiff soils better transfer the load to the surrounding soil than soft soils. A larger influence zone for hard soils is expected. Further investigation is needed to quantify this.

- Eventually it would be better to have a 2D model. The addition of an extra degree of freedom will significantly increase the possible internal resonance and therefore better describe the reality.
- The value for alpha is kept constant throughout the different test simulations. Further investigation is needed to quantify the value of alpha. Alpha describes the static resistance against penetration for a certain type of element. Laboratory or full scale field tests might be performed to determine the static resistance against penetration for a certain type of element at different soil conditions. The results need to be correlated to the cone resistance and then implemented in the model. This will significantly improve the accuracy of the model.
- The computing time of this simple model is 25 minutes. Increasing the complexity will enlarge the computing time. One should look for other method to reduce the computing time.

# 8

## Model results & validation

The purpose of the model is to simulate the penetration process of an element in the ground. The model must be able to determine the total installation time and quantify difficulties during penetration. The model uses the CPT data to obtain its parameters. Different field test results are used to validate the model. It is assumed that for all tests the maximum vibration frequency of 180Hz is used to vibrate the element into the ground. Per test the applied load and the soil characteristics are different depending on the test location.

### 8.1 Introduction

Validation of the model is only possible for the tests at which sufficient and accurate data about the installation is available. The model should be able to simulate the installation process in both strong and soft layers. Therefore, the response of the elements to different types of soil should be known. Only tests 1, 3, 4 & 5 fulfil these requirements. The elements used in these tests are 8 meters in length and reach both strong and soft layers when fully inserted. During the execution of these tests the time needed for the element to penetrate one meter of soil was recorded.

**Table 8.1 Field tests for validation**

Test nr.	Description	Test location
Test 1	Closed 300 mm	1
Test 3	Open 300 mm	2
Test 4	Open 300 mm	5
Test 5	Closed 400 mm	3

In the next chapter the CPT data at the particular test location is briefly elaborated. Subsequently the model is used to mimic the installation process using different sets for CPT reduction factor alpha and the damping amplification factor beta. The model uses a constant dynamic load and constant frequency of 180 Hz throughout the process. The different tests were performed with weight compensation (WC) and without weight compensation. The pull down load with WC is max 4 ton, without WC the max pull down load varies between 8-10 ton.

### 8.2 Results

The field test results of test 1 and 5 presented in Figure 8.1. The figure shows the effect of an increase in diameter (test 1 300 mm and test 5 400 mm). The larger the diameter the greater the resistance and the longer it takes for the element to be fully inserted. In the right figure the test results of test 3 and 4 are depicted. Test 3 and 4 were both performed using 300 mm open-ended elements. The field test results of test 4 show a more linear development of the penetration when compared to the results of test 3. This difference can be appointed to the different soil conditions at the test location 2 and 5.

According to the crane operator test 4 was fully performed with weight compensation. However, the results show that penetration time is more in agreement to a test without weight compensation (8-9ton), test3.2 & 3.2. In consequence, it is assumed that test number 4 is performed without weight compensation.

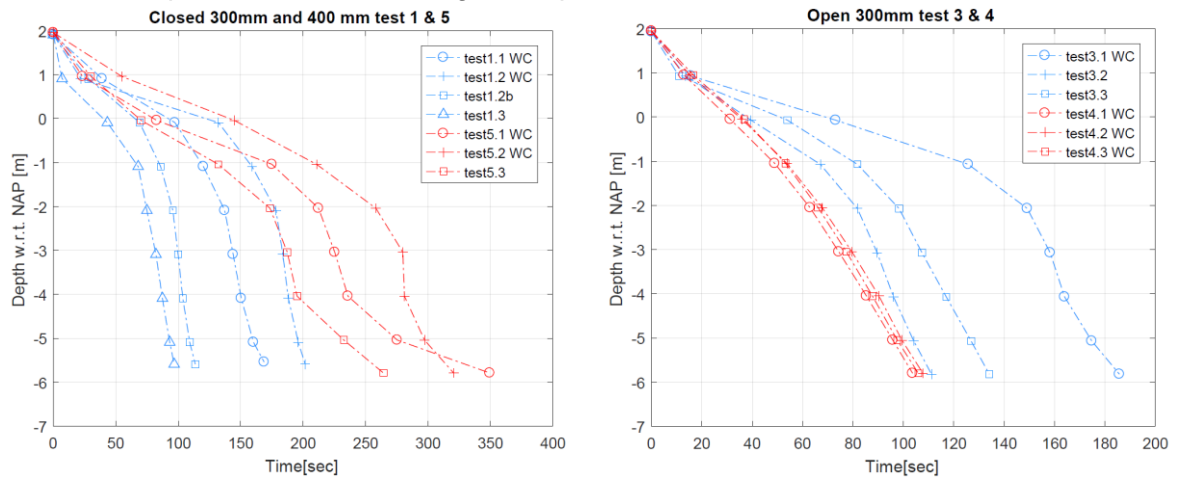


Figure 8.1 Field test results open- and closed-ended elements

### 8.2.1 Test 1

The first test is performed at test location 1. A 300 mm in diameter closed-ended element shaped as a vibroflot was vibrated, whilst pushed, into the ground. During this test the crane leader was directly positioned on ground surface. This caused some disruptions during the test as a result of instability of the crane leader. The CPT data shows two hard soil layers in the first four meters of soil with in between a small soft soil layer. Beneath these layers only relatively soft types of soil can be found.

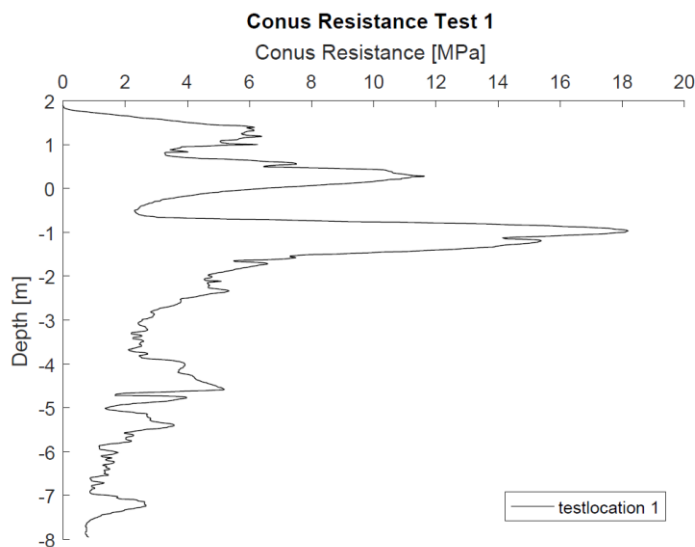


Figure 8.2 CPT data test location 1

Three different type of tests have been performed at this test location. The first two tests were performed with a pull down load of 4 ton and the last two tests with 8 ton. In the last test water is added at the tip of the element to enhance the penetration rate. The model is not capable in modelling the addition of water during the installation process.

Therefore the comparison between the results of the model and test 1.3 is not representative.

**Table 8.2 test description location 1**

Test nr.	Description
1.1	4 ton load
1.2	4 ton load
1.2b	8 ton load
1.3	8 ton load + addition of water

During the different tests the installation process had to be stopped for several times to realign to crane leader with the element. This extra time has been excluded from the data set. In Figure 8.3 the test results model results are plotted.

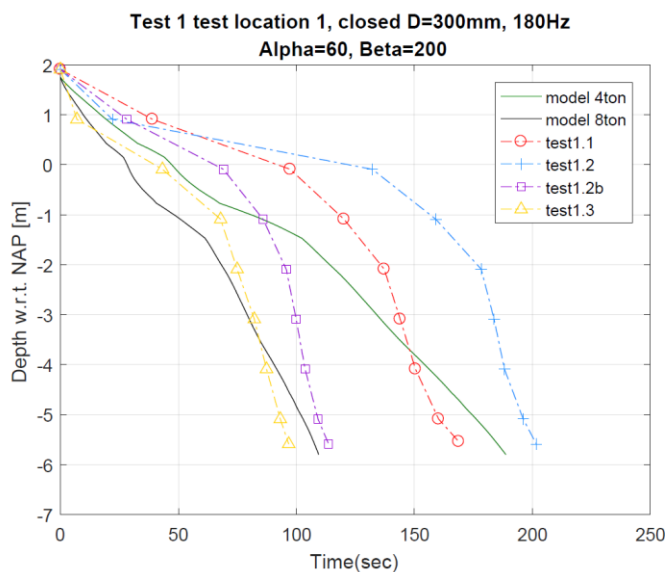


**Figure 8.3 Model vs field test data test location 1**

The inclination of the curve represents the penetration rate of the element. The model seems to respond differently to the strong and soft layers than the element in the field. The field test results show a large decrease in penetration rate in between 1 and 0 m NAP while this reduction in the model is only minimal. At this particular depth the first 'strong' sand layer can be found. The maximum cone resistance of this layer is only 11 MPa and such a large reduction in penetration rate is therefore not expected. After this strong soil layer, a softer soil layer, with a thickness of around 1 meter, can be found. The model results show an increase in penetration rate in this layers until the penetration of the element becomes influenced by the second strong layer at -0.75 m NAP. The increase in penetration rate also appears to be present in the field test results. The inclination of the curve in these layers is similar at the model and field test. The influence of the second strong layer at around 1 m NAP is not visible in the field test results. The peak value of the cone resistance is even higher than the value of the first peak and a strong reduction of the penetration rate is therefore expected. The penetration rate in the field test results only increases after the first peak is penetrated. The second strong layer seems to be completely absent at the locations where the tests were performed.

The model results are largely affected by the second strong layer in the CPT data. A high value for beta is needed to approach the field test results. The large value for beta results in a under estimation of the penetration rate in the soft soil layers.

The CPT data used to model test 1 does not deliver the desirable results. The CPT data from test location 2 (next to test location 1, figure A.1) seems to be more in agreement with the soil conditions at test location 1. The results are displayed in Figure 8.4. The large resistance against penetration due to high cone resistances at 1 m NAP is still not present in the CPT data of test location 2. Nevertheless, the overall penetration curve is more in agreement with the field test results. Especially the penetration rate obtained in the softer layers. A lower value of beta can be used to approximate the field test results.

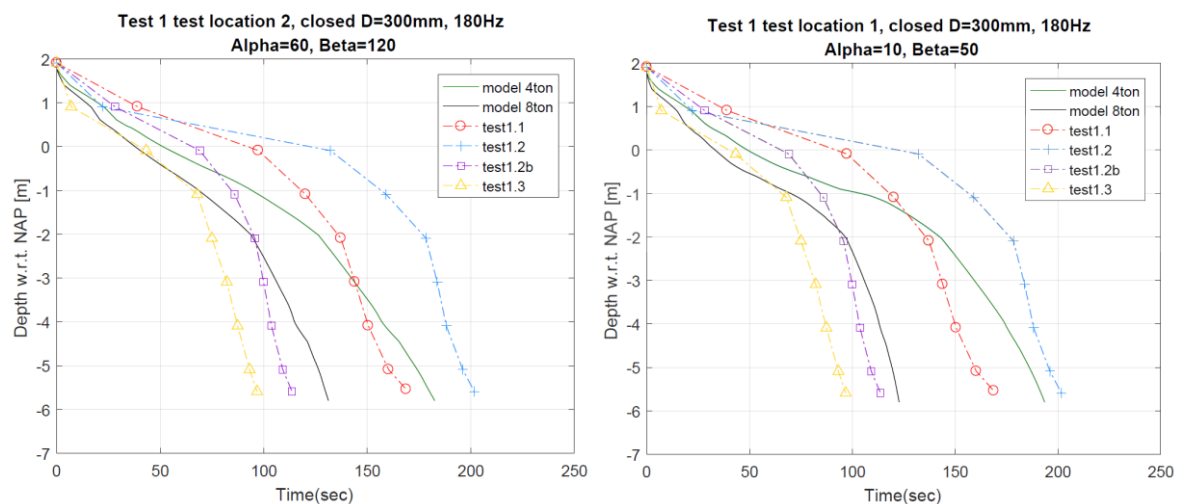


Figure 8.4 Model vs field test data test location 2

### 8.2.2 Test 3

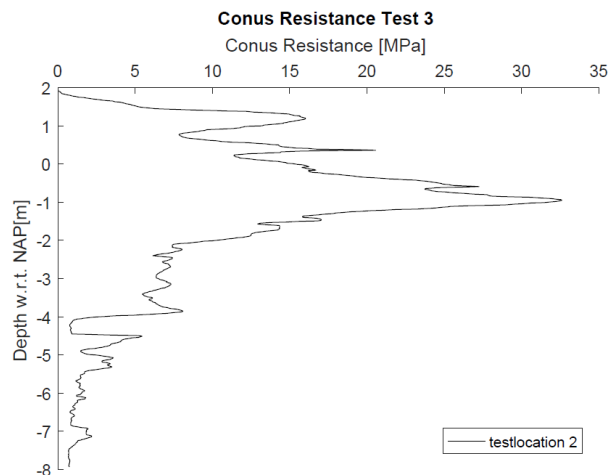


Figure 8.5 CPT data test location 2

The third test was performed at test location 2. The CPT data obtained for the test location 2 is characterized by a single large peak of 33 MPa. The two distinct peaks as observed at other test locations are not pronounced at this location. At this testlocation three different tests have been performed with a open-ended element with a diameter of 300 mm.

From this point on the crane leader is stabilized on a wooden board as explained in Appendix A The use of the wooden board greatly improved the stability and thus the installation process. The following tests have been performed:

**Table 8.3 Test description location 2**

Test nr.	Description
3.1	4 ton
3.2	10 ton
3.3	10 ton

The model is used to simulate the behavior of the pile penetrating the soil. No real difficulties were encountered at this particular test location.

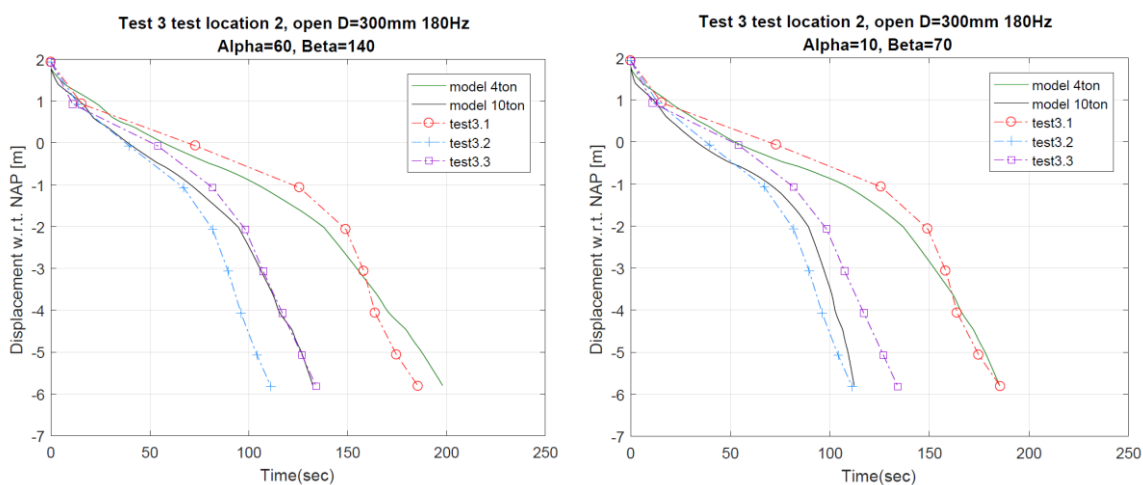


**Figure 8.6 Model vs field test data test location 2**

The obtained model results for test 3 are more in agreement to what can be seen at the field test. This suggests that the right input data is used for the determination of the soil characteristics. The results show that the model has a bit less difficulties in penetrating the first 4 meters than the results from test 3.1 and 3.3. The penetration rate of the model at the deeper layers is very similar to that of the field test. This indicates that the accumulation of shaft resistance with depth is in agreement to what is happening in the field.

### 8.2.3 Test 4

The fourth test was performed on test location 5. There are two distinct peaks visible. This test was one of the only tests that went very smooth without having difficulties. Three open-ended elements with a diameter of 300 mm were installed.

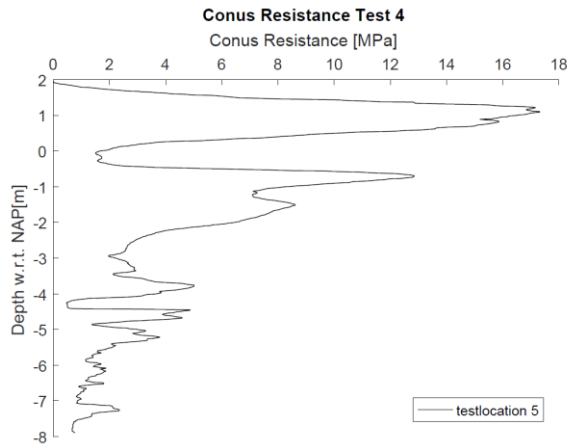


Figure 8.7 CPT data test location 5

The three different tests were all performed under the same conditions.

Table 8.4 Test description location 5

Test	Description
4.1	4 ton
4.2	4 ton
4.3	4 ton

The three field test results are very similar. It seems likely that these tests were performed under the same conditions.

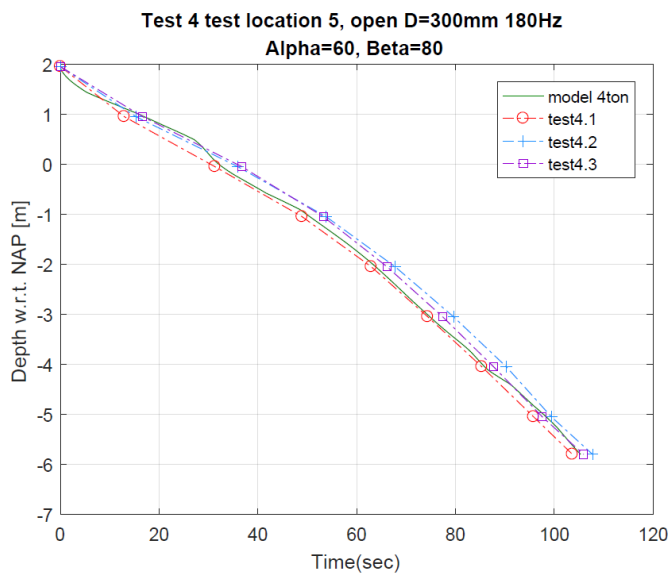


Figure 8.8 Model vs field test data test location 5

The model is in good agreement with the test results. There are no large differences visible. The model seems to respond a bit stronger to the soft layer at +/- 0.5m NAP. However, this does not affect the further response of the model.

As been mentioned before it seems that the test was performed without weight compensation considering the penetration time of 105 seconds. The model is again used to simulate the penetration but now with a load of 8 ton.

**Table 8.5 Test description location 5 (adapted)**

Test	Description
4.1	8 ton
4.2	8 ton
4.3	8 ton

The applied load is changed to 8 ton and new values for alpha and beta can be obtained.

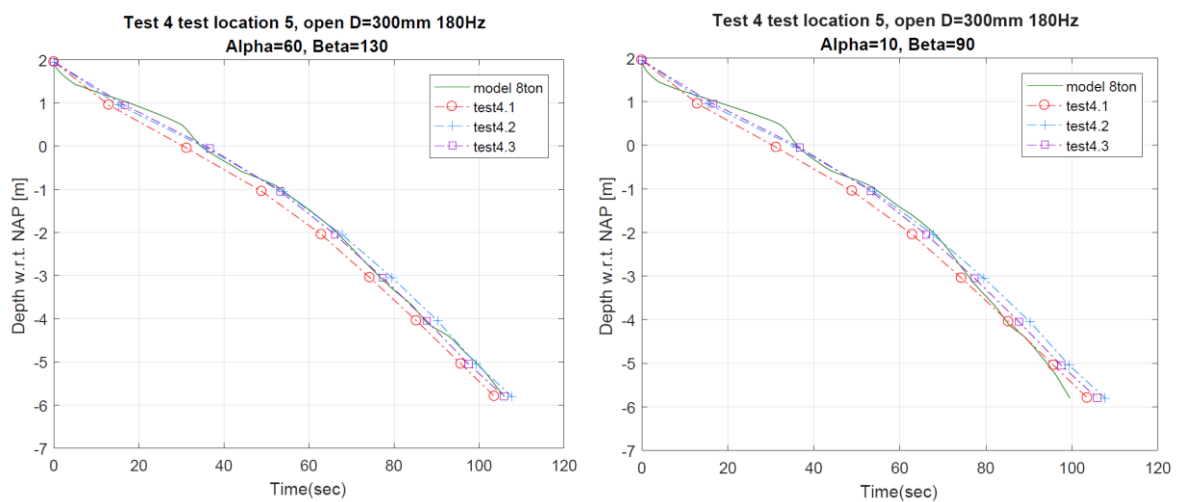


**Figure 8.9 Model vs field test data test location 5**

Again, the model is able to perfectly describe the penetration of the element in the ground.

### 8.2.4 Test 5

The fifth test was performed at test location 3. The CPT data is similar to that of test location 5 only the second peak value for the cone resistance is greater at this test location.

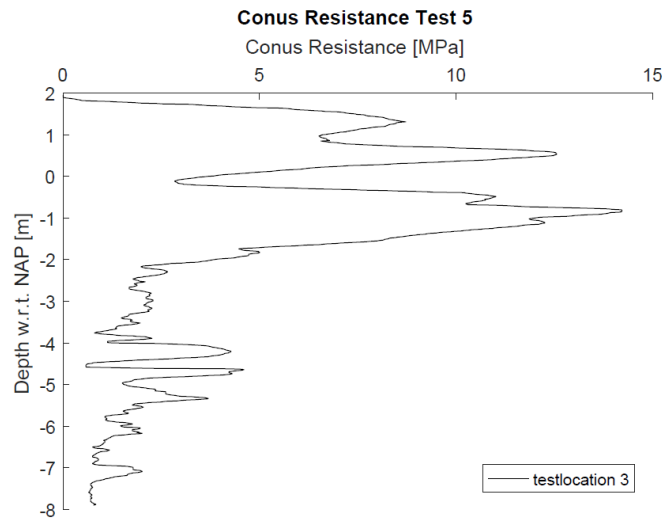


Figure 8.10 CPT data test location 3

At this test three tests with a 400 mm in diameter closed-ended element were performed.

Table 8.6 Test description location 3

Test	Description
5.1	4 ton
5.2	4 ton
5.3	8 ton + water

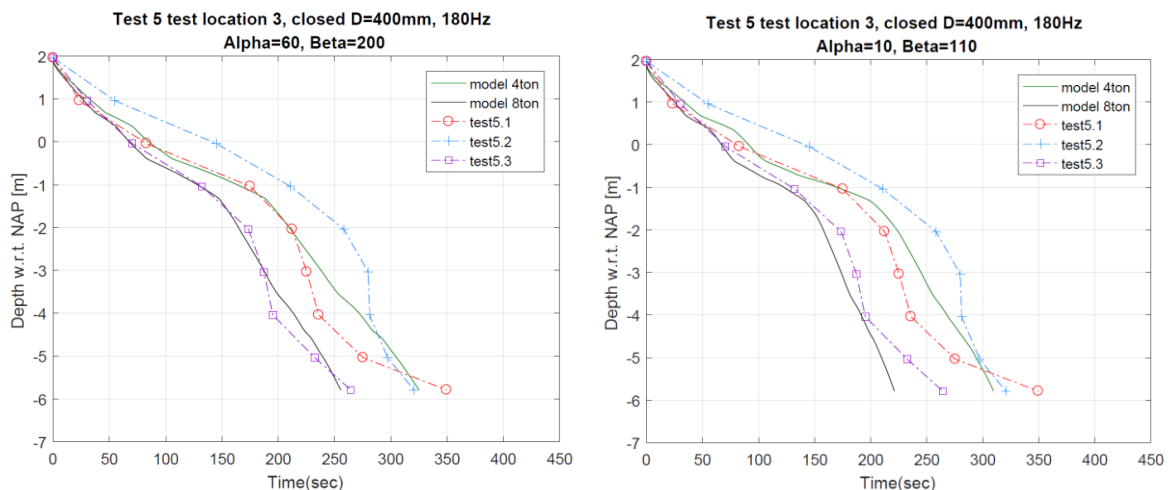


Figure 8.11 Model vs field test data test location 3

The results show that the model underestimates the penetration rate in the deep soft layers ( $d < -2$  m NAP). Test 5.2 seems to be shifted to the right in comparison to test 5.1. This might indicate an error in the time/depth registration at the start of the test.

### 8.3 Conclusions model

The results show that the model is able to fairly well describe the installation process for open-ended elements. At closed-ended elements the model underestimates the penetration rate in the soft soil layers deeper than -2 m NAP (test 5) but still gives a reasonable fit.

The CPT data that is used to model the tests in test 1 seems to be not in line with the local soil conditions. The field test results indicate that the element was probably subjected to a stronger soil layer, at a depth of +/- 0.5 m NAP, than the CPT data indicates. The second strong layer at a depth of -1 m NAP may not even exist at the location of the different tests. The presence of this second strong layer greatly influences the model results. The resistance along the shaft becomes more amplified by strong layers and therefore decreases the penetration in the deeper layers. This explains why the penetration rate at the deep soil layers greatly differs between the model and the field test. The CPT data corresponding to test location 2 seems to be more in line with the local soil conditions. Although the model still overestimates the penetration in the first 2 meters of soil. Another explanation for the deviation between the model and the test results can be appointed to the disruptions during the installation process. The model assumes a constant pull down load over time while during the field test the installation was stopped several times to realign the crane leader. The realignment was not in favour for the installation time and occurred mainly in the first 4 meters of soil. Even though the stopwatch was paused during the realignment of the leader it is still possible that some extra time is included in the test data. This causes the curve to shift to the right. As the elements got deeper into the soil more stability is gained from the surrounding soil. The increase in stability enhanced the installation rate in later stages.

The model shows good results when simulating the installation process at test 3. There are only small differences between the model and field test results. The differences are mainly due to different soil conditions in the first four meters between the model and the field test. The small deviations might be the results of the small peak values of cone resistance in the first 2 meters of soil. At deeper layers the average cone resistance becomes stable resulting in a constant and equal penetration rate of both the field test results as the model results. The similar penetration rate indicates that the accumulation of shaft resistance with depth is in line to what is happening in the field. The deviation between test 3.2 and test 3.3 might indicate that the tests were performed at locations with different soil characteristics or the installation process went differently.

In test 4 no striking differences can be seen. The three different tests were properly executed under the same conditions and gave equally results. The model is able to perfectly describe the installation process for test 4.

The model at test 5 is in line with the field test results in the first 4 meters of soil. Beneath -2 m NAP the model starts to underestimate the penetration rate. This phenomena can also be seen in test 1 when using the CPT data from test location 1.

At the different models the factor alpha was used to define the shape of the model. The factor alpha determines the reduction in static resistance. For a value of alpha equal to 1 the static resistance is equal to the cone resistance multiplied with the area of the tip. The larger the value of alpha the lower the static resistance against penetration. The best fit of the model curve is obtained by changing the value for beta while alpha is kept constant. The factor beta determines the amount of damping at the tip of the element. At

low values of alpha the curvature of the model is more in agreement with the field test results.

Table 8.7 Factors  $\alpha$  and  $\beta$  for the different tests

Test nr.	Test location	Factor $\alpha$	Factor $\beta$	Ratio $\alpha/\beta$	Load (ton)	Type element
1	1	60	200	0.30	4 & 8	300 mm Closed
1	2	60	120	0.50	4 & 8	300 mm Closed
1	2	10	50	0.20	4 & 8	300 mm Closed
3	2	60	140	0.43	4 & 10	300 mm Open
3	2	10	70	0.14	4 & 10	300 mm Open
4	5	60	80	0.75	4	300 mm Open
4	5	60	130	0.46	8	300 mm Open
4	5	10	90	0.11	8	300 mm Open
5	3	60	200	0.30	4 & 8	400 mm Closed
5	3	10	110	0.10	4 & 8	400 mm Closed

At higher values of alpha higher values for beta are needed to obtain an equal penetration rate. This relation is not considered to be linear. A good comparison between the values for alpha and beta at open-ended and closed-ended elements cannot be made. This is due to the lack of correct CPT data at test 1 and due to difficulties fitting the model with the field test results at closed-ended elements. Furthermore, the field test results of test 1 and test 3 show equal penetration results, see Figure 8.12.

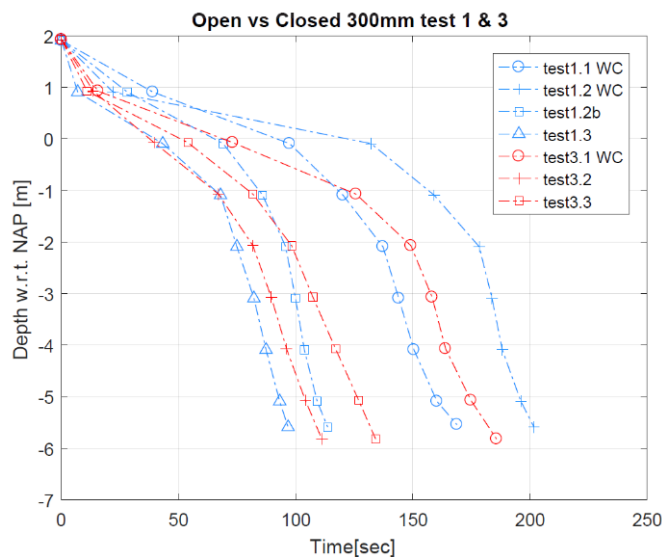


Figure 8.12 Installation curve open- vs closed-ended elements

The equal penetration time is due to plug formation at the tip of the open-ended element. The closure of the tip causes the open-ended element to behave similar to a closed-ended element. Nevertheless, an increase in beta can be recognized when comparing test 3 & 4 with test 5. The increase in beta indicates more damping at closed-ended elements. The closed-ended elements are considered to be soil displacement elements.

Large volumes of soil have to be moved in order to create room for the element to penetrate the soil. The movement of soil particles increases the amount of damping. Furthermore, the pile soil interface at the tip is larger for closed-ended elements than it is for open-ended elements. The closed-ended elements more or less push its ways through the soil while the open-ended elements cut through the soil.

The model is not capable in correctly simulating closed-ended elements. The simulation of test 5 shows an under estimate of the penetration rate in the soft soil layers. The amount of damping/static resistance in these particular layers is too high. When modelling open-ended elements this is not visible.

The differences between the model and field test data are influenced by various factors both due to human action as on the soil characteristics. In case of using different CPT data it does not necessarily mean that the model is wrong it only describes the installation of an element at different soil conditions.

Nevertheless, the model is a simplification of reality. The installation process is far more advanced than the model describes. There are multiple explanations for differences between the model and the field test results. The different CPT data from the different test locations show large deviations in cone resistances. Especially the cone resistance in the first 4 meters of the soil differs throughout the test field. The soil in the first four meters is very disturbed and contains lots of debris, Appendix D. The soil resistance is measured by the cone penetration test. As the cone comes in contact with large pieces of debris it will measure higher cone resistances than there actually are in the surrounding soil. This negatively influences the results of the model.

During the execution of the tests the large crane had to be moved to the selected test location. The crane had to drive across other test locations in order to reach its final destination. The heavy weight together with vibrations, developed during driving, modifies the soil conditions in the top section of the subsoil. The CPT data used to simulate the field test results does not take this into account.

The total test field covers an area of 45 by 100 meters and is subdivided in 15 different test locations. Each test location is represented by one CPT. The centre to centre distance in between the different tests was in some cases only 7 meters. The CPT data between the different test locations show large deviations. The CPT data might not always correspond with the soil characteristics at the location of a test. This causes a difference in the results obtained with the model and the field tests.

The model considers constant values for the vibration frequency and the static load throughout the installation process. However, during the field test these parameters were not kept constant all the time. The change of vibration frequency and static load greatly influences the penetration rate of an element in the soil.

The installation of the elements was not always a continuous process. In some tests the installation process had to be stopped to realign the crane leader or for maintenance of the crane. As the vibrator starts to slow down it passes the natural frequency of the soil. Vibrations at the natural frequency the soil greatly contributes to the densification of the soil and changes the soil characteristics. The same is happening during restart of the vibrator. Furthermore, the unloading of the soil causes an elastic uplift of the soil and a redistribution of stresses. The soil near element might behave different as the installation process proceeds again. The model does not take any change in soil characteristics into account.

During installation of the element a small leak in one of the hoses arose. Due this leak the static pressure might be different than what it should be according to the level of the hydraulic pressure. Unfortunately, this was not measured. As the operation time of the crane increases the hydraulic fluid starts to heat up. The viscosity of a liquid such as oil is dependent on its temperature. Larger temperature will decrease the viscosity of the fluid and influences the potential static pressure of the crane.

During the different tests the time needed for an element to penetrate one meter of soil was measured with a stopwatch. In between the intervals no information is available about the penetration rate of the element. The proposed installation curve presented in the different figures can differ from the actual installation curve. The last data point of field test is not representative for the total installation time. As the element reaches it maximal depth the penetration rate was lowered to prevent the vibrator from touching the soil.

# 9

## Sensitivity analysis

In the sensitivity analysis the uncertainty in model output is attributed to the uncertainty in model input. The sensitivity analysis is performed to gain more understanding in how the parameters influence the model results.

The results from test4 are used to perform the sensitivity analysis. Test 4 showed the most consistent results throughout the different tests and therefore the influence of side effect is assumed to be limited.

### 9.1 Parameters

For each parameter multiple values are generated in a defined space. The contribution to the penetration time is then treated. For each case only one parameter value is changed while the other ones stay at their original value. The sensitivity of the following parameters is investigated:

- Factor alpha
- Factor beta
- Poisson ratio
- G-modulus (small/large strain)
- Dynamic frequency
- Pull down force

#### 9.1.1 Factor alpha

The value of alpha is used to get the static tip resistance from the CPT data using equation 45. High values of alpha reduce the static resistance against penetration. The value of beta is kept constant at 95.

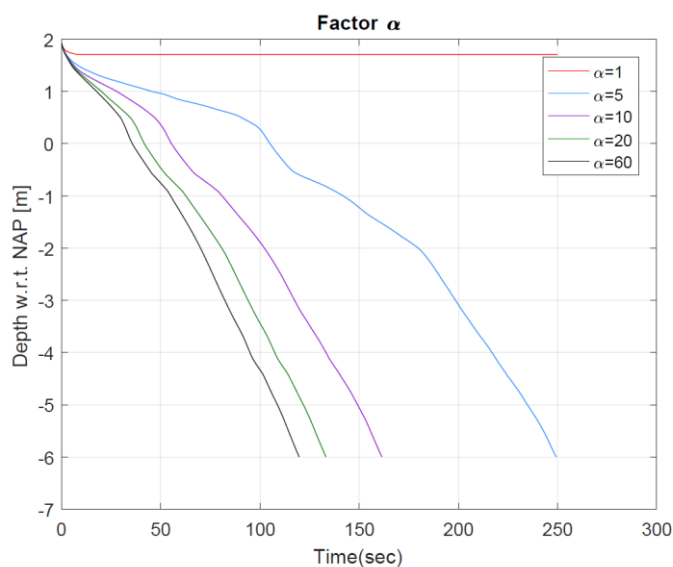


Figure 9.1 Sensitivity analysis reduction factor  $\alpha$

The model shows to be more influential to hard layers for low values of alpha than at high values for alpha. Without any reduction in the static resistance the crane is not able to drill the element through the hard soil layer. Increasing the value of alpha allows the element to penetrate through the hard soil layers. The larger the value for alpha the less alpha influences the penetration rate. At very large values of alpha the influence of the damping becomes determinative instead of the static resistance. The depth at which penetration of the element becomes impossible depends on the value of alpha for a particular value of the cone resistance. The penetration rate in the soft soil layers is not affected by the value of alpha.

### 9.1.2 Factor beta

The factor  $\beta$  increases the development of damping at the tip of the element. By increasing the factor more damping is involved resulting in a lower penetration rate.

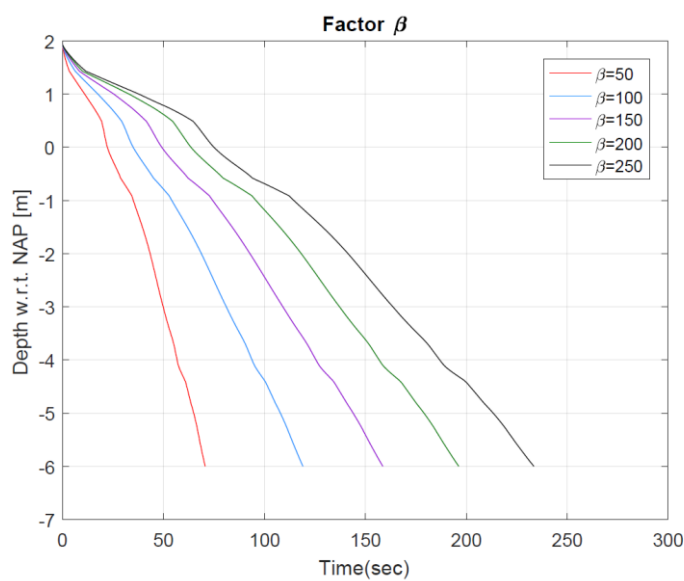


Figure 9.2 Sensitivity analysis amplification factor  $\beta$

The interval between the curves of different values for beta is almost constant at particular depths. By increasing the value of beta the curve rotates anticlockwise. For a value of beta equal to zero there is no damping and the soil element will penetrate the entire soil profile in zero seconds after the applied force exceeds the static resistance force.

### 9.1.3 Poisson ratio

The Poisson ratio is the ratio between the lateral extension and the axial compression. Sandy soils behave drained when they become compressed, the water is free to flow out of the pores resulting in a volume reduction of the bulk. When clay is loaded it behaves more undrained. In undrained conditions the water is not able to flow out of the voids. The bulk becomes incompressible and no volume change occurs. A Poisson ratio equal to 0.3 is assumed when considering drained conditions and a value of 0.5 for undrained conditions.

The Poisson ratio is used in the formula for the conversion of the E-modulus to the G-modulus and for the determination of the spring stiffness and damping at the tip, equation 30.

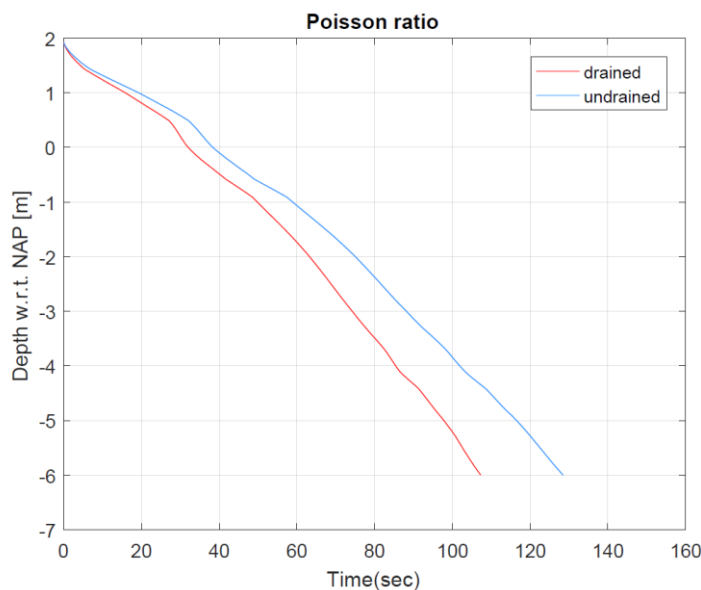


Figure 9.3 Sensitivity analysis Poisson ratio

Increasing the Poisson ratio to simulate undrained behaviour result in an decrease of shear modulus. The soil particles are free to move when being sheared. The decrease in shear modulus affects both the shaft resistance and the tip resistance. At the shaft the interaction between the soil and the element is solely dependent on shear forces. A reduction in shear modulus reduces the values for the spring stiffness and the damping at the shaft. Below the tip both shear forces and compressional forces describe the pile soil interaction. An increased value for the Poisson ration result in an increase of the damping and spring stiffness at the tip. The tip resistance is determinative when considering the penetration time and therefore results in an increase in penetration time at undrained conditions.

### 9.1.4 G-modulus

The shear modulus forms the basis for the determination of the different components of the model. Increased values for the shear modulus raises the amount of damping and increases the stiffness of the spring.

The dynamic properties of soil are different at small strains ( $\xi < 10^{-3}\%$ ) than at larger strain. Especially the stiffness of the soil. Stiffness is defined as the inclination of the

stress/strain curve. The inclination of the curve decreases with increasing strain resulting in a reduction of the tangential and secant shear modulus. The maximum stiffness can be found at small strains. The tangent line to the stress-strain curve starting at the origin corresponds to the small strain stiffness  $G_0$  and is known as the maximum shear modulus.

S. Oztoprak et al. collected the modulus degradation curves of 454 tests from the literature and created a hyperbolic relationship to approach the test results (Oztoprak & Bolton, 2013).

$$\frac{G}{G_0} = \frac{1}{1 + \left(\frac{\gamma - \gamma_e}{\gamma_{ref}}\right)^a} \quad (49)$$

$\gamma_e = \text{elastic threshold}$   
 $\gamma_{ref} = \text{reference strain}$   
 $a = \text{curvature parameter}$

The different values for  $\gamma_e$  and  $\gamma_r$  depend on the sand type (i.e. uniformity coefficient), soil state (i.e. void ratio, relative density) and mean effective stress. The database covers a wide variety of sandy soils. The results hold sand in dry, wet and saturated conditions. Results were obtained using both reconstituted and undisturbed samples. The different samples contained clean sands, gravels, sands with fines and/or gravels, and gravels with sands and fines, representing 60 different materials (e.g. Toyoura sand, Ottawa sand, undisturbed Ishikari sand). The different tests were performed at both drained and undrained conditions in static and dynamic tests, resulting in a wide variety of different results.

S. Oztoprak et al. indicated a lower and upper bound within the different test results can be found.

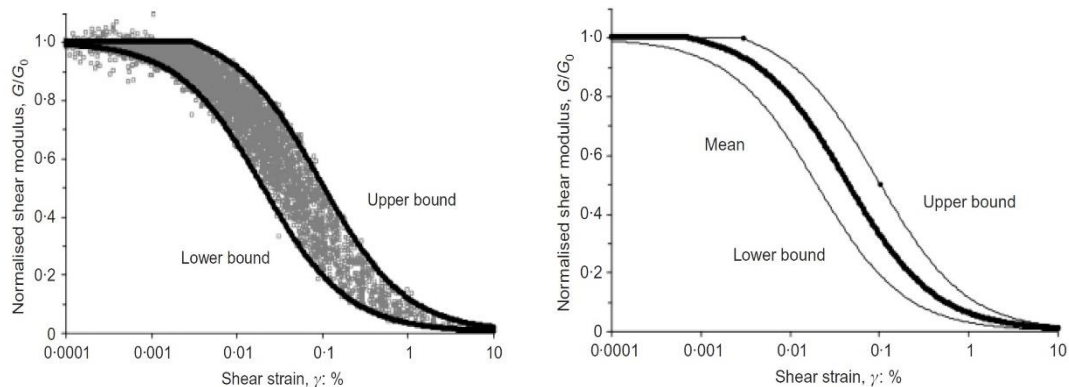
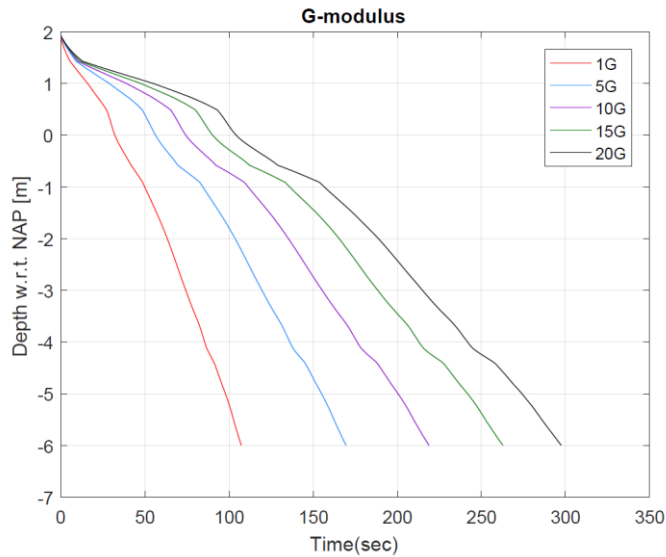


Figure 9.4 Shear modulus reduction curve

Table 9.1 Shear modulus reduction curve characteristics

	Lower bound	Mean	Upper bound
$\gamma_r$ [%]	0.02	0.044	0.1
$\gamma_e$ [%]	0	0.0007	0.003
$a$ [-]	0.88	0.88	0.88

Deformations in geotechnical structures generally stay below 0.5 % strain. The stiffness modulus obtained by the relation proposed by Robertson is defined as the stiffness that is mobilized at 0.1 % strain. The value for the small strain stiffness can be 5-25 times higher than stiffness used in the model. The shear modulus in the model is varied to see the influence on the penetration time.



**Figure 9.5 Sensitivity analysis shear modulus**

The higher the G-modulus the stiffer the response and the larger the penetration time is.

### 9.1.5 Dynamic frequency

The SonicSampDrill vibrator can reach frequencies up to 180 Hz. During the installation of the elements frequencies between the 150-180 Hz were used. It generally applies that higher frequencies corresponds to larger energy consumption. A larger frequency does not always increase the penetration rate of the element. Even though the influence of different frequencies is small there is a decrease penetration rate for larger values of the dynamic frequency.

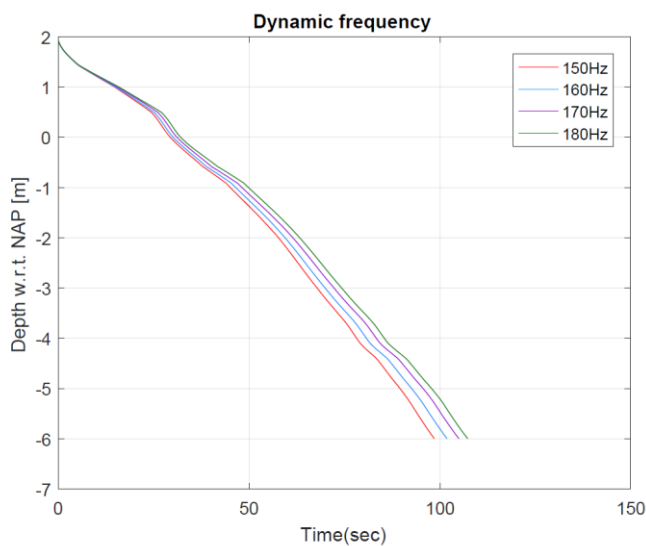


**Figure 9.6 Sensitivity analysis dynamic frequency**

The decrease in installation time at higher frequencies is due to the structure of the model. The displacement of the mass is obstructed by large values for the damping components. The dashpots slow down the displacement of the mass. At increasing frequencies, the dashpots do not have enough time to respond to the applied force and therefore lower the displacement. The frequency at which the dynamic frequency contributes to the penetration rate can be found at lower frequencies. Higher frequencies do not contribute to an increase in the penetration rate of the model.

### 9.1.6 Pull down load

The pull down load is the static load that the crane is able to transfer to the element. The pull down load that was applied during the field test can be found within 4 and 10 ton. During the test the load varied.

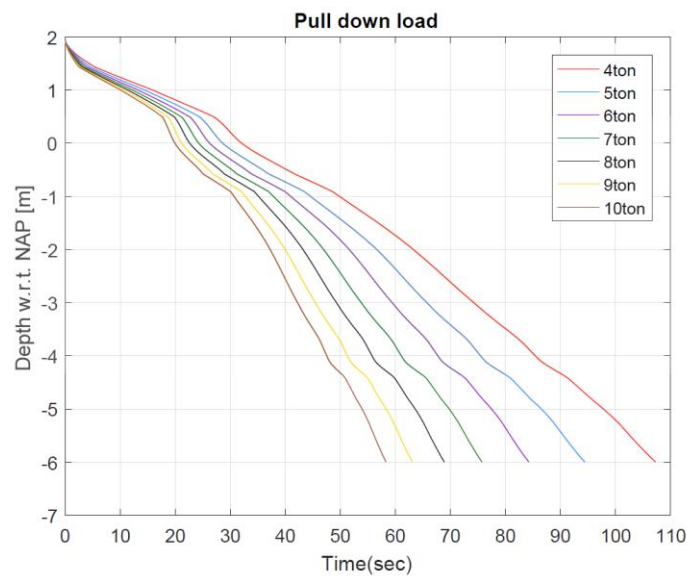


Figure 9.7 Sensitivity analysis pull down load

The influence of the pull down on the penetration time is considerably large. It is therefore from importance to know how the static load evolves during the installation.

### 9.1.7 Conclusion

The influence of the Poisson ratio and frequency on the penetration time are relatively small. The values for the G-modulus, pull down load and the factor alpha and beta significantly influence the results. More investigation is needed to reduce the possible range of these values.

# 10

## Optimization

### 10.1 Introduction

The drilling process is optimized to improve the penetration rate in order to save time and eventually costs. The penetration rate can easily be improved by increasing the pull down load as can be seen from the sensitivity analysis. However, high loads cause reduced stability of the crane leader during installation and obstruct proper installation. Another way to increase the applied static load is to increase the weight of the element. A thicker wall or another type of steel contributes to a heavier element. The increase in weight might reduce the vibration amplitude of the element due to the extra inertia effects explained in Chapter 6.2. Another possibility is to use a longer element. A longer element decreases the resonance frequency of the element to a frequency that is within the frequency range of the vibrator, however the current crane setup cannot deal with elements longer than 8 meters of length. Experiments with water were also carried out during the field test. The results show a decrease in penetration time. During the process fines were washed out of the soil by the water and transported to the surface. This influences the soil characteristics and affects future use of the soil.

Changing the dynamic frequency of the system is also a way to increase the penetration rate. The frequency at which the displacement amplitude is at its greatest is considered to be the optimal for the model. The optimal frequency for a simple undamped spring mass system is the natural frequency. At this particular frequency the system starts to resonate resulting in an increase in displacement amplitude.

Natural frequency for a simple mass spring without damping is:

$$\omega_0 = \sqrt{\frac{k}{m}} \quad (50)$$

The damping influences the natural frequency of the system, especially when it reaches the critical damping. For values of  $c_e$  equal or larger than the critical damping the development of a harmonic displacement is obstructed. The ratio between the damping and the critical damping is indicated with the Greek letter zeta. A damping ratio equal to one indicates critical damping. For values larger than one the system is called overdamped. The critical damping is given by:

$$c_{cr} = 2\sqrt{km} \quad (51)$$

$$\zeta = \frac{c_e}{c_{cr}} \quad (52)$$

The closer the value of zeta comes equal to 1 the faster the displacement amplitude decreases to zero.

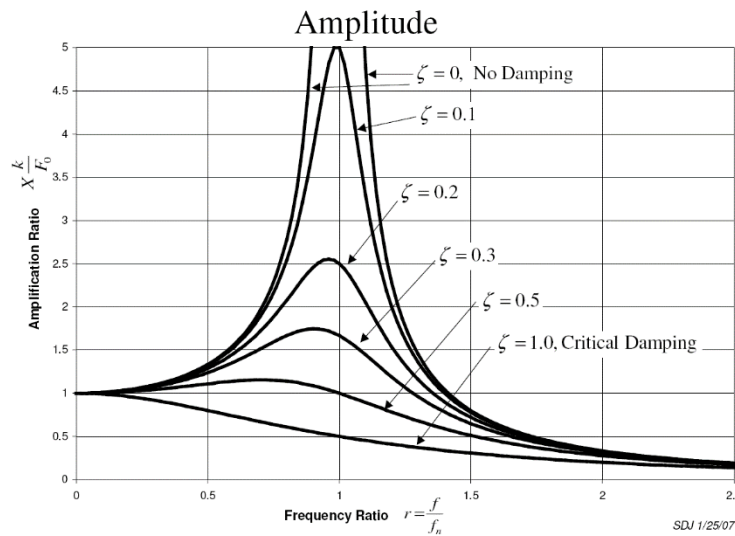


**Figure 10.1 Resonance frequency at different damping ratio's**

For values of zeta smaller than 0.707 the amplification ratio becomes larger than one and resonance of the system is possible, Figure 10.1. Decreasing the damping ratio and thus the amount of damping causes the peak at which resonance occurs to shift to the right. At zero damping to total system fully resonates at the natural frequency of the system and the amplification amplitude reaches an infinite value. The peak value for an undamped system can be found at a frequency ratio of one and is equal to the natural frequency  $\omega_0$  of the system.

The peak frequency at which resonance occurs for a damped system can be calculated with:

$$\omega_{peak} = \omega_0 \sqrt{1 - 2\zeta^2} \quad (53)$$

As the element penetrates the soil the parameters values  $k$  and  $c_e$  change. As a consequence, the peak frequency of the system changes. The alteration of the frequency is the consequence of having more interaction with the soil with increasing penetration depth and reaching new layers with different stiffness's. The value at which resonance occurs changes and the model has to constantly modify the applied frequency to maintain resonance. Generally, it applies that for increasing values of damping the frequency at which resonance occurs decreases and for increasing values of the spring stiffness the frequency increases.

## 10.2 Test location 5

The possibilities to optimize the installation process of an element in test location 5 are further investigated. To clarify the optimization of the installation process the CPT data at the location is simplified. The soil strata are divided in to different layers with constant values for the cone resistance  $q_c$  and friction ratio  $R_f$ .

Table 10.1 Soil characteristics test location 5

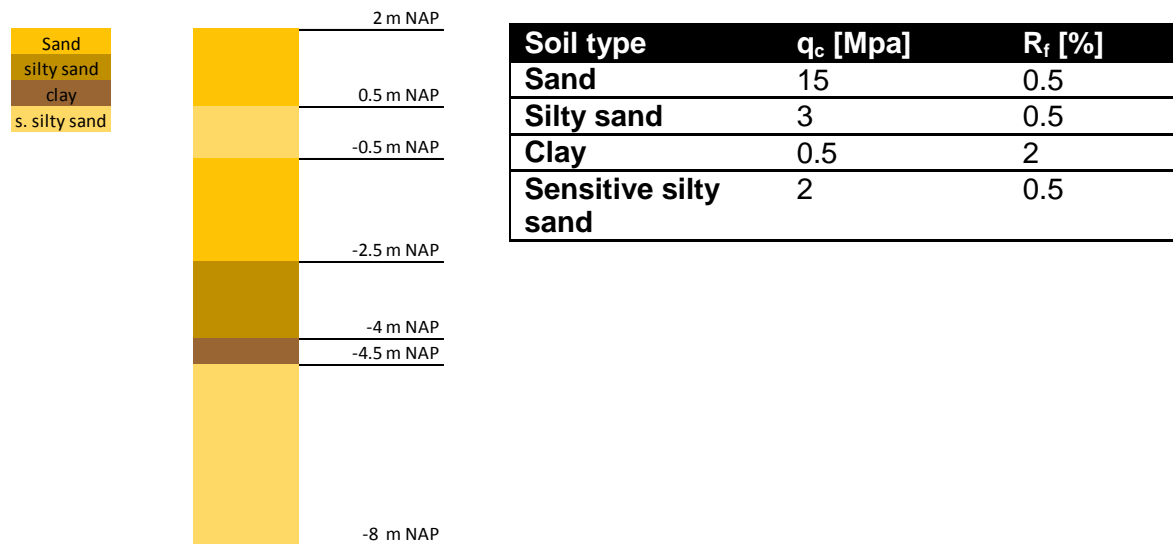


Figure 10.2 Simplification soil strata test location 5

The two peak values in the first four meters of soil are taken to be equally. The cone resistance over depth is illustrated in Figure 10.2. The parameter values for both the damping and the spring stiffness for the different types of soil can be found in Appendix G.

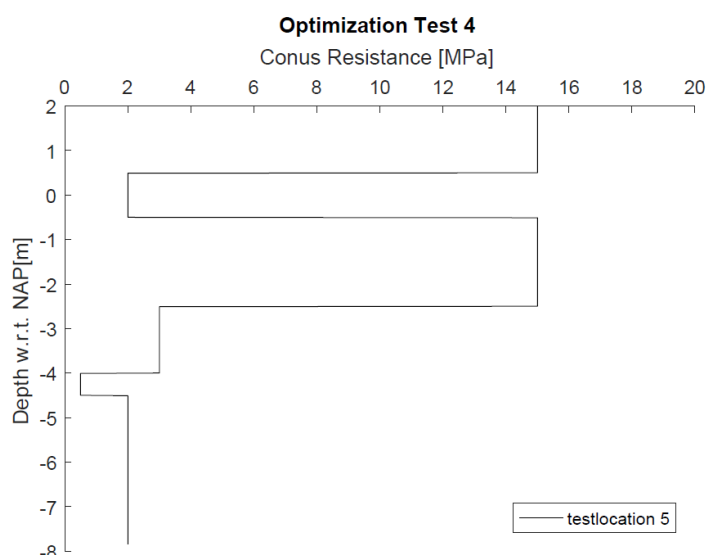


Figure 10.3 cone resistance with depth test location 5

In case of an undamped system the resonance frequency is given by equation 48. As the element penetrates the different soil layers the resonance frequency changes as result of

a changed spring stiffness. The frequency at which the system resonates is mainly dependent on the tip resistance of the element. The contribution of the shaft resistance to the resonance frequency is limited and can be recognized by the inclination of the curve in Figure 10.4. In a particular soil layer, the tip resistance stays constant while the shaft resistance increases with penetration depth. Equation 48 shows that increasing values for  $k$  raises the resonance frequency. The spring stiffness is again dependent on the shear modulus. The stiffer the soil the larger the value for  $k$ . The resonance frequency for the undamped system is illustrated in Figure 10.4.

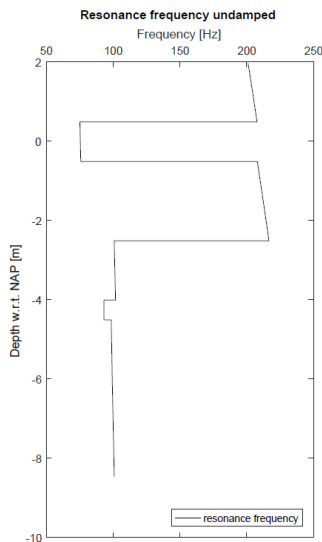


Figure 10.4 Resonance frequency undamped system test location 5

Damping plays an important role in the installation process and can therefore not be neglected. As the damping is activated in the system the peak resonance frequency drops to 87 Hz at the start. As the element penetrates the soil the value for the damping ratio increases as more and more damping of the system occurs. The frequency at which resonance can be obtained decreases to a value zero as the damping ratio reaches a value of 0.707. The system becomes critically damped, there is no frequency anymore at which resonance of the system can be achieved. At a frequency of 0 Hz no penetration is possible, see Figure 10.5.

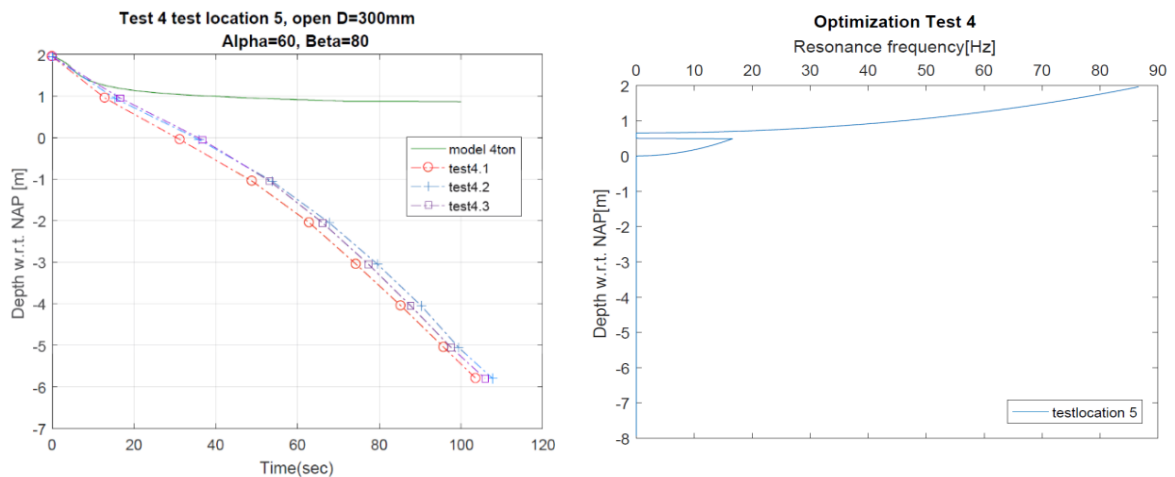


Figure 10.5 F.I.t.r penetration, resonance frequency test location 5

The large degree of damping in the stiff soil layers makes the penetration of the element impossible. This does not necessarily mean that there would not be penetration in practice. It only shows the behaviour of this model at the resonance frequency of the system.

### 10.3 Conclusion

One must be aware that calculated resonance frequency is the best frequency for this mathematical system and does not necessarily agree with the resonance frequency of the sonic drill system. The reality is far more complex than this model and therefore the optimal frequency might be different. As has been explained in Chapter 7.9.1 the frequency at which the steel element starts to resonate is not taken into account by this model. The resonance frequency of a steel element is much larger than the frequency calculated. The natural frequency of a steel element with a length of 8 meters can be found in the order of 360 Hz according to equation 6.

The damping in the system greatly influence the possibilities to improve the penetration rate by using a dynamic frequency equal to the resonance frequency of the system. As the amount of penetration of the element in the soil increases both the damping as the spring stiffness increases, see Appendix G. The increase of spring stiffness raises the resonance frequency while the increase in damping lowers the resonance frequency. For the damped system the damping becomes determinative resulting in resonance frequency which reduces with depth.

For the damped situation it is not possible to increase the penetration rate by vibrating at the resonance frequency of the system. The damping becomes too high and the system starts to behave overdamped resulting in no penetration of the system. This is in contradiction with the field test observations. An increase in frequency seemed to have a positive influence on the penetration. A explanation for this is that higher frequencies positively contribute to the development of excess pore water pressure, the degradation of the shear resistance and an improvement of the energy transfer of the steel element. In the model the parameters are independent of the dynamic frequency and are not able to mimic this behaviour.

Soft soil layers are characterized by low stiffness's and strong layers by high stiffness's. For high stiffness's the damping ratio increases and for low stiffness's the damping ratio decreases. As the element reaches the first soft silty sand layer the value for the damping ratio decreases and becomes smaller than 0.707. At this point the resonance frequency rises to around 15 Hz. As the element penetrates the soil the damping increases due to the increase of shaft area that comes in contact with the soil and resonance frequency is lowered to a value of zero again. The effect of the damping on the resonance frequency is clearly visible. Together with the results obtained using no damping one can see that the damping predominates the resonance frequency.

# 11

## Discussion

The dynamic process of the installation of elements is considered to be very complex and is not fully understood yet. A model is developed to better understand the process and make estimation of the expected installation time for an element in certain soil profile. The overall reliability of the model is considered to be low as there is no clear routine of the factors  $\alpha$  &  $\beta$ , but can give a first approximation. One should be aware that the knowledge about the high frequency drilling is still limited at the moment. This thesis only focusses on the contractive soils which respond undrained to cyclic loading.

The final conclusion is based on the field test results, the model and the soil conditions. Relevant aspects and shortcomings for each of them is discussed separately in this chapter.

### 11.1 Field test

The test was performed in a week of extremely bad weather. Because of this bad weather it was difficult to monitor all the data. One of the shortcomings is the absence of information about the static load that was applied over time at the different tests. It seems clear that the applied load was not kept constant. The influence of the static load on the penetration rate is considered to be significant. A data log with the static load over time would greatly improve the model results.

At some tests the installation process was put to a halt to realign the crane leader. During realignment the load was removed, and the vibrations were stopped. After realignment of the crane leader the load and vibrations were reapplied. The magnitude of the load and the frequency of the vibration were changed to enhance the penetration rate. The changes that were applied during these events were not explicitly registered.

The location at which the field test was performed is characterized by a large spread of different soil characteristics. Especially the first 4 meters of soil show large deviations in cone resistance throughout the field. This made the comparison between different tests at different locations difficult.

The magnitude of the vibrations in the close vicinity of the elements ( $d < 2\text{m}$ ) are uncertain due to errors in the geophone data. Even in the geophones at greater distance there are significant amount of errors in the data present. The exact frequency of vibration is also uncertain. The geophones measured different frequencies even though the vibrator was vibrating at a constant frequency. The geophone installed at a radial distance of 10 meters from the vibratory source was not capable of measuring the particle acceleration. The excess pore water pressure it assumed to be totally dissipated as the element is retracted from the soil. So, no further deformations were expected.

The installation per meter length of the element was monitored by using a stopwatch. The penetration rate within this meter might fluctuate. This is not taken into account.

To reach the different test locations the crane had to drive over the other locations. The large load of the crane together with the vibrations might influenced the soil characteristics. The degree of influence of the crane on the soil conditions is not elaborated.

The open-ended 300 mm element suffered from plug formation. The behavior of plugged is more in line with a closed-ended element. The difference in penetration resistance between the open-ended elements and closed-ended elements was therefore not noticeable from the field test and no conclusion on the different values of alpha and beta in the model can be drawn.

## 11.2 Model

The model is a simplification of the reality and therefore has limited usage. The model does not capture the complex behavior of waves traveling through the soil and element. The zone of plastic deformation depends on the degree of development of excess pore water pressure. The increase of pore water pressure is the results of pressure waves. The attenuation of pressure waves in the surrounding soil does greatly affect this process. Wave propagations in the element can have influence on the penetration rate as well. Especially at higher frequencies ( $f \rightarrow f_{\text{natural}}$ ) this effect becomes significant but is not captured by the model.

The model does not explicitly take the displacement of the soil into account. Extra volume is added to the soil as the element penetrates the soil. Depending on the type of soil and displacement this can lead to hardening or softening of the soil.

The model uses the CPT data to obtain the parameters needed for the model to work. The different CPT's show large deviations within the test field. The used CPT data might not be representative for the soil conditions that can be found at the location where the element was installed. This result in a deviation between model results and field test results.

The correlations proposed by Robertson are developed for normally consolidated uncemented silica sands with low fines content. These correlations between the CPT data and the soil parameters do not have any theoretical background as they are purely empirical. The relations between the cone resistance and other parameters is strongly influenced by other parameters such as: fine content, intergranular friction, horizontal and vertical stresses, mineralogy, compressibility and crushability and over consolidation ratio.

The static resistance against penetration underneath the pile tip is calculated using the average cone resistance over a length of two times the diameter of the element. Methods used for the determination of the static bearing capacity of the pile tip show a similar approach. The influence zone of in these methods is often larger and do take the soil above the pile tip into account. The dynamic behavior of the element does not allow the soil to redistribute the force over a larger area and therefore a smaller influence zone is justified. The exact zone of influence might be different and changing at different soil types. See also Appendix C.

The damping from internal mechanisms of the element are neglected. The damping is considered to be much smaller than the damping obtained from the surrounding soil and is therefore neglected (Novak, 1974).

The model uses constant elastic stiffness parameters while the system undergoes plastic deformation. Large strains will affect the stiffness of the soil. The sensitivity analysis show that the stiffness greatly affects the penetration rate of the system. In other studies, a residual strength is chosen to be the maximum allowable shear resistance. This model uses the stiffness as input parameter and therefore the stiffness degradation seems more logical.

The model uses the same mathematical approach for both closed as open-ended elements. The model seems to work better at open type of elements than for closed ones. The different response of open-ended and closed-ended becomes evident by using different sets of alpha and beta. The available data to validate the model is limited and therefore no clear difference between the simulation of open-ended and closed-ended elements can be seen.

The influence of water is not approached separately. At cyclic loading the water pressure increases resulting in a degradation of the shear resistance. The degradation of shear resistance is captured by the factors alpha and beta together with other processes that still need to be identified properly. The degradation is dependent on the frequency of the cyclic loading and load- and displacement amplitude. In this current model this is not taken into account.

The formula's to obtain the values for the different model components were not originally intended to describe high frequency loading. The formulation for the damping at the tip proposed by Lysmer underestimates the amount of damping that occurs. The formulation proposed by Lysmer provides the damping at low frequency vibrations and relatively small displacements at homogenous soil conditions. The model is used for high frequency vibrations and large displacements on inhomogeneous soil conditions. The factor  $\beta$  is used to increase the amount of damping to make the model correspond more to the field test results. An increase in amount of damping with an increase of frequency is in agreement with the findings of Dash et al. (Dash & Sitharam, 2016).

The model describes a one-dimensional problem. Mechanism in the horizontal plane are not taken in consideration. The model assumes that there is always contact between the soil and the element.

The model uses larger strain stiffness. The small strain stiffness can be 20 times higher than the stiffness at large strains. The strain per loading cycle is minimal is considered to be very small however the time between each cycle is also very small. The displacement over time is similar to a case where just a static load is applied. Furthermore, the stiffness degrades as result of the development of EPP.

There are only displacements after the static resistance is exceeded. In reality there are often minor displacements before this load is reached. These extra displacements are not taken into account by the model.

The model assumes that during the installation the sonic vibrator always vibrated at its maximum frequency. It should be mentioned that this was not always the case. During the different tests the frequency varied between the 140Hz and 180Hz. The sensitivity analysis shows that the frequency in that particular range has minimal influence on the penetration rate and therefore the use of 180Hz in the model for all the tests is justified.

### **11.3 Soil**

To obtain values for the Poisson ratio the assumption is made that the soil is normally consolidated. For hydraulic fills this assumption is justified as the soil never experienced higher stresses than the current stress acting on the soil.

The soil parameters are determined using the CPT data belonging to the test location. The CPT data used might deviate from the soil characteristics at the exact test location. This will directly influence the model results. The deviation can be appointed to the fact that the elements were not exactly installed on the same spots as were the CPT data taken. From the different CPT data it can be seen that the soil at Centrumeiland is very inhomogeneous. The CPT represents an entire test location while there might be great differences in cone resistances within the test field. The first few meters of soil contain large pieces of debris, see appendix D. These pieces will negatively influence the CPT results. Besides that the ground surface at the test location was also not entirely flat. During the different tests it was assumed that the elements were installed from the same level of ground surface as the CPT. There might be a difference in ground surface. However, this difference is considered to be minimal and therefore neglected. When the cone penetrates the soil, it might happen that the cone starts to undergo an inclination. The influence of this inclination on the CPT data is not taken into account. Next to the inclination of the cone the installation speed influences the results this also plays a minor role in obtaining wrong data. Finally, incorrect data may arise in unsaturated zones as a result of the presence of inherent cohesion. This effect however will be minimal.

# 12

## Conclusion

### **General conclusion**

Conventional densification techniques face difficulties when penetrating hard soil layers to reach the loosely packed layers. A technique that is capable in penetrating hard types of soil is the sonic drill technology. By increasing the penetration rate through hard soil layers the total densification process can be shortened, this will eventually reduce the costs. The sonic drill installation itself is not able to densify the surrounding soil. Once on depth, a conventional vibro-densification method can take over the densification process of the soil.

The sonic drill technology uses high frequency vibrations up to 180Hz to strongly reduce soil resistance. The resistance of the element against penetration is reduced by liquefaction, inertia effects and a temporary reduction of porosity of the soil.

Field test results show that the system is able to easily penetrate soil layers with cone resistances up to 40 MPa with minimal disturbance to the surroundings.

### **Theoretical concepts sonic driving**

A Sonic vibrator transfers a high frequency displacement at the top of an element via a rigid connection. The back and forth movement of the vibrator is repeated periodically, creating sinusoidal compressive and expansive pressure waves. The elasticity together with the inertial properties of the element allow the waves to propagate through the element. As the pressure waves travel through the element, they become partially transmitted to the surrounding soil. Shear waves and compression waves propagate in a spherical wave front from the pile toe. At the sides of the pile mainly vertical shear waves are transmitted. The shear waves travel outwards over a conical wave front.

As the pressure wave propagates from the source to the surrounding soil energy is lost and the wave amplitude decreases. The attenuation of wave amplitude is also known as decay and can be appointed to scattering, radial damping and proper damping.

The pressure waves develop liquefaction of the soil underneath the tip of the element.

Liquefaction causes the soil to lose a large percentage of its shear resistance.

Liquefaction of the surrounding soil is induced by flow liquefaction and cyclic mobility, depending on the confining stress and the void ratio. In both cases it gives rise to a net development of EPP. The moment the pore water pressure increases the effective stress decreases. The build-up of EPP is dependent on the stress/strain amplitude, cyclic frequency, initial effective stress and the number of cycles applied to the soil. At the sides, inertial effects prevent the soil from sticking. Furthermore, a reduction in shaft resistance can be appointed to friction fatigue. During friction fatigue the vibrations cause the soil in the vicinity of the element to lose its initial structure and start to densify locally. The densification decreases the horizontal stress acting on the element and lowers the shear resistance. The strong reduction in resistance enables the element to penetrate through hard soil layers.

### **Modelling pile installation**

A mathematical model is developed to simulate the installation process. In the model the surrounding soil behaves as a Bingham viscoelastic viscoplastic material. The soil behaves viscoelastic until it reaches a certain yield stress. As the stress becomes larger than the yield stress it starts to behave viscoplastic.

The model is able to fairly well describe the installation process on the basis of only CPT data. As input arguments the model needs the shear modulus, the Poisson ratio and the specific weight of the soil. These parametric values are obtained using CPT correlations proposed by Robertson. These are used to obtain the values for the dashpots ( $c_e$  &  $c_f$ ), spring( $k$ ) and friction slider ( $F$ ). As the element penetrates the soil the value for the damping  $c_e$  and the spring stiffness  $k$  accumulates as a result of an increasing contact area between the element and the soil.

The response of soft soil to cyclic loading differs from the response of hard soil. Soft types of soils are more likely to suffer from flow liquefaction, while hard soils will suffer from cyclic mobility. Flow liquefaction results in a fast loss of shear resistance and therefore a reduction in stiffness at soft soil layers is applied.

The static resistance against penetration is obtained by multiplying the interface area of the element with the local cone resistance. A reduction factor alpha is introduced to scale down the resistance. The reduction factor alpha comprises the influence zone around the pile tip, the type of pile and the shape of it. The greatness of alpha determines the degree at which the model responds to strong layers. The damping of the soil surrounding the tip of the element is approached with the parameter  $c_f$ . An amplification factor of  $\beta$  is needed to make the model better fit with the reality. The factor beta comprises an increase of damping due to the use of high frequencies, development of EPP and large plastic strain.

The total resistance is the sum of the friction along the shaft and at the tip of the element. The more the element penetrates the soil the larger the contribution of the shaft to the total resistance. Around 25% of the total damping in strong layers can be attributed to the shaft. In weak layers the contribution can be as high as 70%. For the spring stiffness applies that in strong soil layers the contribution of the shaft is around 15% and in weak layers around 80%. These values highly depend on the penetrated depth and on the local soil conditions.

### **Practical approach**

The possibilities of further optimizing the process have been examined. Increasing the pull down/static load and the elongation of the element are not feasible with the current crane setup or needs further investigation. The test results show that the addition of water increases the penetration rate. However, it washes out the fines which can have negative influence on the long term stability of the soil. The frequency used during installation can be modified to enhance the penetration rate. The use of the resonance frequency of the system increases the relative displacement of the mass. As the spring stiffness increases the resonance frequency increases too, while the resonance frequency decreases with increasing amount of damping.

For the damped situation it is not possible to increase the penetration rate over the long run by vibrating at the resonance frequency of the system. During penetration the damping becomes too high and the system starts to become overdamped. This reduces the resonance frequency to 0 Hz.

# 13

## Recommendations

This research mainly focusses on better understanding the sonic drill process. The element/soil interaction is considered to be very complex and not well understood. A simple mathematical model is developed to better understand the principles behind Sonic drilling and to improve the penetration process. The results look very promising. However, there are still numerous points that require extra attention and/or need further investigation. A few of the most pressing opportunities for improvement or further investigation are elaborated.

As been mentioned before the current sonic drill setup is not able to densify the surrounding soil. Nevertheless, it showed great success in penetrating strong soil layers. To make the setup applicable for densification I would recommend installing an extra vibrator. This vibrator should be able to vibrate at low frequencies (10-20 Hz). The vibrator can either be an external vibrator or internal vibrator. The best results can be obtained with an internal vibrator which is capable in vibrating in horizontal direction. The possibilities to improve the crane setup should be further investigated.

To be able to better calibrate the model and better understand the factors  $\alpha$  &  $\beta$  more field tests need to be performed. It is highly recommended to perform these tests at a test location with more homogeneous soil conditions. During those tests more detailed information about the pulldown load and vibration frequency need to be monitored. Additionally, pressure transducers can be installed on the element to register the development of EPP. The contribution the EPP to the degradation of shear resistance is significantly and is therefore of enormous importance. By measuring the friction along the shaft of the element more insight in the development of friction fatigue can be given. In case the shaft friction is known its contribution to the total resistance can be calculated. The ratio between point resistance and shaft resistance is from high interest when calibrating the mathematical model.

Additional geophones at different depths makes is possible to better distinguish pressure waves generated by the tip and the shaft of the element. In this way more information on how the sonic drill process influences the surroundings can be obtained.

The parameters needed for the model to simulate the penetration of a certain element are obtained using the CPT data. The value for the stiffness is constant and not dependent on the strain and development of EPP. Strain and EPP dependency of the stiffness parameter would greatly improve the accuracy of the model.

# 14

## References

- Abel, M., 2014. *Material nonlinearity*. [Online]  
Available at: <https://wiki.csiamerica.com/display/kb/Material+nonlinearity>  
[Accessed 2017].
- Araei, A., Razeghi, H., Tabatabaei, S. & Ghalandarzadeh, A., 2012. *Loading frequency effect on stiffness, damping and cyclic strength of modeled rockfill materials*, s.l.: Soil Dynamics and Earthquake Engineering, Elsevier.
- Ardoino, F., Bertalot, D., Piatti, C. & Zanoli, O., 2014. *Effect of pore pressure build-up on the seismic response of sandy deposits*, Genoa, Italy: D'Appolonia S.p.A..
- Ashmawy, A. K., Salgado, R., Guha, S. & Drnevich, V. P., 1995. *Soil Damping and Its Use in Dynamic Analyses*. Missouri, Missouri University of Science and Technology.
- Baker, H., 2010. *Vibro Systems*, -: Hayward Baker; A Keller company.
- Barkan, D., 1962. *Dynamics of bases and foundations*. New York: McGraw-Hill.
- Barkan, D. D., 1963. *Méthodes de vibration dans la construction*, Paris: Dunod.
- Bauer, 2014. *Soil Improvement*. s.l.:s.n.
- Baziar, M., Shahnazari, H. & Sharafi, H., 2010. *A laboratory study on the pore pressure generation model for Firouzkooh silty sands using hollow torsional test*, s.l.: International Journal of Civil Engineering.
- Berghe, J. F. V., 2001. *Sand strength degradation withing the framework of vibratory pile driving*, Louvan: s.n.
- Berghe, J. F. V. D., 2001. *Sand strength degradation withing the framework of vibratory pile driving*, Louvan: s.n.
- Bolton, M. D. & Wilson, J. M. R., 1990. *Soil stiffness and damping*, Rotterdam: Balkema.
- Booker, J., Rahman, M. & Seed, H., 1976. *A computer program for the analysis of pore pressure generation and dissipation during cyclic or earthquake loading*, Berkeley, Calif: Earthquake Engineering Research Center, Univiversity of California at Berkeley.
- Bornitz, G., 1931. *Über die Ausbreitung der von Groszkolbenmaschinen erzeugten Bondenschwingungen in die Tiefe*. Berlin, Springer.
- Borrow, J. C., 1994. The Resonant Sonic Drilling Method: An innovative Technology for Environmental Restoration Programs. *Groundwater Monitoring & Remediation*, vol 14(Issue 2), pp. 153-160.

- Boskalis, 2013. *Land reclamation artificial island, Punta Pacifica*. [Online]  
Available at: <https://boskalis.com/about-us/projects/detail/land-reclamation-artificial-island-punta-pacifica.html>
- Brinkgreve, R., 2015. *The role of water in soil behavior*. s.l., s.n.
- Brinkgreve, R., 2016. *Small-strain and cyclic loading behavior*, s.l.: s.n.
- Broms, B. B., 1991. Deep Compaction of Granular Soils. In: *Foundation Engineering Handbook*. s.l.:s.n.
- Broms, B. B. & Hansson, Ö., 1984. Deep compaction with the Vibro-Wing method.
- Brown, R. & ASCE, M., 1977. Vibroflotation Compaction of Cohesionless Soils.
- Brown, R. E. & Glenn, A. J., 1976. Vibroflotation and Terra-Probe comparison. Volume 102.
- Castro, G. & Poulos, S. J., 1977. Factors affecting liquefaction and cyclic mobility. *Journal of the Geotechnical Engineering Division*, Volume 103.
- Caterpillar, 2017. *large excavator*. [Online]  
Available at: [http://www.cat.com/en\\_US/products/new/equipment/excavators/large-excavators/1000026487.html](http://www.cat.com/en_US/products/new/equipment/excavators/large-excavators/1000026487.html)  
[Accessed 18 May 2017].
- Chang, C., Kuo, C. & Selig, E., 1983. *Pore Pressure Development during Cyclic Loading*. s.l., ASCE.
- Chern, S. & Chang, T., 1995. *Simplified Procedure for Evaluating Soil Liquefaction Characteristics*. s.l., Journal of Marine Science and Technology, pp. 34-42.
- Converse, F. J., 1950. *Soil Combaction by vibration*, s.l.: s.n.
- Dash, H. & Sitharam, T., 2016. *Effect of frequency of cyclic loading on liquefaction and dynamic properties of saturated sand*. s.l., International Journal of Geotechnical, pp. 487-492 .
- Denies, N., 2010. *Dynamic Behavior of Vibrated Dry Sand*, s.l.: s.n.
- Diaz-Rodriquez, J. & López-Molina, J., 2008. *Strain Thresholds in Soil Dynamics*. Beijing, China, World Conference on Earthquake Engineering.
- DU, S. & Chian, S., 2015. *Excess Pore Pressure Generation in Sand Under Non-Uniform Strain Amplitudes*. Christchurch, New Zealand: 6th International Conference on Earthquake Geotechnical Engineering.
- Elgamala, A., Yang, Z., Parra, E. & Ragheb, A., 2002. *Modeling of cyclic mobility in saturated cohesionless soils*. 19 ed. s.l.:International Journal of Plasticity.
- Evgin, E. & Fakharian, K., 2001. Cyclic degradation of shaft resistance for piles embedded in silica sand. In: s.l.:Department of Civil Engineering, University of Ottawa, Ont., Canada, pp. 1069-1072.

- Faccioli, E., 1972. A stochastic model for predicting seismic failure in a soil deposit. Volume Vol. 1, pp. 293-307.
- Fellin, W., 2000. *Deep Vibration Compaction as Plastodynamic Problem*. s.l.:s.n.
- Fellin, W., Hochenwarter, G. & Geiß, A., 2002. On-line compaction control in deep vibratory compaction. In: *Vibratory Pile Driving and Deep Soil Compaction*. Lisse: Swets & Zeitlinger.
- Gazetas, G., Dobry, R. & Tassoulas, J. L., 1985. *Vertical Responce of Arbitrarily Shaped Embedded Foundations*, s.l.: ASCE.
- Green, R., 2001. *Energy-Based Evaluation and Remediation of Liquefiable Soils*, s.l.: Department of Civil and Environmental Engineering .
- Griffith, C. J., 1991. *Soil Improvement Through Vibro-compaction and Vibro-replacement*, s.l.: University of Maryland, Department of Civil Engineering.
- Hölscher, P., 1992. *Numerical simulation of a fluid-saturated soil under a dynamically loaded pile*, Delft: s.n.
- Ishihara, K., 1986. *Evaluation of Soil Properties for Use in Earthquake Response Analysis.*, Rotterdam, Netherlands: A.A. Balkema Publishers.
- Jamiolkowski, M. & Pasqualini, E., 1992. Compaction of Granular soils - Remarks on Quality Control. In: *Grouting, Soil Improvement and Geosynthetics*. s.l.:s.n.
- Janes, M., 2009. Sonic Pile Driving; The history and the resurrection of vibration-free pile driving. *Piling Canada*.
- Kim, D. & Lee, J., 1999. *Propagation and attenuation characteristics of various ground vibrations*. Taejon, South Korea, Department of Civil Engineering, Korea Advanced Institute of Science and Technology, pp. 305-701.
- Kramer, S. L., 1996. *Geotechnical Earthquake Engineering*. New Jersey: Prentice Hall.
- Lee, K., 2001. Influence of placement method on the cone penetration resistance of hydraulically placed sand fills. Volume 38, pp. 592-607.
- Lenart, S., 2008. *The use of dissipated energy at modeling of cyclic loaded saturated soils*, s.l.: ResearchGate.
- Li, X. & Ming, H., 2000. Unififed modeling of flow liquefaction and cyclic mobility. Volume Vol.19, pp. 363-369.
- Lucon, P. A., 2013. *Resonance: The science behind the art of sonic drilling*, Bezman, Montana: Montana State University.
- Lunne, T. & Christofferson, H., 1983. *Interpretation of Cone Penetrometer Data for Offshore Sands*. Houston, Texas, Offshore Technology Conference.

- Lysmer, J., 1965. *Vertical motion of rigid footings*, Vicksburg, Mississippi: U.S. Army Engineer Waterways Experiment Station, Corps of Engineers.
- Massarch, K. R., 1990. *Deep Soil Compaction Using Vibratory Probes*. Philadelphia, American Society for Testing and Materials.
- Massarch, K. R., 1991. *Deep Soil Compaction Using Vibratory Probes*. Philadelphia, ASTM Special Technical Publication.
- Massarsch, K. R. & Fellenius, B. H., 2015. Chapter 4 - Deep Vibratory Compaction of Granular Soils. In: *COMPACTION, GROUTING AND GEOSYNTHETICS*. s.l.:Elsevier, pp. 111-135.
- Massarsch, K. R. & Westerberg, E., 1995. *The Active Design Concept Applied To Soil Compaction*. Singapore, s.n.
- Mitchell, J. K., 1981. *Soil Improvement*. Stockholm, s.n.
- Mitchell, K. J. & Katti, R. K., 1981. *Soil Improvement, state of the art report*. Stockholm, s.n.
- Nicholson, P., 2015. Chapter 6 - Deep Densification. In: *Soil Improvement and Ground Modification Methods*. s.l.:Elsevier, pp. 115-147.
- Novak, M., 1974. *Dynamic Stiffness and Damping of Piles*. London: Faculty of Engineering Science. University of Western Ontario.
- Oztoprak, S. & Bolton, M., 2013. Stiffness of sands through a laboratory test database. 63(No. 1).
- R.J.Jardine, F.C.Chow, R.F.Overy & J.R.Standing, 2005. *ICP design methods for driven piles in sand and clays*, s.l.: ICE publishing.
- Rahman, M. & Jaber, W., 1986. A simplified drained analysis for wave-induced liquefaction in ocean floor sands. Volume Vol.26, pp. 57-68.
- Rascol, E., 2009. *Cyclic Properties of Sand: Dynamic Behaviour for Seismic Applications*, Suisse: École Polytechnique Fédérale de Lausanne.
- Rinne, N., 1985. *Evaluation of interface friction between cohesionless soil and common construction materials*, s.l.: Department of Civil Engineering, The University of British Columbia.
- Robertson, P., 2010. *Soil behaviour type from the CPT: an update*. Huntington Beach, CA, USA, s.n.
- Robertson, P., 2015. *CPT Guide*, s.l.: s.n.
- Robertson, P., Campanella, R., Gillespie, D. & Greig, J., 1986. *Use of Piezometer Cone data*. s.l., ASCE.
- Rodger, A. & Littlejohn, G., 1980. Study of vibratory driving in granular soils. *Geotechnique*, Vol.30(no.3), pp. 269-293.

- Saito, A., 1977. Characteristics of Penetration Resistance of a Reclaimed Sandy Deposit and their change through Vibratory Compaction. No. 4(Vol. 17).
- Salm, R. v. d., Hölscher, P. & Snethlage, A., 2012. SBR-A richtlijn niet eenduidig voor trillinggevoelige funderingen.
- Sassa, K., Wang, G., Fukuoka, H. & Vankov, D., 2005. *Shear-Displacement-Amplitude Dependent Pore-Pressure Generation in Undrained Cyclic Loading Ring Shear Tests: An Energy Approach*, s.l.: ASCE.
- Sathialingam, N. & Kutter, B. L., 1989. *The effects of high strain rate and high frequency loading on soil behavior in centrifuge model tests*, Arlington: Office of Naval Research.
- Seed, H. & Idriss, I., 1971. *Simplified procedure for evaluating soil liquefaction potential*. 97 ed. s.l.:Journal of the Soil Mechanics and Foundations Division.
- Seed, H., Martin, P. & Lysmer, J., 1976. Pore Water Pressure Changes During Soil Liquefaction. *Journal of Soil Mechanics and Foundations Division, ASCE*, Volume Vol. 97.
- Sekowski, J., 1992. Investigations on Influence of Vibration Parameters on Compacting of Cohesionless Soils. In: *Grouting, Soil Improvement and Geosynthetics*. s.l.:s.n.
- Senneset, K. & Nestvold, J., 1992. Deep compaction by Vibro Wing Technique and Dynamic Compaction. In: *Grouting, Soil Improvement and Geosynthetics*. s.l.:s.n.
- Skempton, A., 1948. *The  $\phi = 0$  Analysis of stability and its theoretical basis*, s.l.: In Proceedings of the 2nd International.
- Skempton, A., 1954. The pore-pressure coefficient A and B. Vol. 4(no. 4), pp. pp. 143-147.
- Thiers, G. & Seed, H., 1968. *Cyclic stress strain characteristics of clay*. s.l.:Soil Mechanics and Foundations Division, ASCE.
- Tokimatsu, K. & Yoshimi, Y., 1983. *Empirical Correlation of Soil Liquefaction Based on SPT N-Value and Fines Content*. 23 ed. s.l.:Soil and Foundations, JSSMFE.
- Verbeek, G., Middendorp, P., Dorp, R. V. & Tara, D., 2005. Pile driving analysis and vibro hammers: a viable combination. pp. 57-59.
- Vermeer, P. A. & Meier, C. P., 1998. *Stability and deformations in deep excavations in cohesive soils*. Darmstadt, s.n.
- Verruijt, A., 2001. *Soil Mechanics*. s.l.:Delft University of Technology.
- Verruijt, A., 2008. *Soil Dynamics*. s.l.:Delft University of Technology.
- Viking, K., 2002. *Vibro-driveability- A field study of vibratory driven sheet piles in non-cohesive soils*. Stockholm, Sweden, Department of Civil and Architectural Engineering.

- Viking, K. & Bodare, A., 1998. *Laboratory studies of dynamic shaft resistance response of a vibro-driven model pile in granular soil by varying the relative density*. s.l., Proc. to XII European Conference on Soil and Foundation Engineering.
- Voznesensky, E. A., Kushnareva, E. S. & Funikova, V. V., 2011. *The Nature and Patterns of Damping of Stress Waves in Soils*, Moscow: Moscow State University.
- Vucetic, M., 2005. *CYCLIC THRESHOLD SHEAR STRAINS IN SOILS*, s.l.: ASCE.
- Waarts, P. & Ostendorf, C., 2006. *Schade aan gebouwen-Deel A uit de Meet- en beoordelingsrichtlijn: Trillingen*. s.l.:SBRCURnet.
- Wallays, M., 1982. *Deep Compaction by Casing Driving*. Bangkok, s.n.
- Wang, H., 1994. *Experimental study and finite element analysis of driveability and static behaviour of various piles installed by vibratory driving*, Houston, Texas: Faculty of the Dep. of Civil and Environmental Engineering, University of Houston.
- Warrington, D. C., 1997. *Closed form solution of the wave equation for piles*, Chattanooga: The University of Tennessee.
- Welsh, J. P., 1991. Ground Modification.
- Westerberg, E., Massarch, K. R. & Eriksson, K., 1995. *Soil resistance during vibratory pile driving*. s.l., s.n.
- White, D., 2009. *A general framework for shaft resistance on displacement piles in sand*, s.l.: Cambridge University Engineering Department.
- Wijewickreme, D., Sanin, M. & Greenaway, G., 2005. Cyclic shear response of fine-grained mine tailings. Volume Vol.42, pp. 1408-1421.
- Yang, J. & Sze, H., 2011. Cyclic behaviour and resistance of saturated sand under non-symmetrical loading conditions. Volume Vol. 61, pp. 59-73.
- Yang, J., Wei, L. & Dai, B., 2015. *State variables for silty sand: Global void ratio or skeleton void ratio?*, s.l.: The Japanese Geotechnical Society.
- Zaalberg, R., 1985. *Het ecosysteem van het IJsselmeer, opbouw en bedreigingen*, s.l.: s.n.

# Appendices

## A Test results

### A.1 Test results

In the period of 27-2-17 until 8-3-17, on a reclaimed land site in Amsterdam, an innovative method for installing elements in dense and hard sand layers was tested. The method focuses on sonic drilling/installation with vibrations up to 180Hz to reduce soil resistance whilst pushing the elements into the ground. This method has shown to generate less disturbances to the surroundings whilst achieving a higher penetration rate in comparison to conventional installation methods.

The tests were performed with an uniquely designed, relatively small crane, provided with a sonic drill generator that is able to push the elements with a load up to 10 ton. The vibrations were generated with a sonic vibrator developed by the company Eijkelkamp. The vibrator is known as the SonicSampDrill and is only able to transmit vertical vibrations onto the element.

The tests consist out of installing open and closed tubes with diameters of 300mm 400 mm and 800mm. During the tests measurements were made of the time needed for penetration and of the vibrations (using Geophones). CPTs were taken before and after the installation to compare the installation effects on density.

### A.2 Location

The tests were performed on a site of reclaimed land at the Pampusweg, Centrumeiland IJburg. At the north side of the island a test location of 100 X 45 meter was prepared.

The total area was split up into 15 different test locations. At each location a different type of test was performed. Each test consists out of three tests which are executed with the same type of element. The elements are installed in different ways to change their degree of influence.

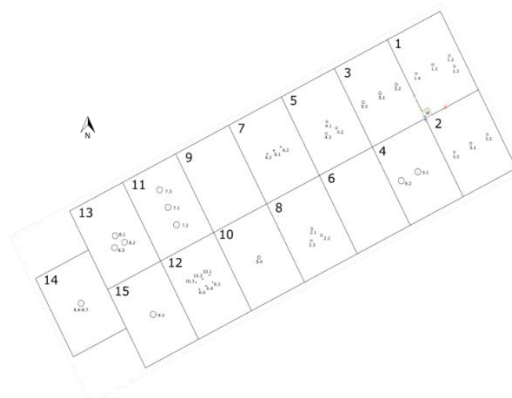


Figure A.1 Test field with test locations 1-15

### A.3 SonicSampDril

The SonicSamDrill generates high frequency vibrations and transmits them on the element via a rigid connection. The sonic generator is installed on the crane leader and has the following specifications:

**Table A.1 Sonic vibrator characteristics**

Type:	LargeRotoSonic (LRS)
Sonic frequency:	0-150Hz
Output dynamic force:	227kN/50k lbf
Rotation speed:	92rpm
Rotation torque clockwise:	8.900Nm@275bar/6.565ft-lbf@3.990psi
Rotation torque counter clockwise:	10.000Nm@310bar/7.375ft-lbf@4.495psi
Head tilt max:	90°
Type of damper:	Air cushion
Max hydraulic pressure on sonic:	310bar/5.000psi
Mass vibrator:	1250kg/2800lbf
Pull up force with sonic:	10.000daN/22.480lbf
Pull down force with sonic:	10.000daN/22.480lbf
Pull up force static:	10.000daN/22.480lbf
Pull down force static:	10.000daN/22.480lbf
Drilling angle:	80° and 10° of perpendicularly

### A.4 Elements

The following elements have been tested:

- Closed steel tube shaped vibroflot diameter 300 mm
- Open steel tube shaped vibroflot diameter 300 mm
- Closed steel tube shaped vibroflot diameter 400 mm
- Open dummy replacement flot diameter 800 mm
- Closed dummy replacement flot diameter 800 mm

The closed 300 mm and 400 mm and the open 800 mm were also used to test to ability to densify the soil with the help of low frequency vibrations. As the elements reached depth a lower frequency vibration (+/- 45 Hz) was used to densify the surrounding soil. The frequency was kept constant for 40 seconds. Table A.2 shows at which test location the different tests were performed and if low frequency vibrations were used to densify the surrounding soil.

**Table A.2 Test overview**

Test nr.	Description	Densification	Test location
Test1	Closed 300 mm		1
Test2	Closed 300 mm	X	8
Test3	Open 300 mm		2
Test4	Open 300 mm	X	5
Test5	Closed 400 mm		3
Test6	Closed 400 mm		10
Test9	Open 800 mm		11
Test10	Open 800 mm	X	13
Test11	Open 800 mm	X	14

<b>Test12</b>	Open 800 mm	X	4
<b>Test13</b>	Open 800 mm*	X	15
<b>Test18</b>	Open 300 mm**		6

\*executed in loosened soil

\*\*partly executed with a vacuum -0.45bar

## A.5 CPT

CPT's were performed by the company Inpijn-Blokpoel. On the 23th of February 2017 in advance of the test 15 CPT's were performed according to NEN-EN-ISO 22476-1. The CPT data consist out of the cone resistance and the local shaft friction. At CPT-3 and CPT-10 also the pore water pressure was registered.

On the 8<sup>th</sup> of March again 15 CPT's were performed to measure the installation effects on the density. The post CPT's were performed in test locations 5, 8, 11, 13 & 14.

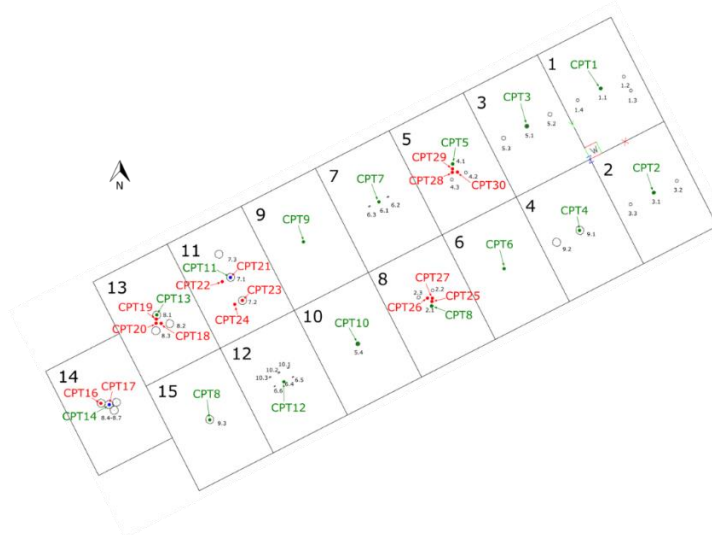


Figure A.2 CPT location, in advance of the tests (green) and afterwards (red)

The results of the Geotechnical investigation at the Pampuslaan show that the first 4 metres mainly consist out of dense/strong sand. Small interceptions of silty layers cause of reduction in cone resistance in the first 4 meters of soil. These thin silty layers are the result of segregation of grains that occurred during the hydraulic placement of the sand. The maximum cone resistance in the silty layer is around 10 MPa. In the sand layer the cone resistance rises to value of 20-30 MPa. CPT number 15 shows an even higher value for the cone resistance of 39.50 MPa. The soil at beneath a depth of -2 m NAP is dominated by silt. At -4 m NAP small interception of a clay layer can be found. The thickness of this layer varies throughout the area. The cone resistance in the silty layer is around 2 MPa and in the clay layer around 1 MPa.

The pore water pressure measurement show that the phreatic surface can be found at around -0.3 m NAP.

## **A.6 Time-Depth Registration**

During the installation of the elements the time for 1 meter length of penetration was recorded. Together with the CPT's data the applicability of the sonic drill to penetrate particular layers can be identified.

## **A.7 Execution tests**

In advance of each test the best test location was determined according to the CPT-data. The crane moves to that particular location and an element is installed onto the sonic drill. A wooden board is positioned next to the drill location. The crane leader is positioned on this board. This wooden board prevent that the crane leader sinks into the ground when pressure is applied. The crane leader ensures extra stability of the element during installation. As the elements are installed the pull down force can be changed. However, a higher pull down force result in less stability of the crane leader. There are two options in which the element can be installed:

- With pull down force limitations
- Without pull down force limitations

To ensure the stability of the crane leader the pull down force on the element is limited to 4 tons. As more force is applied to the element less pressure is taken by the crane leader. As result the crane leader starts to slip from the wooden board because it cannot obtain enough resistance when the normal force on the board is too low. However, the extra pull down force increases the penetration rate. The downside is that in case of slippage the installation has to be stopped to realign the leader with the element. This takes extra time. The maximum pull down force that can be achieved with this crane setup is 10 tons.

In some cases, water is used to enhance the penetration rate even further. Water was added with low pressure at the tip of the element. As the element penetrates the soil the water surrounds the element and reduce the friction along the length of the element.

## **A.8 Results**

### *Installation time*

The time-depth registration shows that the penetration of the first 4 meter takes the most time. This is in agreement with the CPT-data. The first 4 meters consist out of strong sandy layers with high values of cone resistance. In the next layers the time needed for the element to penetrate the soil decreases. The shortest time recorded was at the moment that the element reaches the clay layer. The low cone resistance can directly be related to a faster penetration time.

Table A.3 Installation data closed-ended element 300 mm

Test 1 Test location 1	Depth (m)	Cumulative installation time (s)	Installation time per meter length (s)	Removal time (s)
Test 2	1	22.01	22.01	10.70
	2	132.21	110.2	17.85
	3	159.12	26.91	23.93
	4	178.36	19.24	30.37
	5	183.8	5.44	36.65
	6	188.2	4.4*	42.87
	7	196.15	7.95	46.57
	7.5	201.73	5.58	49.63

\*start clay layer

The same conclusion can be drawn for the open-ended element. The lowest penetration time can be found when the element penetrates the clay layer.

Table A.4 Installation data open-ended element 300 mm

Test 3 Test location 2	Depth (m)	Cumulative installation time (s)	Installation time per meter length (s)	Removal time (s)
Test 1	1	15.6	15.6	10.48
	2	73.13	57.53	20.53
	3	125.78	52.65	28
	4	149.19	23.41	34.85
	5	158.26	9.07	41.41
	6	164	5.74*	47.74
	7	174.81	10.81	52.35
	7.75	185.76	10.95	56.08

\*start clay layer

From the data also appears that the installation time without the limited pull down force is reduced. However, the stability of the leader cannot be guaranteed. In some of the tests the leaders slipped off the wooden board and had to be realigned with the element again. This realignment takes extra time this is not included in the time-depth registration. In test nr. 3 water was added from the toe of the element to measure the influence of water on the installation time.

Table A.5 Influence conditions on installation time

Test1	Installation time (s)	test nr.
Limited pull down force	168.81 & 201.73	1 & 2
No pull down force limitation	113.66	2b
Addition of water	96.75	3

*Influence type of element*

As been mentioned before at the different test locations different tests have been performed. The CPT data from the different locations show a spread of cone resistances

throughout the area. Especially in the sand layers a large spread of cone resistances throughout the test area can be found. The cone resistance of the silty layers beneath the sand (<-4m NAP) do not show this large spread. To compare the installation time of different type of elements in this silty layer the influence of the type of element can be investigated. The installation time of the different type of elements at 5 to 7 meters of penetration is compared. The penetration corresponds to a depth of -3 m NAP up to -5 m NAP. Only the tests which were performed with limited pull down force are compared.

The results show that the 300 mm closed-ended element was installed in similar amount of time as the open version. This unlikely result is probably due to the maximum pull down speed of the motor. The resistance obtained during penetration was too little to affect the installation time at the closed 300 mm element in respect to the open version.

**Table A.6 Comparison closed/open-ended elements**

Type of element	Average installation time [5-7m] (s)	Notes
Closed 300 mm	20.42	Test 1 test location 1
Open 300 mm	25.62	Test 3 test location 2

A larger difference between the closed 300 mm and the closed 400 mm is noticeable. The large surface causes more resistance and leads to a larger installation time.

**Table A.7 Comparison diameter elements**

Type of element	Average installation time [5-7m] (s)	Notes
Closed 300 mm	20.42	Test 1 test location 1
Closed 400 mm	63.01	Test 5 test location 3

No comparison between the closed 800 mm with the closed 300mm and 400 mm is made because of the length of the element. The 800 mm tube has only a length of 4 meter and therefore does not reach the silt layer at -4 m NAP.

*Correlation cone resistance and installation time*

A correlation can be found when the installation time is plotted against the cone resistance. The data of only the first four meters is used because of the spread of cone resistance. A higher cone resistance leads to a lower penetration rate and thus a longer installation time. This relation can be found from the results obtained for Test 1 but also from the Test 5, 3 & 4, 9 & 10 & 11 and 18, see **APPENDIX1**

**Table A.8 Installation time vs cone resistance**

Test 1	Depth (m)	Average qc (MPa)	Installation time per test (s)			
			1.1	1.2	1.2b	1.3
1	4	39.04	22.01	28.14	6.97	
2	7	58.34	110.2	40.91	36.26	
3	6	22.82	26.91	16.84	24.67	
4	11	17.05	19.24	9.82	7	

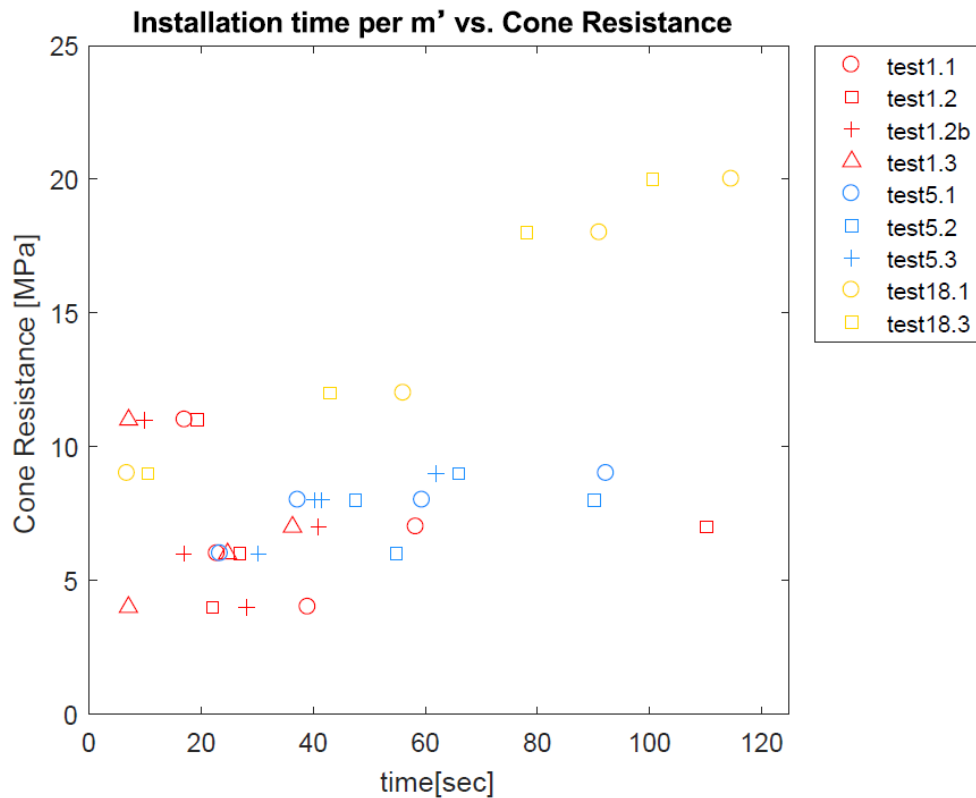


Figure A.3 Installation time per m' vs. cone resistance tests 1, 5 and 18

*Vibrations*

During the tests measurements were made of the vibrations using Geophones. The geophones record the particle acceleration, velocity and the frequency in x, y and z direction. The geophones were installed at 2m, 5m and 10 m distance from the vibratory source. The magnitude of the velocity and acceleration of the vibration wave tells something about the zone of influence. Both the acceleration as the velocity are frequency dependent.

Table A.9 Installation different geophones

Alignment test location 1	Geophone nr.	Radial distance to vibrating element
	428	2m
	458	2m
	15	5m
Alignment other test locations	458	2m
	428	5m
	15	10m

Results obtained at a distance of 2 meters from the element show too many errors in the data-log to be used for further processing. Therefore, the geophone installed at 5m distance is used to obtain the following results.

The following conclusions can be drawn:

- The particle velocity and accelerations decrease with distance from the element, the frequency of the vibration stays the same.
- Vibrations of 140 Hz were used to install the elements. The average particle velocity was 1.0-2.0 mm/s during the installation. See **APPENDIX 3**.
- During the densification process a frequency of 40-45 Hz was used to densify the surrounding soil. The frequency was kept constant for 40 seconds. The geophone at 5 meter distance recorded at particle velocity of only 2 mm/s, **APPENDIX 4**.
- Lower velocities were recorded when the pull down force was limited to 4 tons, **APPENDIX 5**.
- Lower velocities were recorded when water was used to reduce the friction, **APPENDIX 5**.
- High particle velocities were found when the elements were vibrated at 50 Hz. At 50 Hz resonance of the crane occurred, **APPENDIX 3**.

### *CPT*

The installation of the elements does not result to an increase of cone resistance according to the CPT data. Also the use of low frequency vibrations did not result in the densification of the surrounding soil. Some of the tests are further elaborated to explain this more extensively.

### **Test2**

Test location 8

Appendix 6

### Pre

The first 4 meters is dominated by sand with two peak values of 25 MPa. Between those peaks the average cone resistance is 15 MPa.

### Post

The vibrations created by the element resulted in a decrease of cone resistance at the peak values. In contradiction to the cone resistance an increase in shaft resistance can be seen at the layers beneath -2 m NAP. These layers are characterized by soft layers. The increase of shaft resistance is probably the result of plastic deformation of the soil.

### **Test4**

Test location 5

Appendix 7

### Pre

At a depth of 1 m NAP and -1 m NAP a strong sand layer can be found with a maximal cone resistance of 19 MPa.

Post

From CPT 28 & 30 an increase in cone resistance can be seen while at CPT 29 the cone resistance decreases. Remarkably for all the CPT's the shaft resistance increase. This is the result of plastic deformation in the horizontal plane.

**Test9**

Test location 11  
Appendix 8

Pre

From the data can be seen there is a strong layer at 0 m NAP. The maximum value for the cone resistance in this particular layer is 35 MPa.

Post

CPT were performed both on the exact test location as just next to the it. On test location 11 three open-ended elements with a diameter of 800 mm were vibrated into the ground. After the elements were removed some subsidence of the ground surface was visible. The subsidence of 25 cm only occurred inside the element. CPT 21 & 23 were performed in this hole, Figure A.. The data show an enormous reduction in cone resistance. The subsidence was therefore not caused by the densification of the soil but probably due to formation of a plug at the toe of the element. The soil clogs the element and enables the element to push the plug further into the ground. The soil inside the element becomes looser as result of the vibrations. Pushing the plug down into the ground causes a plastic deformation at -2 m NAP. The CPT data shows a small increase in cone resistance.

**Test10**

Test location 13  
Appendix 9

Pre

Two peak values in the first 4 meters of the ground, respectively 14 & 17 MPa.

Post

Over the entire length of the element a reduction of cone resistance can be found.

**Test11**

Test location 14  
Appendix 10

Pre

Two peak values in cone resistance can be found at a depth of 1 m NAP and -2 m NAP. Between the peak values a soft layer can be found with a cone resistance of only 1 MPa at 0 m NAP.

#### Post

The results show an increase of the cone resistance in the soft layer of 5 MPa. This increase in cone resistance is only visible in this CPT.

### **A.9 Conclusions**

The following conclusion can be drawn from the results:

- The post CPT data show that there was almost no increase in cone resistance as result of the vibrations. One can conclude that it was not possible for the crane to densify the soil.
- The test shows that the at further distances from the vibrator the value both the acceleration as the velocity of the particles decreases. This is due to the damping of the soil.
- The installation time of the elements reduces when more load is applied on the elements, 10 tons instead of 4.
- Reduction of the installation time when water is used to reduce the friction
- The same installation time for both the closed as the open 300 mm element are the result of the maximum driving force of the motor and probably not due to the resistance.
- A closed-ended element and a larger diameter element leads to a higher installation time
- High particle velocity can be found at 50 Hz. The rapid increase in particle velocity is caused by resonance of the crane.
- During the densification process low frequency vibrations of 40-45 Hz were used. The particle velocity did not exceed 2 mm/s. at a frequency of 50 Hz the velocity becomes 7 mm/s. The increase in particle velocity is not related to the surrounding soil but to the natural frequency of the crane. The crane starts to vibrate and transmits these vibrations onto the soil via the crane leader.
- In case of no limitation to the pulls down force lower velocities were recorded by the geophones. When there is maximum pull down force on the element there is limited load on the crane leader. The vibrations caused by the crane cannot be transmitted to the ground and therefore the geophones measure less particle velocities.
- The use of water leads to a reduction in particle velocity as well. The water damps the vibrations even more.
- Soil layers with low cone resistance causes were easier to penetrate for all the different type of elements.

## A.10 Appendices

### A.10.1 Appendix 1

Time registration vs average cone resistance for different tests. These data is used to obtain a correlation between the cone resistance and the installation time

Test 1	Depth (m)	Average qc (MPa)	Installation time per test per meter length (s)			
			1.1	1.2	1.2b	1.3
1	4		39.04	22.01	28.14	6.97
2	7		58.34	110.2	40.91	36.26
3	6		22.82	26.91	16.84	24.67
4	11		17.05	19.24	9.82	7

Test 3	Depth (m)	Average qc (MPa)	Installation time per test per meter length (s)		
			3.1	3.2	3.3
1	8		15.6	13.56	10.88
2	11		57.53	25.98	43.08
3	24		52.65	27.5	27.78
4	16		23.41	14.69	16.54

Test 4	Depth (m)	Average qc (MPa)	Installation time per test per meter length (s)		
			4.1	4.2	4.3
1	8		12.92	15.26	16.63
2	8		18.36	20.66	20.09
3	7		17.65	17.87	16.52
4	7.5		14	13.98	12.89

Test 5	Depth (m)	Average qc (MPa)	Installation time per test per meter length (s)		
			5.1	5.2	5.3
	1	6	23.37	54.84	30.19
	2	8	59.45	90.14	40.13
	3	9	92.32	65.88	61.83
	4	8	37.26	47.48	41.38

Test 9	Depth (m)	Average qc (MPa)	Installation time per test per meter length (s)		
			9.1	9.2	9.3
	1	4	25.87	26.43	40.96
	2	6	44.06	23.99	271.04
	3	20	219.55	38.36	319
	4	21			

Test 10	Depth (m)	Average qc (MPa)	Installation time per test per meter length (s)		
			10.1	10.2	10.3
	1	6	36.63	34.09	21.84
	2	7.5	34.42	149.35	28.83
	3	7	51.56	82.04	43.38
	4	11			

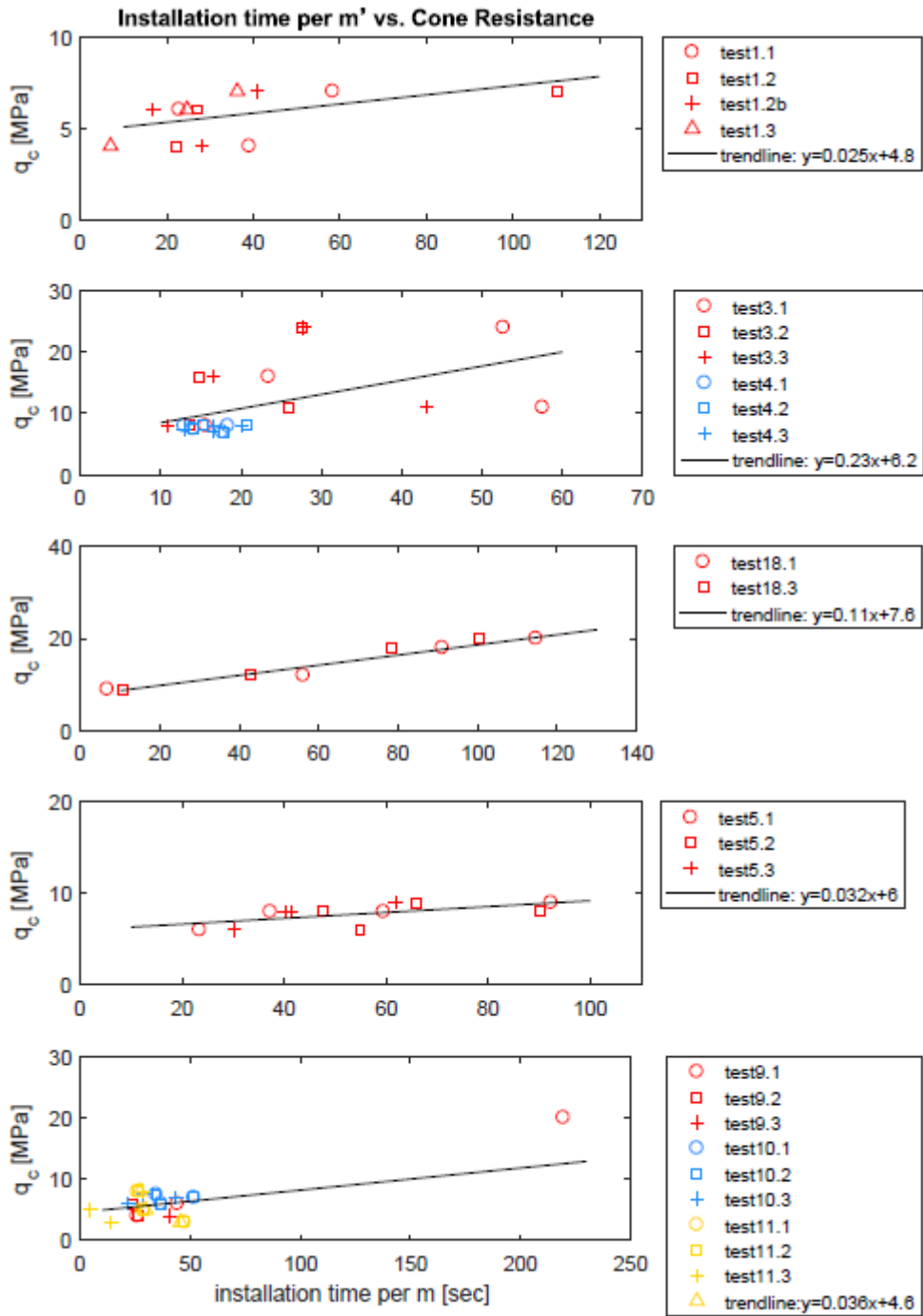
The additional value of a sonic drill in a new compaction method

---

Test 11	Depth (m)	Average qc (MPa)	Installation time per test per meter length (s)			
			11.1	11.2	11.3	11.4
	1	8	25.98	28.32	28.32	27.11
	2	5	28.48	32.79	4.47	29.76
	3	3	47.27	46.77	13.98	45.45
	4	14				

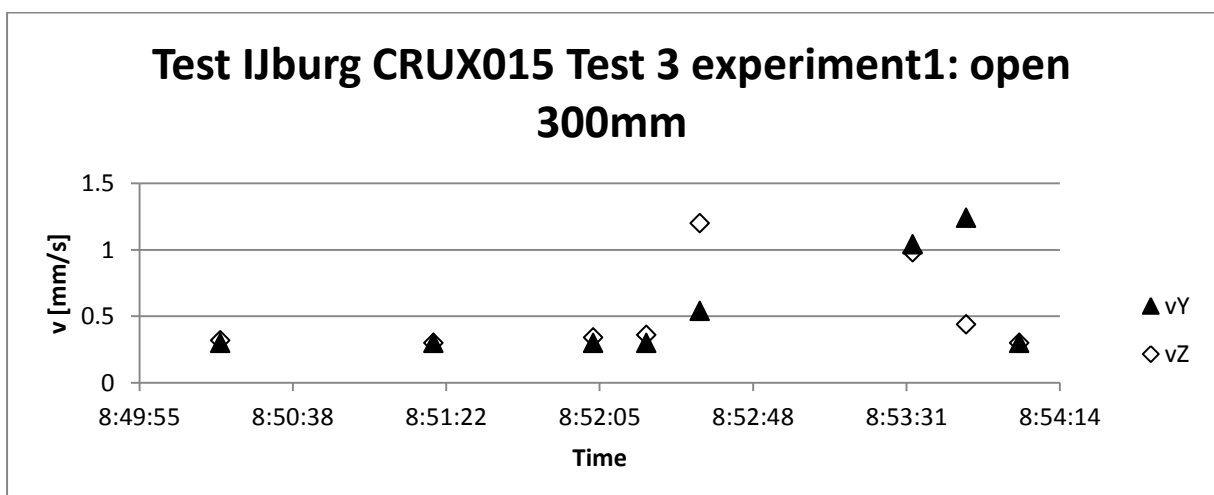
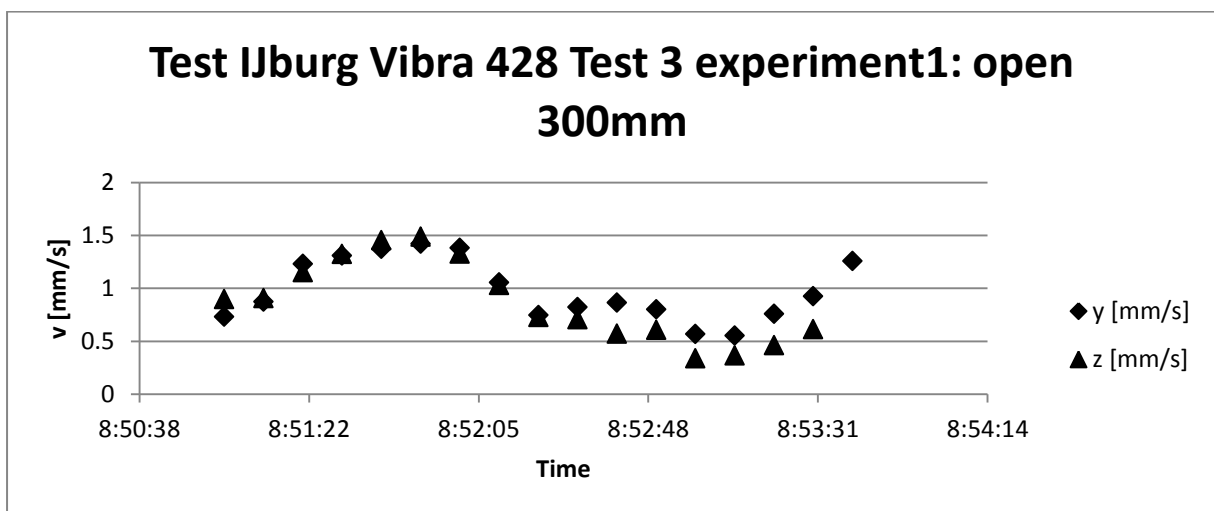
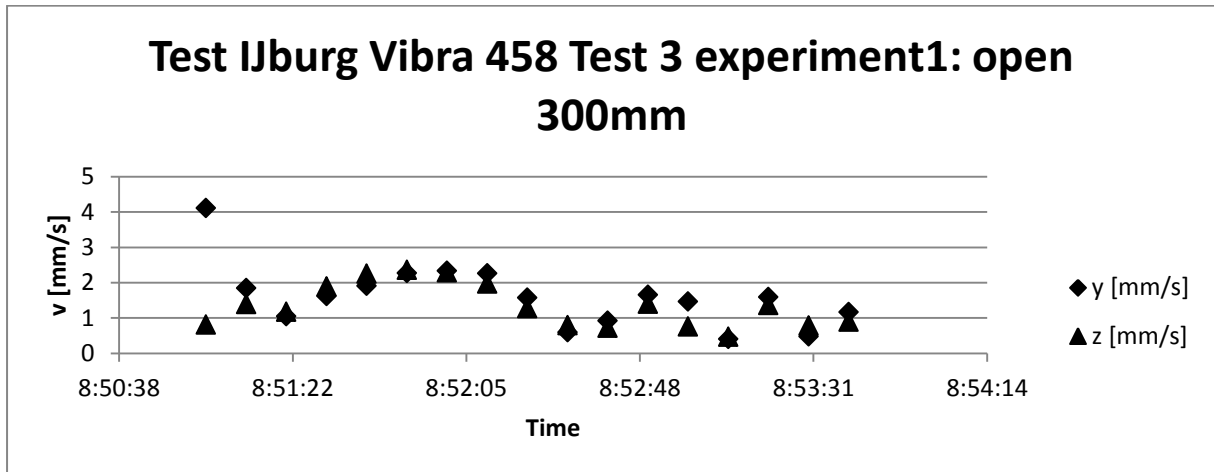
Test 18	Depth (m)	Average qc (MPa)	Installation time per test per meter length (s)		
			18.1	18.2	18.3
	1	9	6.75	-	10.49
	2	12	56.1	-	42.97
	3	18	91.11	-	78.13
	4	20	114.68	-	100.55

Correlations between the installation time and cone resistance.



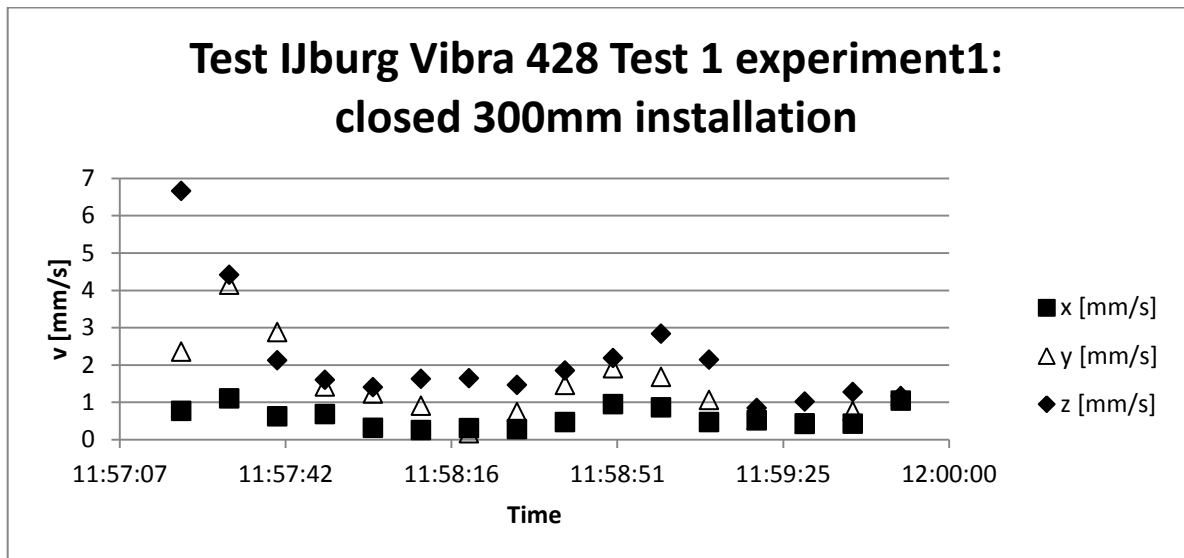
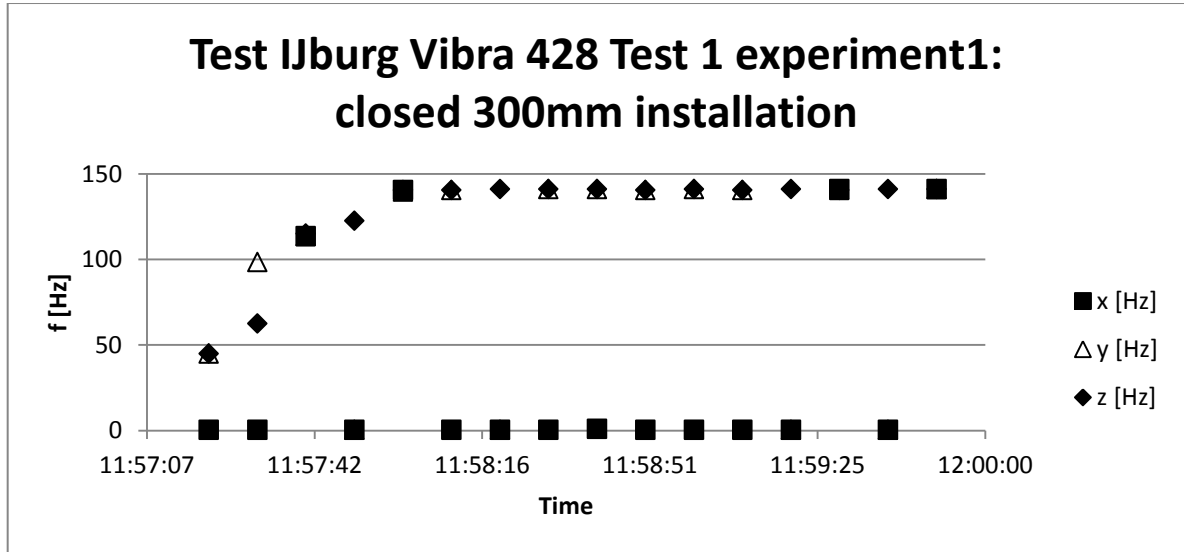
### A.10.2 Appendix 2

Decrease of particle velocity at greater distances from the vibratory source. Graph are shown of the geophone installed at 2m (458),5m (428) and 10 m (CRUX015) from the element.



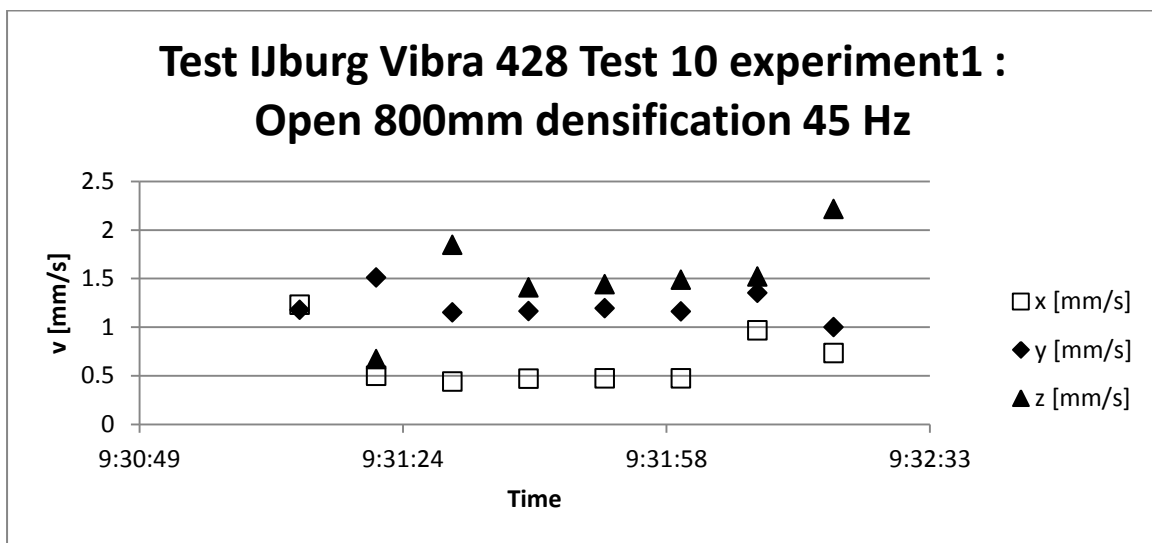
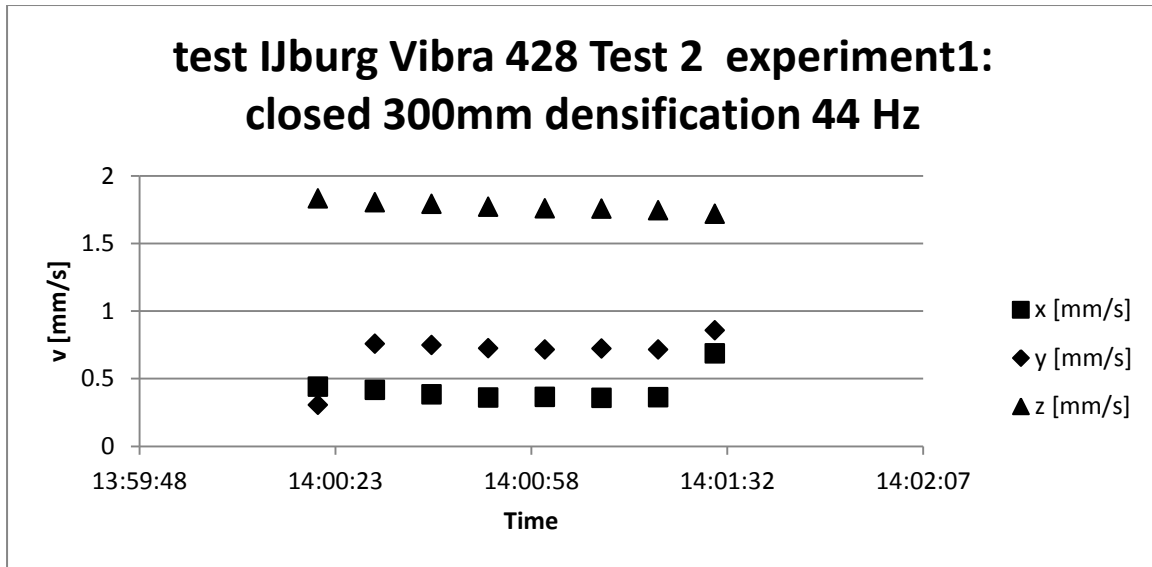
**A.10.3 Appendix 3**

Particle velocity over time



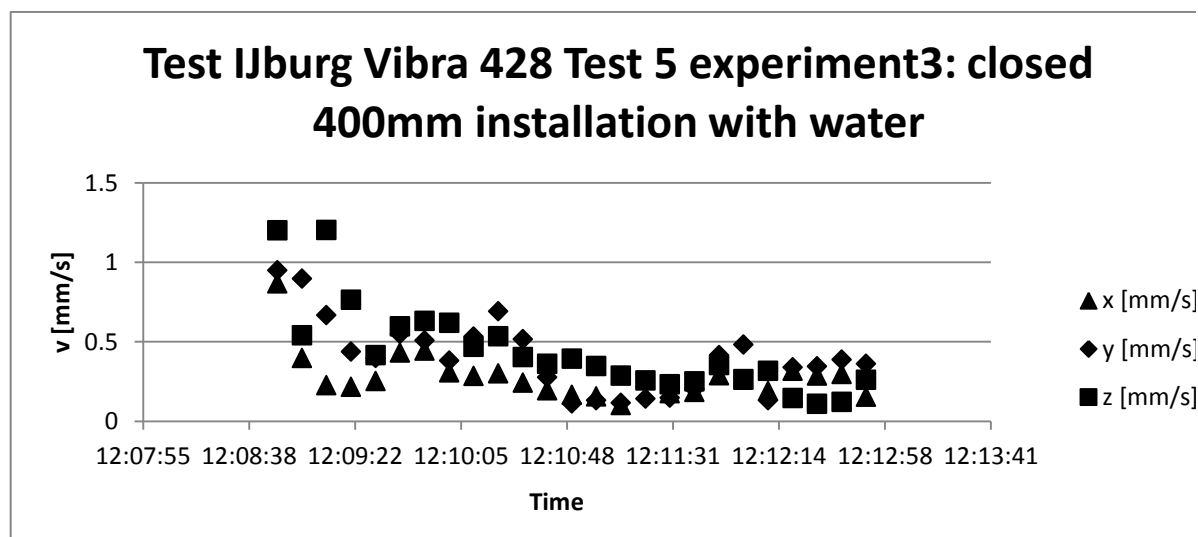
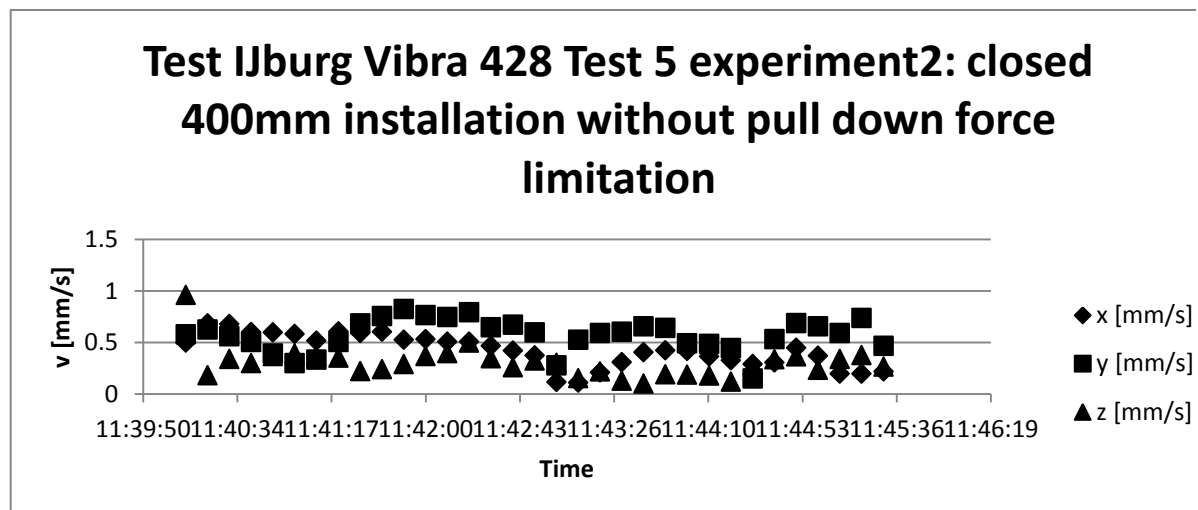
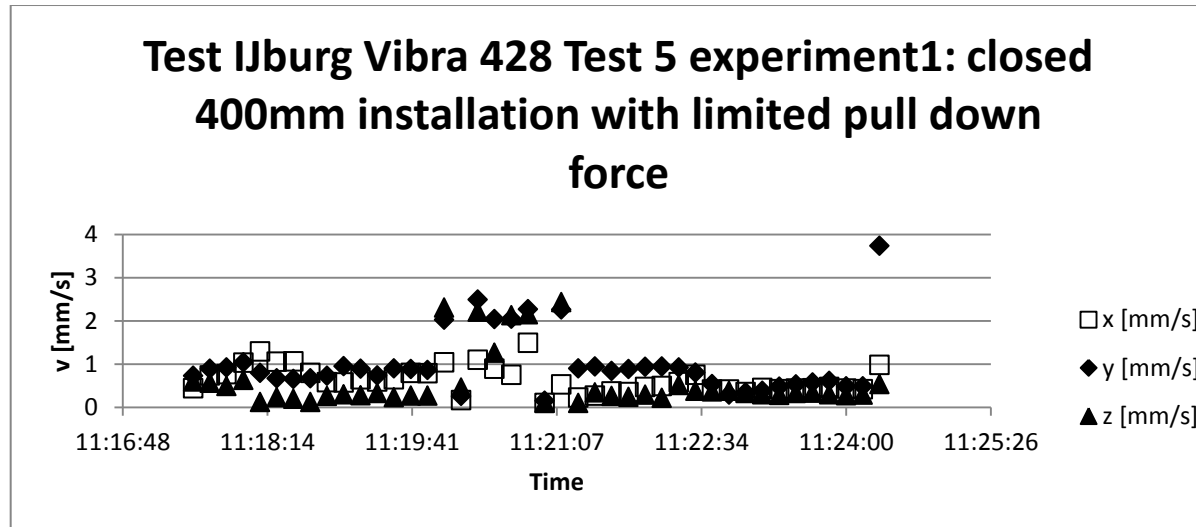
**A.10.4 Appendix 4**

Densification process



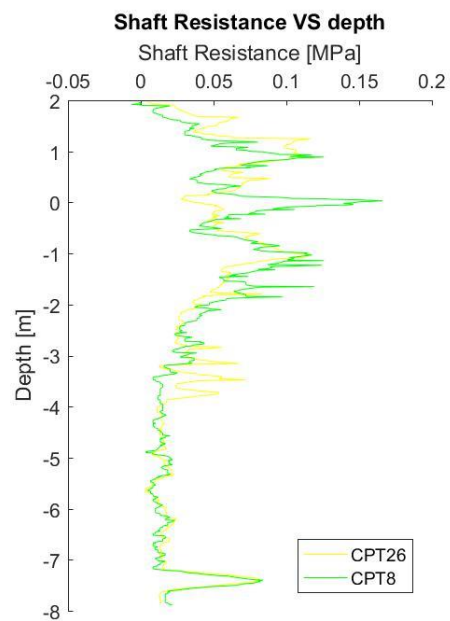
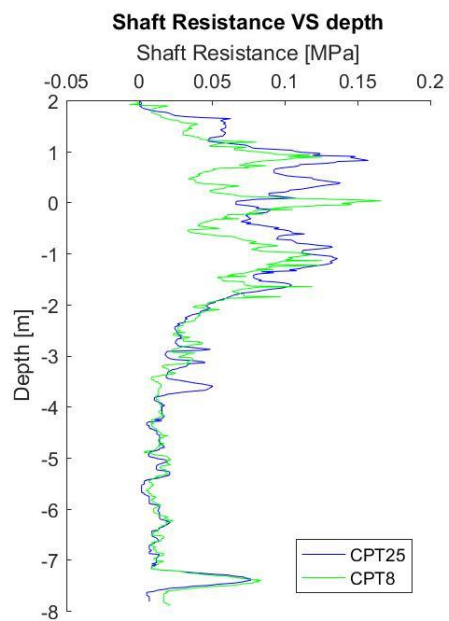
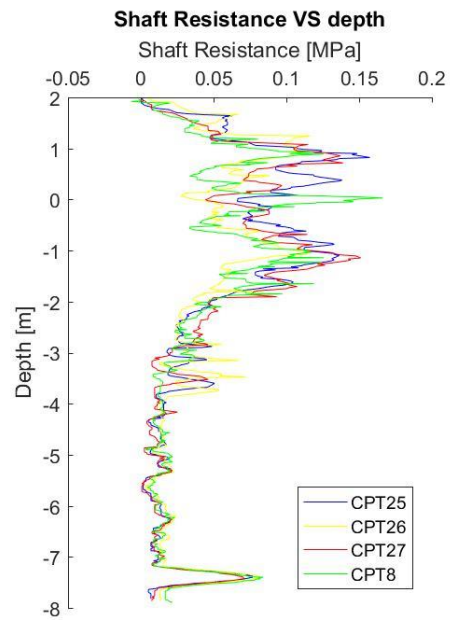
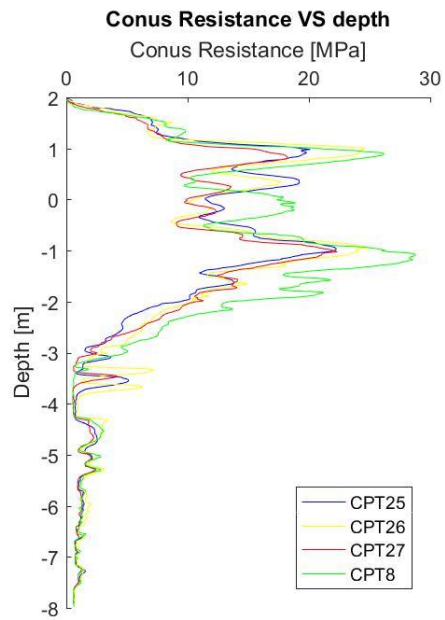
**A.10.5 Appendix 5**

Influence of the pull down force and water on the installation time.



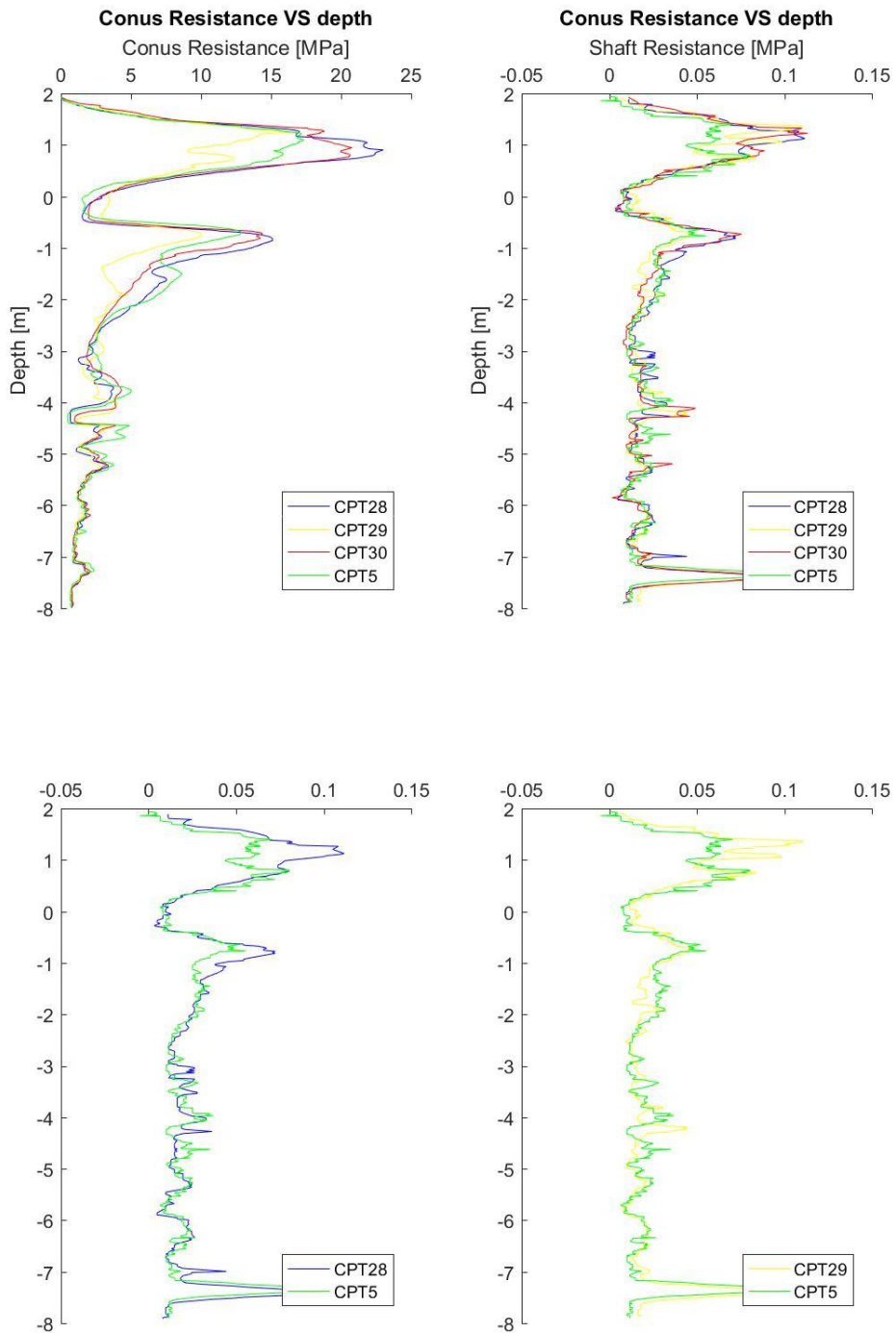
### A.10.6 Appendix 6

#### CPT data Test2 location 8



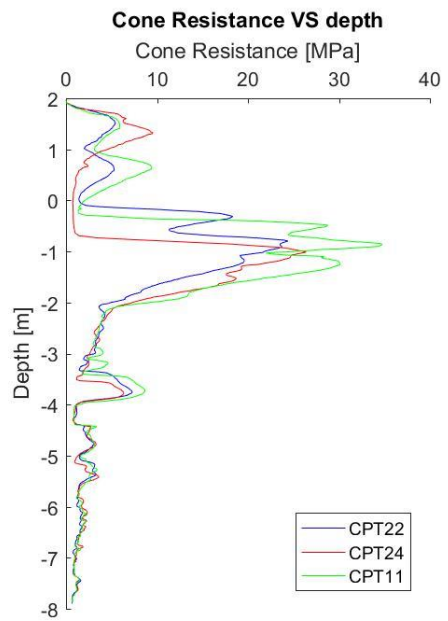
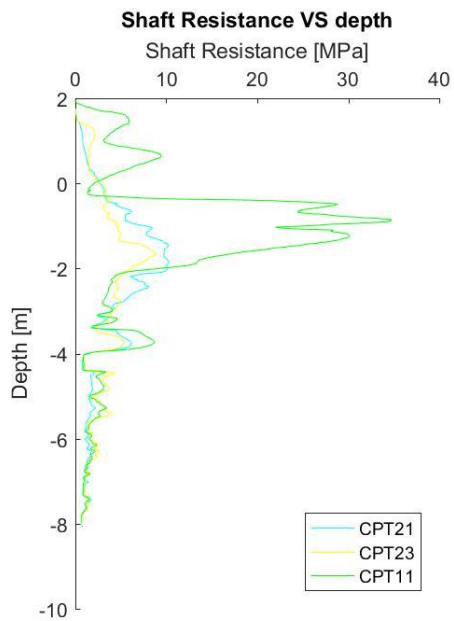
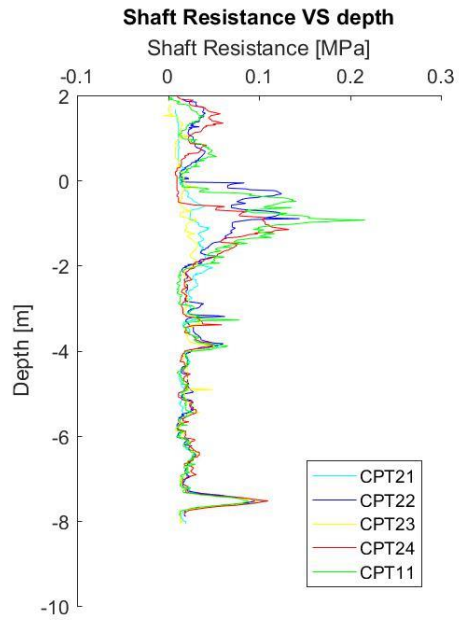
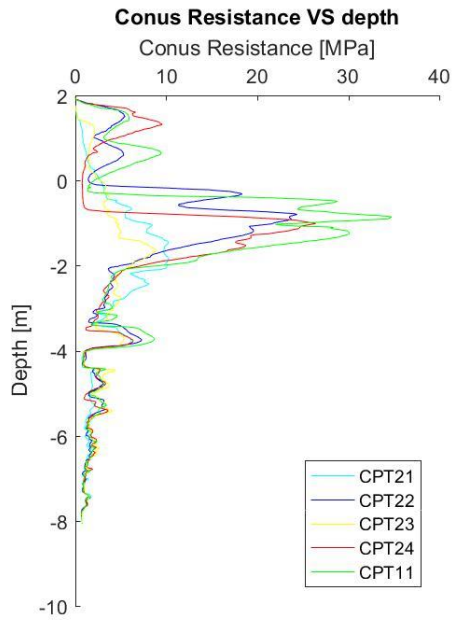
### A.10.7 Appendix 7

CPT data Test 4 location 5



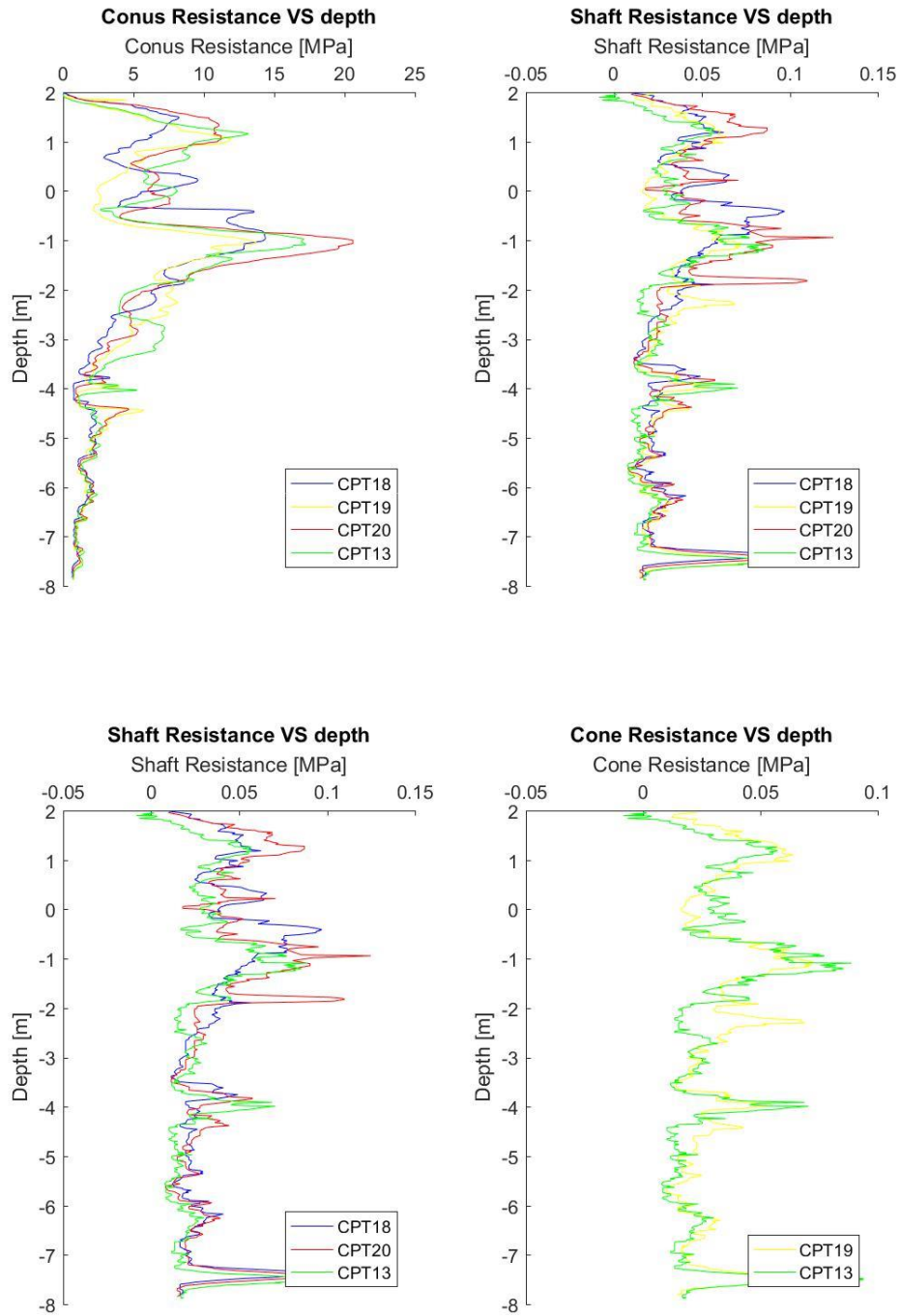
### A.10.8 Appendix 8

CPT data Test 9 location 11



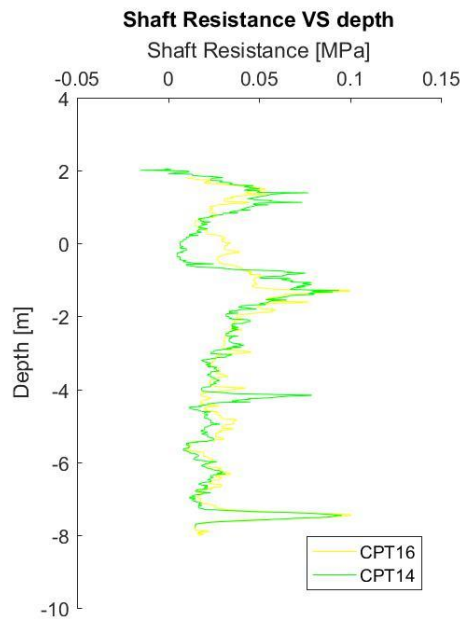
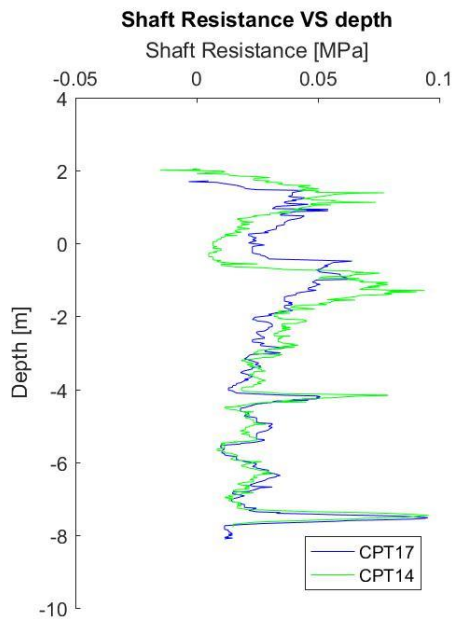
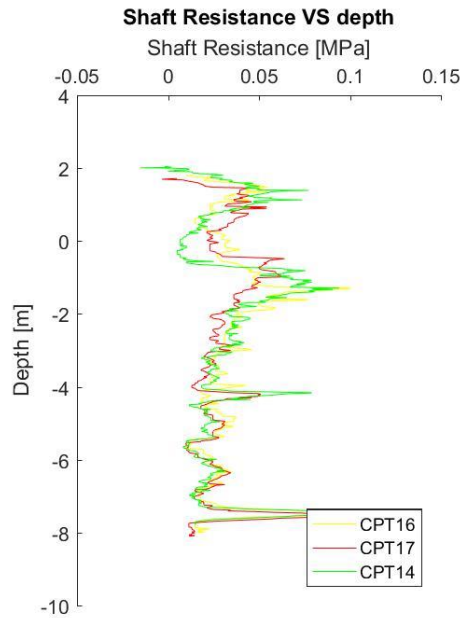
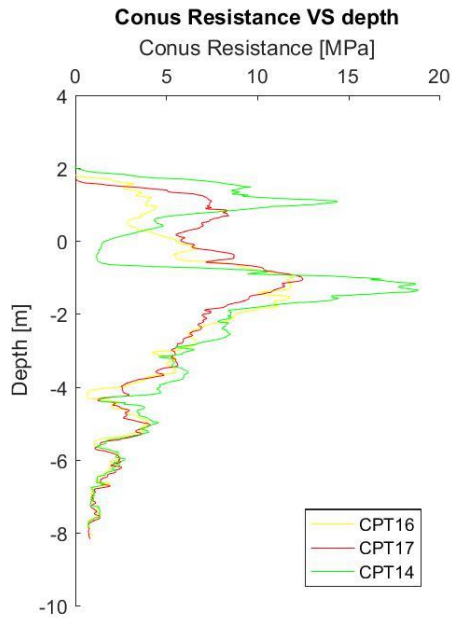
### A.10.9 Appendix 9

CPT data Test 10 location 13



### A.10.10 Appendix 10

CPT data Test 11 location 14



# B Modelling

## B.1 Introduction

The differential equations are solved with a ode45 which is integrated in the Matlab software. Two sets of ode solvers need to be implemented. Each of the ode solvers calculates the displacement  $u_1$  and  $u_2$  and checks if the applied frictional force becomes larger than the critical force.

The ode's will be solved for each time step. At each time step an 'if statement' checks the status of the model.

## B.2 Pseudo code

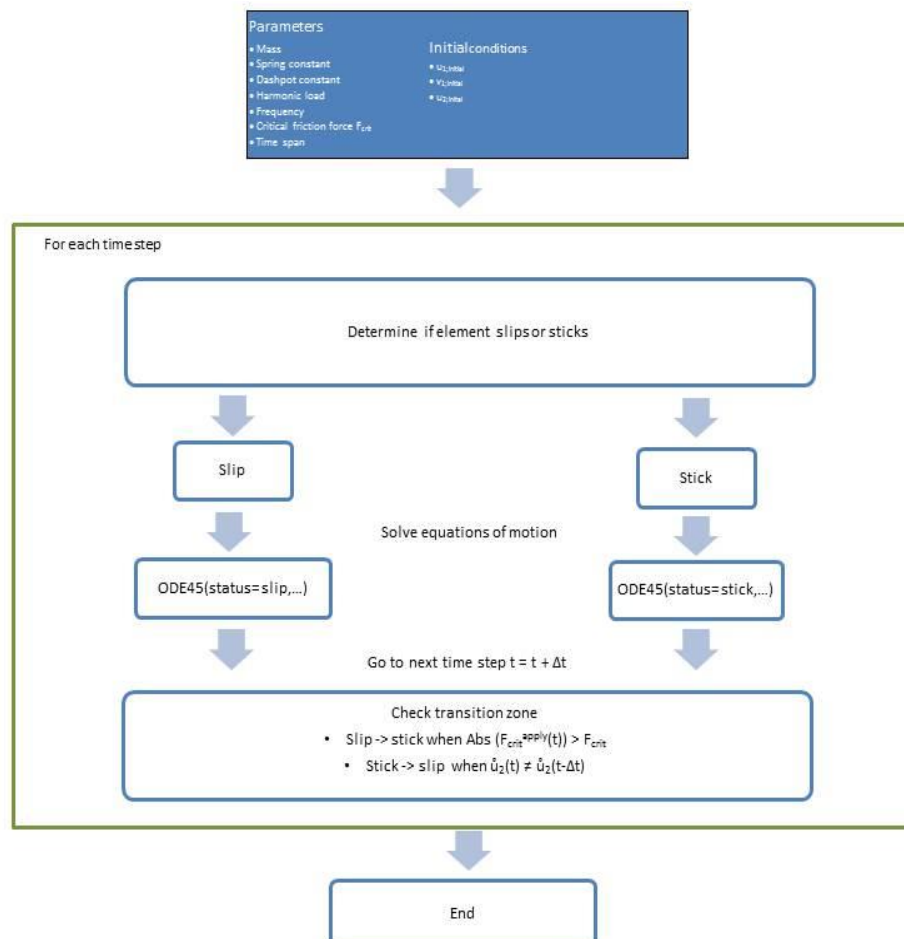


Figure B.1 Pseudo code model

### Spring-Mass system

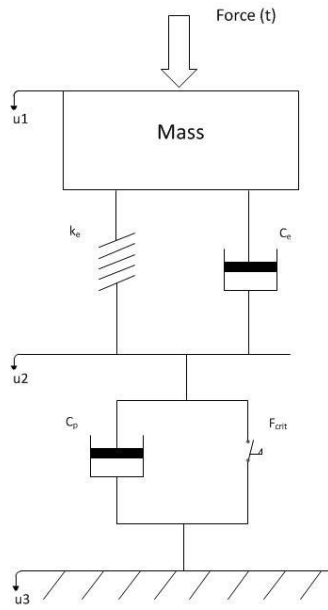


Figure B.2 spring mass system

### B.3 Governing equation

#### Equations of motion:

Slip condition:

$$m\ddot{u}_1 + c_e(\dot{u}_1 - \dot{u}_2) + k_e(u_1 - u_2) = \text{Force}(t) \quad (54)$$

$$c_e(\dot{u}_1 - \dot{u}_2) + k_e(u_1 - u_2) = c_f\dot{u}_2 + \text{sign}(\dot{u}_2) \cdot F_{fric}^{kin}$$

Rearrangement:

$$\ddot{u}_1 = \frac{\text{Force}(t) - c_e(\dot{u}_1 - \dot{u}_2) - k_e(u_1 - u_2)}{m} \quad (55)$$

$$\dot{u}_2 = \frac{c_e(\dot{u}_1) - k_e(u_2 - u_1) - \text{sign}(\dot{u}_2) \cdot F_{fric}^{kin}}{c_f + c_e}$$

Stick condition:

$$m\ddot{u}_1 + c_e(\dot{u}_1) + k_e(u_1 - u_2) = \text{Force}(t) \quad (56)$$

Rearrangement:

$$\ddot{u}_1 = \frac{Force(t) - c_e(\dot{u}_1) - k_e(u_1 - u_2)}{m} \quad (57)$$

The model should be able to determine if slip or stick occurs. Slip occurs when the applied force exceeds the critical force. The model stays in the slip condition until the value for the velocity changes from sign.

$$\text{Stick} \rightarrow \text{Slip: } \text{Abs}(F_{\text{fric}}^{\text{apply}}(t)) > F_{\text{crit}} \quad (58)$$

$$\text{Slip} \rightarrow \text{stick: } \text{sign}(\dot{u}_2(t)) \neq \text{sign}(\dot{u}_2(t-\Delta t))$$

### Transition zones:

Stick status:

The applied frictional force on the friction slider is the sum of the force in the spring and in the dashpot. The relative displacement of  $u_1$  with respect to  $u_2$  determines the force in the spring. The force in the dashpot is dependent on the relative velocity at  $u_1$  and  $u_2$ . However, in case of the stick status the displacement at  $u_2$  stays constant and therefore the velocity  $v_2$  will be equal to zero.

The applied force is:

$$F_{\text{fric}}^{\text{appl}} = k(u_1 - u_2) + c_e(\dot{u}_1 - \dot{u}_2) \quad (59)$$

Slip status:

The slip status is activated when the applied frictional force becomes larger than the critical force. During the slip status  $u_2$  is able to move as result of the harmonic load. As the force retreats the applied force becomes less, leading to a decrease in velocity  $v_2$ . The moment when the velocity changes sign the stick status is activated again.

The stick status is activated when:

$$\text{sign}(\dot{u}_2(t)) \neq \text{sign}(\dot{u}_2(t-\Delta t)) \quad (60)$$

## B.4 Model processes

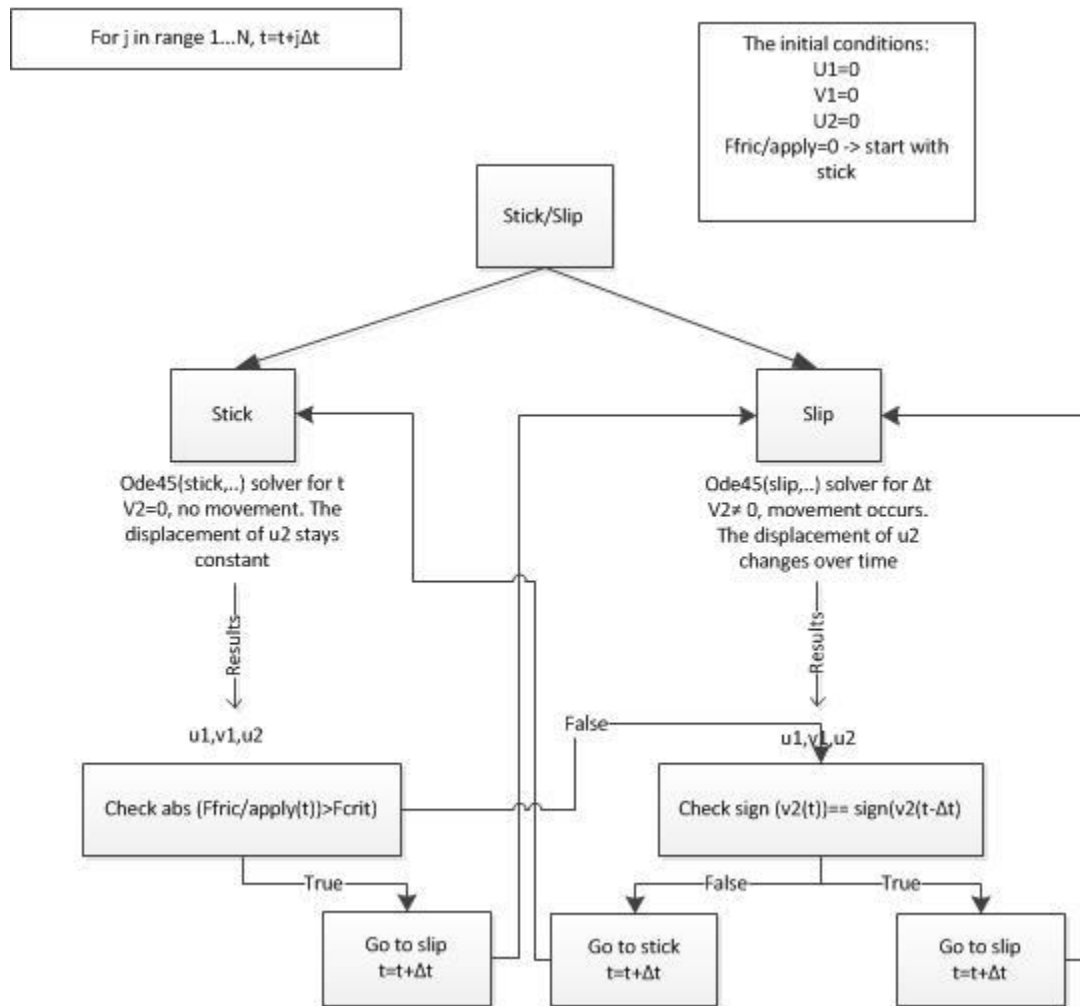


Figure B.3 Model processes

# C Zone of influence

As the pile penetrates the soil it experiences resistance from the soil underneath the tip. The load applied by the element on the underlying soil is spread over a certain area underneath the pile tip. Soft soil layers decrease the tip resistance while stronger layers increase it. When a stiff layer overlays a soft layer the penetration resistance is greatly influenced by the soft layer when the pile tip reaches this layer. Because of the rapid cyclic loading the load does not have enough time to redistribute itself over a larger area therefore an influence area of two times the diameter is chosen to be an adequate zone. In case the influence zone is equal to zero the penetration resistance is greatly affected by the soil strength/stiffness directly at the tip of the element. At large peak values for the cone resistance, which can be found at test location 2, the model overestimates the resistance resulting in overestimation of the penetration time.

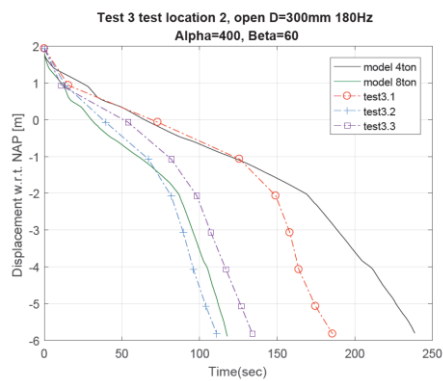


Figure C.1 influence zone 0D

When an influence zone of two times the diameter is chosen. The peak values are scaled down by taking the average cone resistance over a length of two times the diameter beneath the pile tip. The model seems to be more in agreement with the field test results.

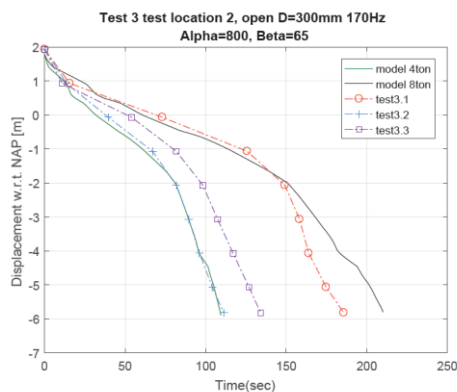


Figure C.2 Influence zone 2D

## **D** Test field conditions

The top soil layer contains large pieces of debris. Large pieces negatively influence the CPT data. In case the cone comes in conflict with a large piece of debris it will measure larger cone resistances than there actually are. The model uses the CPT data for the determination of the amount of damping and the spring stiffness. Large values of cone resistance increase these parameters and lower the penetration rate. This causes a difference in results obtained with the model and with the field test results.



Figure D.1 Soil condition test location IJburg, Amsterdam

# E Influence factor Beta

The value for beta is probably soil dependent. By changing the value for beta at the different types soil more accurate results can be obtained. The model results show that the value for beta is larger in strong soil layers than it is in soft soil layers.

The value for beta in the strong sand layers is equal to 200 and in the soft soil layers 100

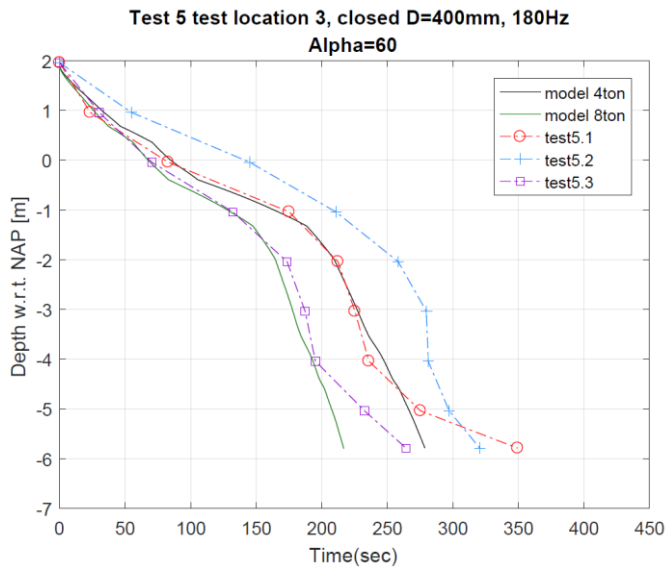


Figure E.1 variable beta

The model results are greatly improved by this correction of beta at the soft soil layers.

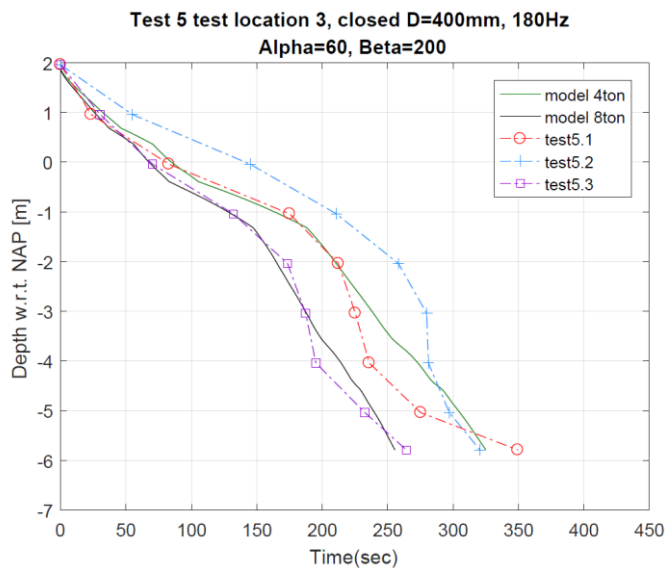


Figure E.2 Variable beta

By changing the value for beta it is even possible to directly overlay the field test results.

# F Damping

It is interesting to see that the same that the penetration rate in the beginning is more or less the same when using a frequency that much smaller than the frequency used in the test.

As the element penetrates the soil there is more damping. The larger the damping ratio the smaller the frequency at which resonance can be obtained for a damping ratio equal to 0.707 the resonance frequency is equal to 0 Hz. At 0 Hz no penetration of the element is possible.

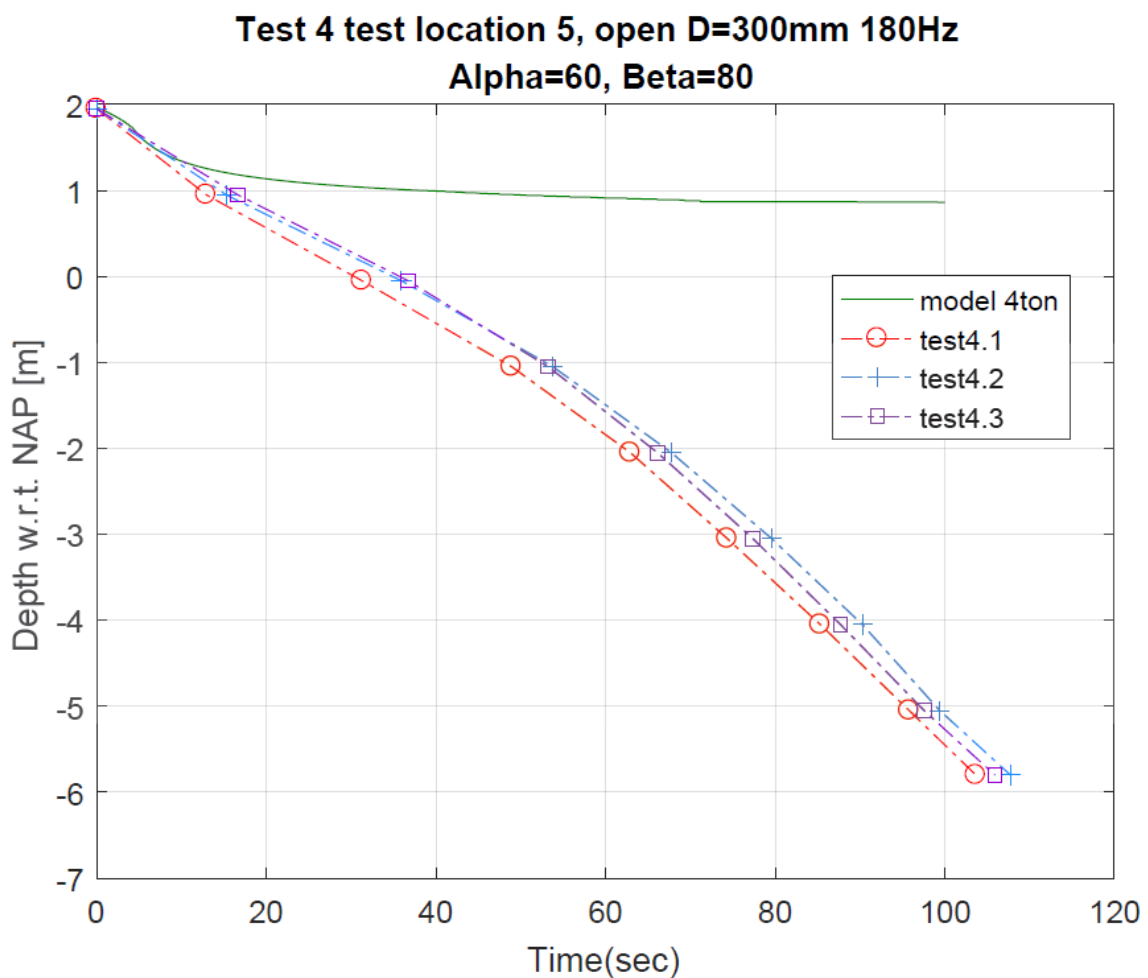


Figure F.1 Overdamped response

# G

## Parameter values damping and spring stiffness

The model makes use of the following parameter values for the damping and the spring stiffness.

**Table G.1 parameters values mathematical model**

Variable	Value	Unit
Sonic drill bit spring $k_t$		
Sand	3.00E+10	N/m <sup>3</sup>
Silty sand	2.59E+9	N/m <sup>3</sup>
Clay	1.59E+9	N/m <sup>3</sup>
Sensitive silty sand	2.11E+9	N/m <sup>3</sup>
Sonic drill spring rate along the length $k_s$		N/m <sup>3</sup>
Sand	1.03E+8	N/m <sup>3</sup>
Silty sand	8.90E+6	N/m <sup>3</sup>
Clay	4.68E+6	N/m <sup>3</sup>
Sensitive silty sand	7.27E+6	N/m <sup>3</sup>
Sonic drill bit damping $c_t$		
Sand	3.00E+10	N.s/m <sup>3</sup>
Silty sand	2.59E+9	N.s/m <sup>3</sup>
Clay	1.59E+9	N.s/m <sup>3</sup>
Sensitive silty sand	2.12E+9	N.s/m <sup>3</sup>
Sonic damping along the length $c_s$		
Sand	0.24E+6	N.s/m <sup>3</sup>
Silty sand	0.67E+5	N.s/m <sup>3</sup>
Clay	0.47E+5	N.s/m <sup>3</sup>
Sensitive silty sand	0.60E+5	N.s/m <sup>3</sup>

As the elements penetrates the soil the value for the damping and spring stiffness increases. As the elements becomes in more contact with the soil

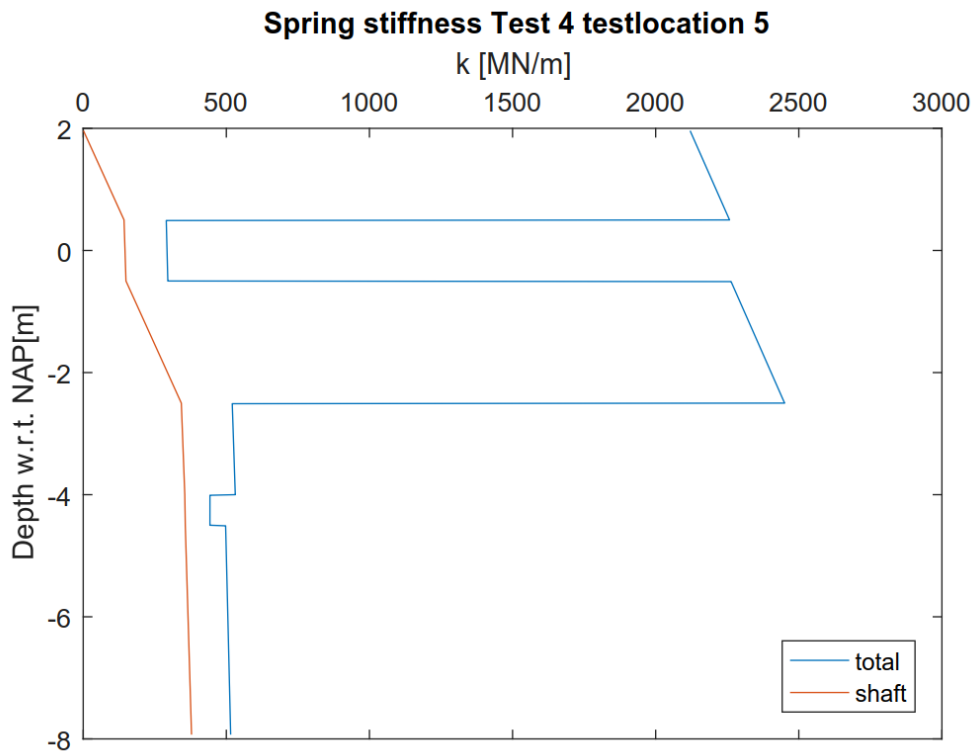


Figure G.1 Development spring stiffness

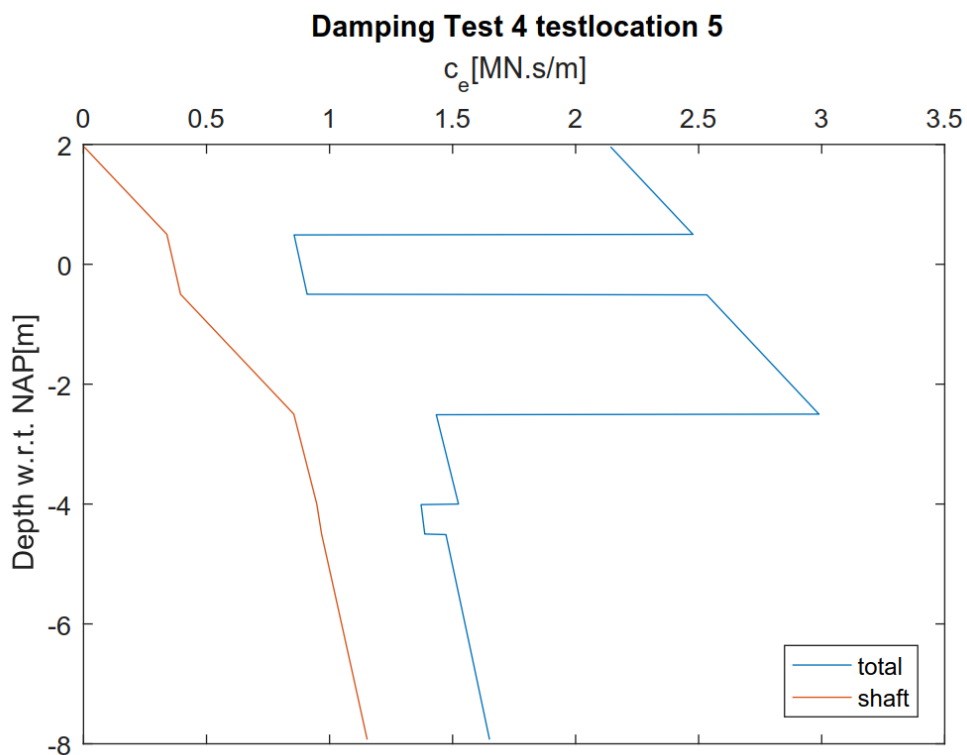


Figure G.2 Development damping

# H Pore pressure ratio

Several researches came up with different formula's to determine the pore pressure development at cyclic loading.

Tokimatsu K. and Yoshimi Y. came up with the following relation (Tokimatsu & Yoshimi, 1983) which is similar to the formula proposed by Seed B.H. et al.

$$r_u = \frac{1}{2} + \frac{1}{\pi} \sin^{-1} \left( 2F_L^{\frac{1}{\alpha_1 \beta_1}} - 1 \right) \quad (61)$$

Where  $\alpha$  and  $\beta$  are soil related constants and F is the factor of safety against liquefaction.

In 1976 Booker came up with his own relation between the number of load cycles and the pore water pressure ratio.

$$r_u = \frac{2}{\pi} \sin^{-1} \left( \frac{N}{N_l} \right)^{\frac{1}{2\alpha}} \quad (62)$$

The value for  $K_0$  largely influences the soil response (Chern & Chang, 1995). Therefore a better failure criterion needs to be determined.

C.S. Chang et. al came up with an empirical relation which takes the consolidation stress ratio  $\sigma'_{1c}/\sigma'_{3c}$  into account for the determination of the number of cycles needed to develop 50% of the confining pressure (Chang, et al., 1983).

$$r_u = \frac{1}{2} + \frac{1}{\pi} \sin^{-1} \left( \left( \frac{N}{N_{50}} \right)^{\frac{1}{\alpha}} - 1 \right) \quad (63)$$

The value of alpha is dependent on the stress consolidation ratio.

$$N_{50} = \left( \frac{CSR}{a} \right)^{\frac{1}{b}} \quad (64)$$

The values for a and b are dependent on the consolidation stress ratio  $k_c$ . Larger the value for  $k_c$  the more remaining residual strength after N load cycles.

Berghe proposed another correlation for cohesive types of soil (Berghe, 2001).

$$G_{Sn} = \Delta \cdot G_{S1} \quad (65)$$

Where  $G_{S_n}$  is the secant modulus at the  $N^{\text{th}}$  load cycle and  $G_{S_1}$  the secant modulus at the first load cycle. The degradation index is indicated with  $\Delta$ .

$$\Delta = N^{-t} \quad (66)$$

The parameter  $t$  is equal to the degradation parameter and is dependent on the plasticity of the soil.

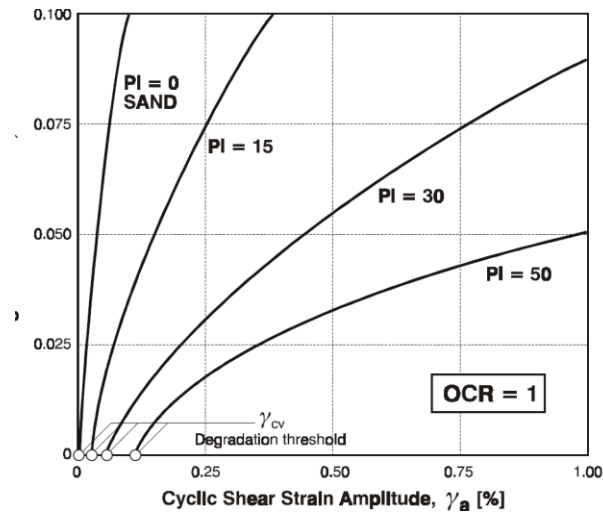


Figure H.1 Degradation curve



## Cyclic mobility

### *Isotropically consolidated samples with stress reversal*

As the cyclic load on the sample proceeds more excess pore water pressure is built up and the mean effective stress moves towards zero stress. When the effective stress reached zero momentarily at zero deviatoric stress, initial liquefaction was said to occurred. At initial liquefaction large axial strain occurs. As the the deviatoric stress becomes non zero again the specimen recovers some of its effective stress and shear stiffness as result of dilation (Yang & Sze, 2011).

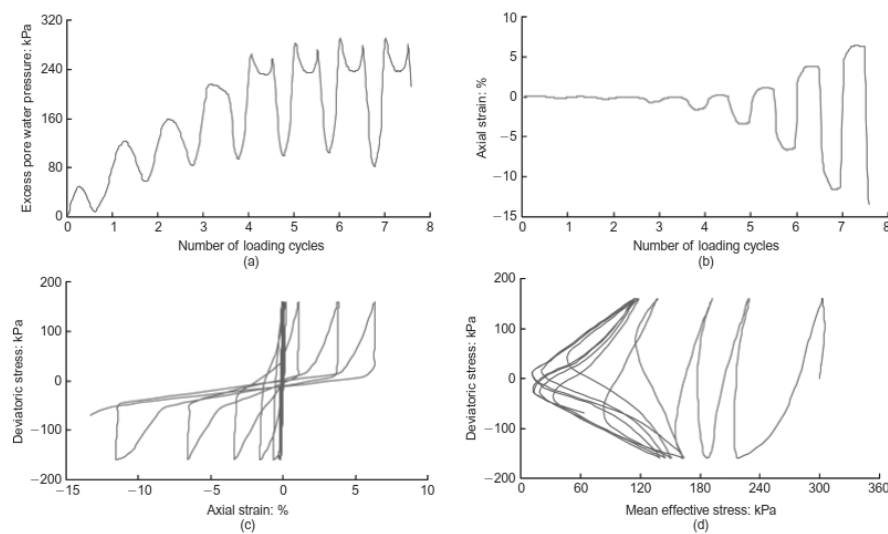


**Figure I.1 Undrained response of medium dense sand under symmetrical cyclic loading ( $D_{rc}=50\%$ ,  $\sigma'_{nc}=300\text{kPa}$ ,  $q_s=0$ ,  $q_{cyc}=160\text{kPa}$ ) (Yang & Sze, 2011)**

The pore water pressure accumulates per loading cycle. At small shear strains the soil has the tendency to contract, resulting in an increase in pore water pressure and a reduction in effective stress. If the cyclic shear stresses become larger than the steady state strength the soil faces instability, Figure . Temporary flow liquefaction occurs, and significant shear strain develops without an increase in shear stress; the soil fails and reacts perfectly plastic. The soil reaches the steady state line from this point and the soil starts to behave dilatant. This change in behavior happens when the curve reaches the phase transformation surface(PTS). The increase in shear strain increases the shear stress and the soil starts to dilate. The dilatancy of the soil result in an increase in effective confinement and an increase in stiffness and strength, a phenomenon which is also known as strain hardening (Elgamala, et al., 2002). As the next load cycle is applied the soil first contracts again and the pore water pressure rises until the stress condition reaches the PTS. For low strain amplitudes the net pore water pressure is positive

### *Anisotropically consolidated samples with stress reversal*

For anisotropically consolidated samples there is an initial static shear resistance which is not equal to zero. The response of the non-symmetrical loaded sample tends to have more axial strain on the compressive site than the symmetrical loaded sample. The pore water pressure built up does not reach the level of the confining pressure. When the effective stress level reaches almost zero a transient strain softening occurs resulting in an increase in strain. As the cyclic stress increases again the specimen regains a substantially part of its initial stiffness. The dilation of the soil occurs already in the first load cycle for the anisotropically consolidated samples.

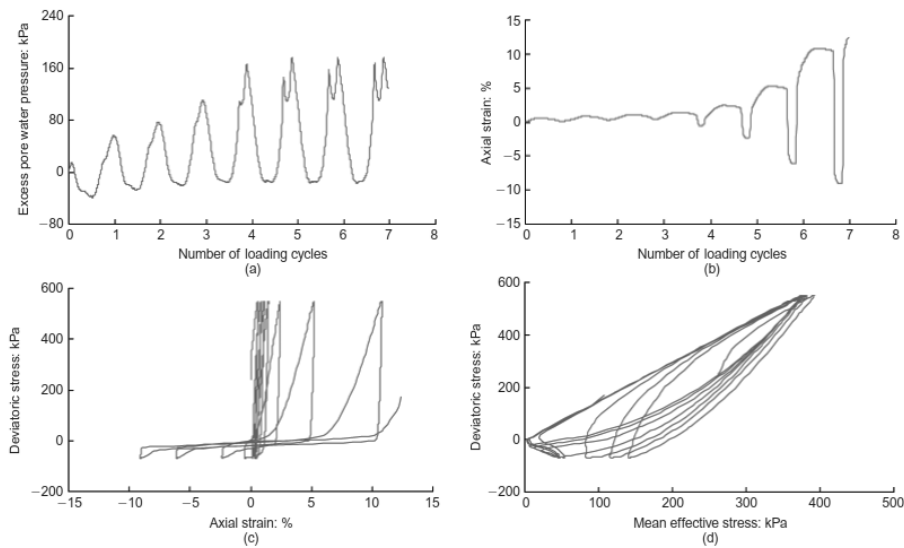


**Figure I.2 Undrained response of medium dense sand under non-symmetrical cyclic loading ( $D_{rc}=50\%$ ,  $\sigma'_{nc}=300\text{kPa}$ ,  $q_s=240$ ,  $q_{cyc}=310\text{kPa}$ ) (Yang & Sze, 2011)**

Anisotropically consolidated samples without stress reversal

No cyclic mobility occurs. There is only strain accumulation on the compression site. Furthermore, one can see that the increment of axial strain per load cycle is more or less equal.

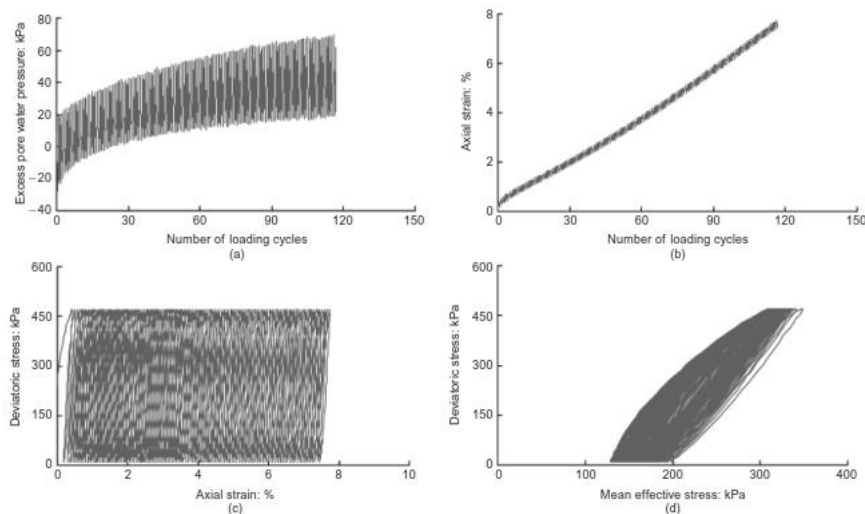


**Figure I.3 Undrained response of medium dense sand under non-symmetrical cyclic loading ( $D_{rc}=50\%$ ,  $\sigma'_{nc}=300\text{kPa}$ ,  $q_s=240$ ,  $q_{cyc}=230\text{kPa}$ ) (Yang & Sze, 2011)**

# J

## Densification based on accelerations

The ability for a stress wave to cause densification is dependent on the acceleration of the particles. To produce densification in the vertical plane an acceleration of at least 1g is required. In the horizontal plane it requires only an acceleration of 0.1g to obtain densification of the soil according to the SBRCUR-A (Waarts & Ostendorf, 2006).

Barkan came up with a densification model based on publications (Barkan, 1962). The model is able to determine a threshold value for the acceleration below no densification occurs. The threshold value for the acceleration can be determined with:

$$\eta_0 = \frac{a_0}{g} = \frac{\ln(1 - D_{r,0})}{-\alpha} \quad (67)$$

The value alpha is an empirical parameter and depends on the soil strength and stress level. According to Hergarden to value of alpha varies between 3, high stress level and strength, to 5 for low stress levels and strength. Considering the strong type of soil were the geophone in which the geophone is placed a threshold value of 0.3g needs to be exceeded before there is possible densification of the soil. The SBR limit seems too conservative in respect to the threshold value obtained with the Barkan and Hergarden formulation.

As already mentioned during the start-up of the vibrator the frequency passes the resonance frequency of the unit. At this particular frequency the displacement amplitude increases and this has its effect on the velocity and acceleration of the soil particles in the surroundings. The transition from 0 to 180Hz only takes a few seconds. It is assumed that the increases in amplitude during this phase has limited influence on the densification of the soil. The moment the vibrator reaches its maximum it starts to vibrate the element in to the ground. In the first few seconds the installation is not very stable as the element cannot obtain stability from the surrounding soil mass. This unstable condition results in higher vibration accelerations in the surroundings. The moment the insertion becomes stable the acceleration reaches an equilibrium. The geophone data at two and five meters radial distance are used to explain the absence of densification. The acceleration in the horizontal plane is calculated as follows:

$$a_h = \sqrt{a_x^2 + a_y^2} \quad (68)$$

The result show that for all cases the acceleration becomes lower than the threshold value at stable installation. Considering the threshold value obtained by the densification model proposed by Barkan more or less the entire process seems the be below the threshold value. This seems to be more in agreement with the reality as there was no densification visible.

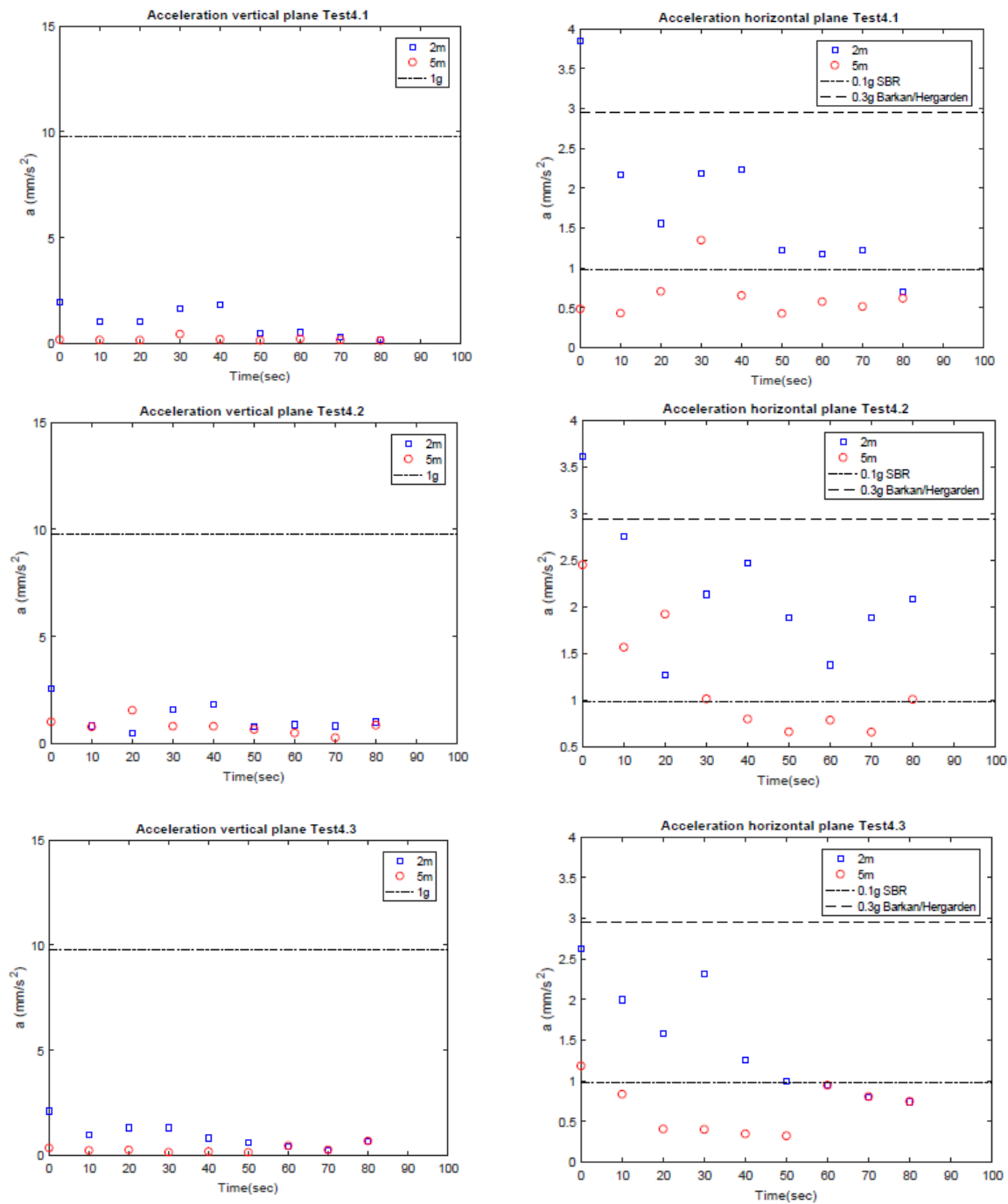


Figure J.1 Attenuation of vibration acceleration

In 2012 R. van der Salm et al. performed research on the influence of the acceleration on the densification of the soil. They concluded that the acceleration is not always the determining factor. They suggested that that for high frequency vibrations it is adequate to use the acceleration however for low frequency vibrations the velocity might be more determinative (Salm, et al., 2012).



## **SONIC INSTALLATION OF ELEMENTS IN HARD SOIL LAYERS CAUSES MINIMAL IMPACT ON SURROUNDINGS**

Jeroen D. Keuzenkamp, Delft University of Technology, Delft, Netherlands, +31-643155779, [jeroenkeuzenkamp@gmail.com](mailto:jeroenkeuzenkamp@gmail.com)

Jelmer Heinis & Almer van der Stoel, CRUX Engineering bv, Netherlands, +31 20 4943070, [heinis@cruxbv.nl](mailto:heinis@cruxbv.nl); [vanderstoel@cruxbv.nl](mailto:vanderstoel@cruxbv.nl)

Jeroen Dijkstra & Jan-Willem Vink, Cofra bv, Netherlands, +31 20 69 34 596, [jeroen.dijkstra@cofra.com](mailto:jeroen.dijkstra@cofra.com); [jan-willem.vink@cofra.com](mailto:jan-willem.vink@cofra.com)

### **ABSTRACT**

The paper describes a full scale test in which an innovative method for installing foundation elements in dense and hard sand layers has been tested. The installation method is based on sonic drilling using vibrations up to 170Hz to reduce soil resistance, whilst pushing different elements into the ground.

The results show that vibrations did not exceed 3 mm/s at approximately 5m distance from the sonic drill at frequencies of >140Hz. In addition, the CPTs show minimal backdrop or increase of cone resistance in the surrounding soil. The setup is able to easily install the elements in highly dense (cone resistance > 34 MPa) sand layers. It took less than 2 minutes to install a 300mm open tube with a length of 8m in a, on average 30MPa, sand layer.

A correlation was found between the cone resistance and the penetration time. This correlation is a first start to find solutions for layers with even higher cone resistances. It can be concluded from the tests performed that the sonic vibration method is an effective solution for installing elements at high speed in challenging ground conditions with minimal vibration and settlement disturbance.

**Keywords: sonic drilling/installation, high frequency vibrations, hard soil, field tests, in-situ measurements, minimal disturbance, soil improvement**

### **INTRODUCTION**

Small size anchors and pipes (diameters of  $\leq 200$ mm) are on many projects successfully installed into very dense ground whilst using vibrations, with frequencies up to 170Hz to reduce soil resistance, in combination with pushing and/or drilling. A trial has been performed to use this innovative installation method for installing larger elements (diameters of  $\geq 300$ mm), for which rapid installation is still challenging, in dense and hard sandy layers.

The performed trial, described in this paper, is part of a master thesis initiated to test this new installation method on the larger diameter elements whilst also investigating the

potentially densification effect. The field test was performed with a newly designed base unit by High Five Solutions BV. The purpose of the trial was also to check the current configuration and current capabilities installing the different types of elements through hard soil layers. Based on the results a qualitative comparison to conventional methods is made and prospects for using the method in future projects are described.



Figure K.1 Unit with sonic vibratory drill set.

## THEORETICAL BACKGROUND

A Sonic vibrator transfers a high frequency displacement towards the top of an element using a rigid connection. The back and forth movement of the vibrator is repeated periodically creating sinusoidal compressive and expansive pressure waves in the element. The elasticity together with the inertial properties of the element allow the waves to propagate through the element to the tip of the element.

The fast up and down movement of the element reduces the friction at the sides considerably as the soil is not able to stick to the element when vibrating at the high induced frequencies.

In saturated soil conditions the sonic drill technique takes advantage of the reduction of shear strength as result of cyclic loading. The rapid movement of the element causes an increase in excess pore water pressure and a consequent decrease of effective stress up to the point that the excess pore pressure become larger than the initial effective stress and very localized liquefaction or failure occurs. In literature related to sonic installation two main types of phenomena that induce liquefaction can be recognized:

- flow liquefaction and
- cyclic mobility.

### ***Flow liquefaction***

This phenomenon is most likely to occur in loosely packed sand soils. Per load cycle the excess pore water pressure increases reducing the effective stress. After a certain number of load cycles, the excess pore pressure is high enough that failure is triggered and the soil is liquefied, completely losing its strength. Large deformations of the soil may occur when the applied shear stress exceed the residual strength of the soil.

### ***Cyclic mobility***

This phenomenon occurs in medium to dense sand. The soil does not fail as result of flow liquefaction but fails as a result of gradual accumulation of strains. As the soil is cyclically loaded the pore water pressure increases progressively resulting in a net softening of the soil. The deformations stop as the cyclic loading ceases because of dilation effects of the soil. Due to the dilatancy the soil recovers a substantially part of its effect stress and stiffness (Yang & Sze, 2011). This is not the case for flow liquefaction. Furthermore, the vibrations of the element enable the surrounding soil to lose its initial structure and start to densify locally. In this way the soil opens a way for the element to penetrate the soil.

The amount of degradation of soil resistance is dependent on shear strain amplitude, relative density and the initial stress state (Berghe, 2001)

## **TRIAL SETUP**

### ***Location***

The test took place on a reclaimed area at IJburg, Amsterdam, The Netherlands. The test field had dimensions of 100mx45m and was divided into 15 compartments. In every compartment one or more tests have been performed and every test has been done three times (subtests) in one compartment in a predefined pattern. Patterns have been chosen such that either influence was expected on the neighbouring location or no influence was expected.

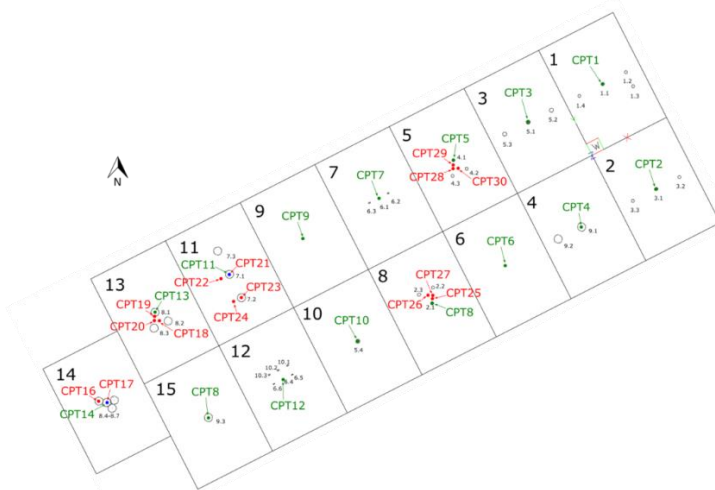


Figure K.2 Test location divided into compartments and patterns, pre CPTs (green), post CPTs (red)

### Tested elements

During the tests open and closed steel elements with diameters of 300mm (length 8m, closed and open), 400mm (length 8m, closed and open) and 800mm (length 4m, closed and open) have been installed. Figure shows the shape of 300mm open-ended element. The steel elements have been tested on driving capability and installation rate. All steel elements were installed over the full length during the tests, except for the tests with the closed 800mm element (tests 12 and 13). Table 1 provides the test details



Figure K.3 Open 300mm element with shape of Vibroflot

**Table K.1. overview of the tests**

Test nr.	Element	Compartment nr.
Test1	Closed 300 mm	1
Test2	Closed 300 mm	8
Test3	Open 300 mm	2
Test4	Open 300 mm	5
Test5	Closed 400 mm	3
Test6	Closed 400 mm	10
Test9	Open 800 mm	11
Test10	Open 800 mm	13
Test11	Open 800 mm	14
Test12	Closed 800 mm	4
Test13	Closed 800 mm	15
Test18	Open 300 mm	6

**Ground conditions**

The test-site consists of reclaimed sand (filled/sprayed). The fill, which is about 4m thick, consists out of sand with high cone resistances up to 34MPa. Below the sand a 1m thick clay layer can be found, followed by loose sand and clay. A characteristic CPT log is illustrated in Figure . CPT data was gathered for all the compartments prior to the execution of the tests.

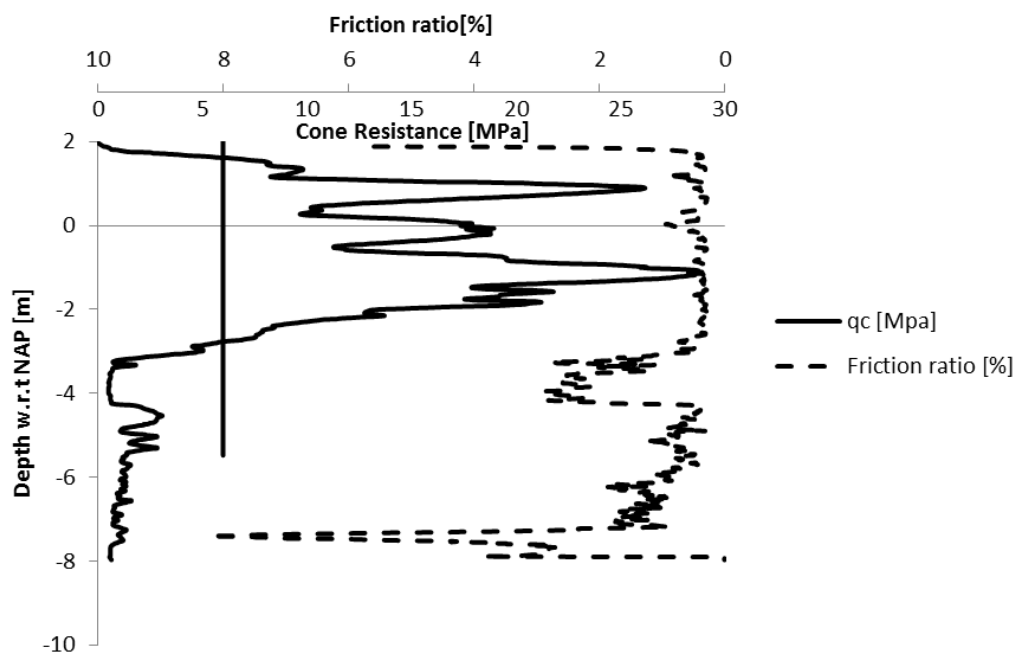


**Figure K.4 CPT compartment 8**

### Execution of the tests

The partition of the tests in the compartments was based on the CPT cone resistance profiles.

All elements were pushed into the ground whilst sonically vibrated. The magnitude of the push force was varied throughout the different tests depending on operational constraints and on the reaction of the element. Water was used in a few tests, applied under low pressure at the tip of the element, to decrease the resistance and enhance the penetration rate.

During the tests the time required per meter of installation was registered. At the same time geophones measured the vibrations at 2, 5 and 10 meters distance from the element. Subsequently for each test settlements were registered before and after the installation.

## RESULTS

### Installation time

The time/depth registration shows that the penetration of the first 4m takes most of the time. This is in accordance with the CPT data, in which the first 4 meters are dominated by dense sand layers with relatively high cone resistances (up to 34MPa). After the first 4 meters the installation time per meter decreases. The lowest installation time per meter is measured when the element penetrates the clay layer at 6m below surface. Figure shows the results for the time-depth registrations for test 3.

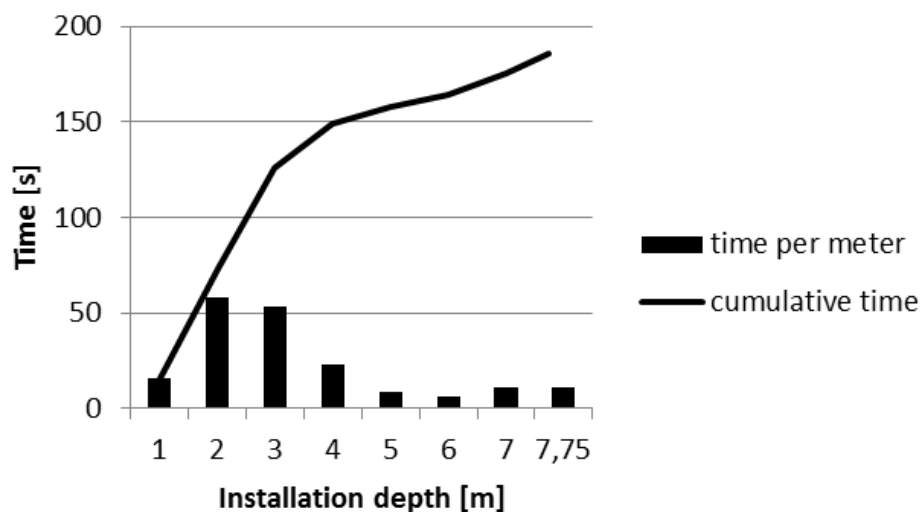


Figure K.5 Installation time per meter and cumulative installation time for test 3 subtest 1

The time dependent registrations show that the ability to lead and push the element into the ground whilst vibrating is creating faster installation speeds. Addition of water leads to a further decrease of installation time. This is shown in Table .

**Table K.2 time registration test 1**

Test 1	Subtest	Installation time [s]
Installation 1	1 & 2	169 & 202
Installation 2(after improvements)	2b	114
Addition of water	3	97

***Influence of element type***

The cone resistance in the first 4m varied considerably between the different compartments. The subsequent layers in the compartments were more consistent with more or less the same cone resistance and soil profiles. The installation time for the different elements at 5m-7m depth below surface is therefore compared to analyse the influence of the element type (open or closed, diameter) on the installation time. The influence of the dense sand layers above the section reviewed, on the penetration rate is considered to be minimal as friction is negligible and is therefore neglected in this analysis.

The comparison points out that the closed 300mm element penetrates the considered layers in about the same time (20s) as the open 300mm element (26s). This seems at first instance unlikely given that the closed-ended element should develop more resistance because of the greater surface. A conclusion that could be drawn from this, but was not investigated further, is that the open-ended element must have a sort of (closed) plug of soil at the bottom and therefore behaves similar to the closed-ended element.

The installation time of the closed 300mm element (20s) and the closed 400mm element (63s) show a considerable difference. This was expected given the greater physical resistance of the 400mm element.

***Correlation between cone resistance and installation time***

The installation time per meter of element differs between the tests in the first four meters of soil. The cone resistance and installation time varies the most in this part. As shown in Figure , the installation time increases in proportion to the cone resistance. This is found for each diameter.

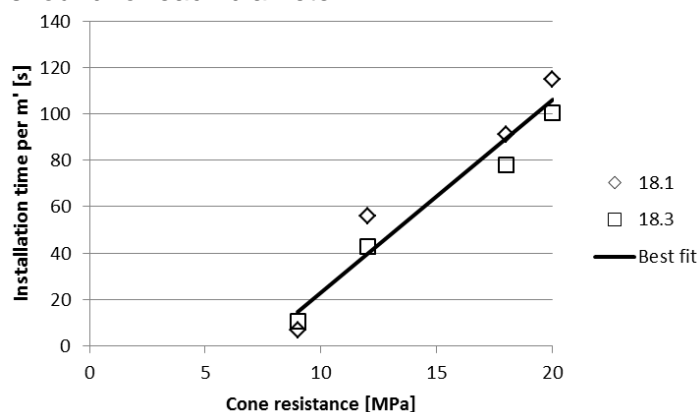


**Figure K.6 Cone resistance correlation Test 18 300mm open,  $y = 8,3062x - 59,961$**

### Vibrations

During the installation of the elements the vibration levels (velocity and acceleration) and frequencies in horizontal (x and y) and vertical (z) directions were measured using geophones. The geophones were buried at 0,3-0,5m depth and installed at radial distances of 2m, 5m and 10m from the element. The data obtained with the geophone at a distance of 2m turned out to be too inaccurate for further analysis. The data at 10m does not show significant vibrations and therefore not further presented here. The analysis below is based on the data obtained with the geophone at a distance of 5m from the element.

The data shows that the sonic drilling causes vibrations in the frequency range of 140-170Hz. When these frequencies are reached the vibration levels are relatively low, about 1-2mm/s. In the non-sonic frequency range of 40-60Hz higher vibration levels (up to 5mm/s) were measured. This is shown in Figure . Presumably, these vibrations were caused by resonance of the excavator in the transition from 0Hz to >140Hz (or >140Hz to 0Hz). Figure shows this phenomenon when the installation/vibration is started or stopped. These vibrations are not caused by the elements, but by movement/vibration of the excavator on the surface. The natural frequency of the excavator can be found at 50Hz. At this particular frequency the excavator starts to resonate, and large vibration amplitudes are generated.

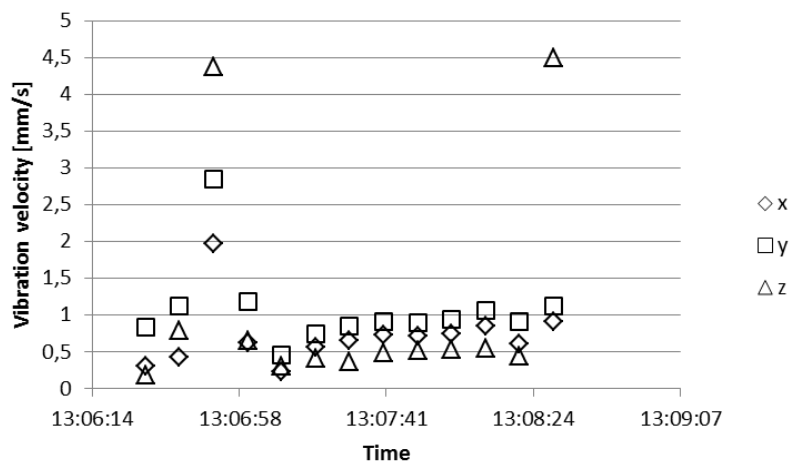
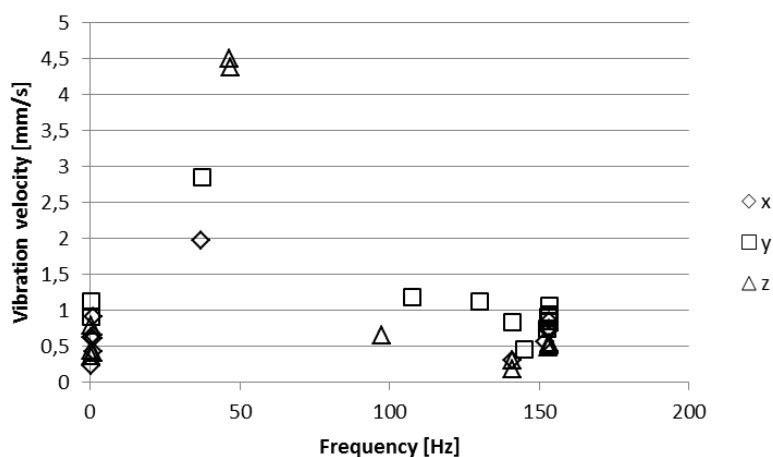


Figure K.7 Vibration speed vs. time test 6 subtest 1



**Figure K.8 Vibration speed vs. frequency test 6 subtest 1**

The levels of vibrations are dependent on the push force applied. When no force is used the vibration levels turn out to be lower than when using a push force. In all probability this has to do with the amount of pressure on the leader which transfers the vibrations from the crane to the subsurface. As the pressure on the leader is reduced, less vibrations are transferred.

Using water also decreases the vibrations. Presumably, the addition of water increases the damping of the vibrations in the soil.

A comparison of the data of the geophones at the different distances shows that the vibration levels decrease considerably with distance from the vibration source. The transfer of high frequency vibrations in soil is very limited.

**CPTs**

CPTs were executed both before and after the tests. The CPT data is used to indicate the effects of the vibrations on the densification of the soil. In general, the post CPTs do not show significant changes in cone resistance. This indicates that the degree of compaction due to installation effects is limited.

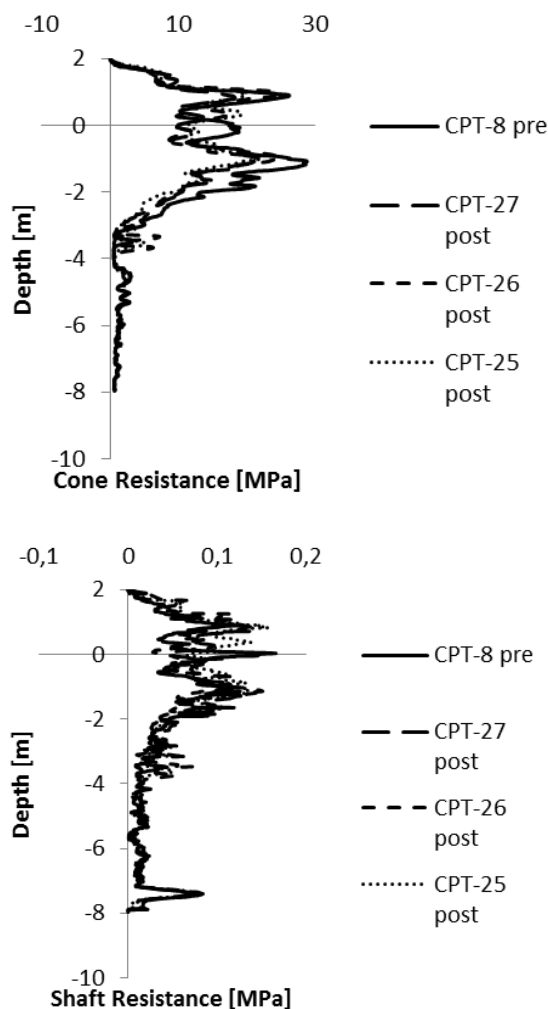


**Figure K.9 Comparison of cone resistance between pre CPT (CPT 8) and post CPTs**

### **Settlements**

After the elements were retracted from the soil a hole remained. Depths up to 1.2m were measured at the locations where open-ended elements were installed. The CPTs do not show any increase in cone resistance but show an increase of shaft resistance at some locations. It is supposed that the settlements are caused by closing of the tip by a soil plug and ground displacement to the sides. No settlements were visible adjacent to the installation locations.



**Figure K.10 Measurement of settlement after retraction of the element**

### **ADDITIONAL TESTS**

In addition to the tests described above, several more tests with different elements were performed to see the installation capabilities of the installation set. The tests were performed with prefab concrete piles and sheet piles. The results and findings are summed up below. The vibrations due to the resonance of the excavator are not taken in to consideration.

#### ***Prefab concrete piles***

Two square 250x250x4000mm prefab concrete piles were installed using sonic vibrations. The installation of 3.5meters of the first prefab concrete pile took 12 minutes. The installed length of the second pile is 2.5m and took about 2 minutes. The second pile is not fully installed because of technical difficulties with the pile clamp. The maximum vibration velocities were 3mm/s and in the frequency range of >140Hz this was 1mm/s.

Some light concrete cracks were detected in the top end of the second pile.

#### ***Sheet pile***

Two sheet piles profile Larssen L604 and length 7,5m were installed. The second sheet pile was installed in the lock of the first sheet pile. Installation took about 8 minutes per sheet pile. The vibration data shows 4mm/s in the 40Hz-80Hz frequency range and 1,5mm/s in the >140Hz frequency range at 5m distance.

### **COMPARISON TO CONVENTIONAL METHODS AND PROSPECTS FOR FUTURE PROJECTS**

The results show that the sonic installation system is capable to install different types of elements up to a length of 8m in challenging / high cone resistance soil conditions at a

relatively high installation rate and with minimal disturbances to the surroundings. Because no tests with conventional methods like traditional pile driving or vibratory pile driving (30-40Hz) were performed a direct comparison cannot be made. However, based on experience from previous projects in comparable soil conditions it can be assumed that the method is potentially faster, more reliable and less risky (in terms of vibrations and settlement impact on the surroundings) compared to conventional methods.

Projects in which the method might prove to be valuable are:

- Installing piles in urban areas (as an alternative to traditional/vibratory pile driving) to have less risks on impact on adjacent buildings, underground cables and pipes and/or other constructions. More specific:
  - installing piles next to buildings/foundations that are sensitive to vibrations (like most shallow foundations);
  - installing piles for sound screens next to roads and/or railways;

The applicability of the specific setup needs to be further investigated before it can be used for any of the before mentioned types of projects.

## **SUMMARY AND CONCLUSIONS**

Several tests have been performed to test an innovative method for installing elements in dense and hard sand layers using sonic vibrations. The goal was to find a new installation method that is capable of installing elements through hard soil layers.

The results show that the sonic vibration installation method can be used to install several types and sizes of elements in hard, granular/sandy soils (up to 35MPa) at a relatively high speed. At the site of the trial the first 4 meters of soil were more densely packed and therefore more likely to show cyclic mobility when cyclically loaded. The soft soil layers underneath are more prone to flow liquefaction.

Additionally, vibrations (using Geophones) and settlements (visually) were registered to research the impact on the surrounding soil. Using sonic vibrations in the frequency range of 140-170Hz, no settlements were visible in the surroundings and the registered vibrations were relatively low at short distance and non-significant from 5m and further.

The promising results show the sonic installation method may have an added value compared to conventional methods for activities like installing piles in urban areas (less risks on disturbing adjacent constructions).

## **REFERENCES**

- Berghe, J.F. (2001). Sand strength degradation within the framework of vibratory pile driving. PhD Thesis, Université catholique de Louvain, Louvain
- Yang, J and H.Y. Sze (2011), Cyclic behaviour and resistance of saturated sand under non-symmetrical loading conditions, *Géotechnique* 61, No. 1, 59–73